EOS MAPPING ACCURACY STUDY

Robert B. Forrest
Thomas A. Eppes
Robert J. Ouellette

Bendix Research Laboratories
Southfield Michigan 48076

March 1973

Final Technical Report for Period
April Through August 1972

Prepared for
GODDARD SPACE FLIGHT CENTER
Greenbelt, Maryland 20771

1. Report No. 6562	2. Government Accession No.	3. Recipient's Catalog No.

4. Title and Subtitle

EOS MAPPING ACCURACY STUDY
Final Technical Report

5. Report Date March 1973

6. Performing Organization Code BRL Report No. 6562

7. Author(s) Robert B. Forrest, Thomas A. Eppes, and Robert J. Ouellette

8. Performing Organization Report No.

9. Performing Organization Name and Address

Bendix Research Laboratories
Southfield, Michigan 48076

10. Work Unit No.

11. Contract or Grant No. NAS-5-21727

12. Sponsoring Agency Name and Address

National Aeronautics and Space Administration
Goddard Space Flight Center
Greenbelt, Maryland
William L. Alford, NASA Monitor

13. Type of Report and Period Covered
Final Technical Report
April Through August 1973

14. Sponsoring Agency Code

15. Supplementary Notes

Prepared under BRL Project No. 2516

16. Abstract

Studies were performed to evaluate various image positioning methods for possible use in the Earth Observatory Satellite (EOS) program and other earth-resource imaging satellite programs. The primary goal is the generation of geometrically corrected and registered images, positioned with respect to the earth's surface. The EOS sensors which were considered were the Thematic Mapper, the Return Beam Vidicon Camera, and the High-Resolution Pointable Imager. The image positioning methods evaluated consisted of various combinations of satellite data and ground control points. It was concluded that EOS attitude control system design must be considered as a part of the image positioning problem for EOS, along with image sensor design and ground image processing system design. Study results show that, with suitable efficiency for ground control point selection and matching activities during data processing, extensive reliance should be placed on use of ground control points for positioning the images obtained from EOS and similar programs.

17. Key Words	18. Distribution Statement
Image Sensor Geometry Earth Observatory Satellite Satellite Image Positioning Accuracy Ground Control Points Attitude Control and Measurement Earth-Resource Data Needs	

19. Security Classif. (of this report)	20. Security Classif. (of this page)	21. No. of Pages	22. Price
Unclassified	Unclassified	137	9.00

PREFACE

OBJECTIVES

The primary objective was to evaluate potential EOS image-positioning methods using various combinations of satellite data and ground control points. Secondary objectives were to assess the merits of the RBV camera for the EOS mission; verify the assumed user requirements for image resolution, coverage, registration, and positioning; model the imaging geometry of a conical-scanning Thematic Mapper to assist in the evaluation of image-positioning methods; and comment on sensor and ground-processing features that, if developed, might enhance system performance.

SCOPE

The study made use of information obtained from literature surveys, discussions with NASA personnel monitoring the program, and discussions with potential users of EOS data. The analyses used to estimate potential accuracies of different image-positioning methods were based on photogrammetric experience and state-of-the-art data. The discussion covers image sensor design factors, position and attitude considerations pertaining to external EOS geometry, and geometric error analysis of positioning methods.

CONCLUSIONS AND RECOMMENDATIONS

EOS attitude control system design must be considered as a part of the image positioning problem for EOS, along with image sensor design and ground image processing system design. With suitable efficiency for ground control point selection and matching activities during data processing, extensive reliance should be placed on use of ground control points for positioning the images obtained for EOS and similar programs.

TABLE OF CONTENTS

LIST OF ILLUSTRATIONS

LIST OF TABLES

SECTION 1

INTRODUCTION AND SUMMARY

1.1 BACKGROUND AND GENERAL COMMENTS

This report describes the results of a study carried out by Bendix Research Laboratories (BRL), Southfield, Michigan, from April through August, 1972, under NASA/GSFC contract NAS5-21727. The work was directed toward mapping accuracy considerations for the Earth Observatory Satellite (EOS) program. Many conclusions are also believed applicable to earth-resource imaging satellite programs in general; the primary goal assumed for such programs is the generation of geometrically corrected and registered images, positioned with respect to the earth's surface. The three EOS sensor candidates of interest were the high-resolution imagers: the Thematic Mapper (Seven-Channel Scanning Radiometer), the Return Beam Vidicon camera (RBV), and the High-Resolution Pointable Imager (HRPI).

The primary study tasks were:

(1) Analyze the relative merits of image-positioning methods using satellite-data only, ground control points only, and advantageous combinations of the two.

(2) Estimate the positional accuracy that can be obtained for each of the methods.

Additional tasks included:

(3) Assess the merits of the RBV camera for the EOS mission.

(4) Verify the assumed user requirements for image resolution, coverage, registration, and positioning.

(5) Model the imaging geometry of a conical-scanning Thematic mapper to assist the analyses of the primary tasks.

(6) Comment on sensor and ground-processing features that, if developed, would further improve system performance.

(7) Define attitude performance requirements in terms of allowable contribution to positional error.

The need for EOS image-positioning on the earth arises from the uses planned for the images. Details of interest on EOS images will be compared with other kinds of information: ERTS images, larger-scale aerial images, maps, tabular, and textual information. The established earth system of latitude and longitude forms a common reference for all these comparisons. A uniform plane-coordinate reference such as the Universal Transverse Mercator grid is useful for some comparisons, and for measuring distance, direction, and area.

EOS image positions should be defined with respect to one or both of these coordinate systems. In addition to this absolute position, the 17-day repeat cycle of the EOS images will be of considerable benefit in making temporal comparisons of phenomena from successive EOS images. Some analyses require comparison on a resolution-element basis. As a result, very accurate relative positioning of one EOS image to an earlier or later image of the same earth scene is sought. This form of relative positioning is called temporal registration here. Finally a single imaging observation of an earth scene is made by several sensors in several spectral bands. Comparison between images from different bands and sensors is very useful, once again on a resolution-element basis. Hence, accurate relative positioning between the resolution elements of different sensors and spectral bands is important. This form of positioning is called event registration. Since the EOS resolution elements will be as small as 20 meters, considerable care must be taken if temporal and event registration are to be done with the desired accuracies.

It is possible to produce the EOS images with no effort toward providing position and registration. This task then would simply be passed to the user, who would have to make the necessary investment in equipment and personnel for his purposes. If there were to be only one user, this solution would be as effective as any other. Since, however, there are many different disciplines engaged in the use of earth-resource data, it is clearly desirable that the image data from EOS be positioned and registered to the maximum extent consistent with production requirements before it is released.

Given that EOS image positioning and registration are to be performed, the next questions are, how and how well? This study is concerned with the answer to these questions. The study is based upon a meeting of two different areas of technology with a common goal: positioning all points in an image with respect to the earth's surface. Assuming the internal geometry of the imaging sensor is well known, six external parameters, three translational and three rotational, are needed to position the image with respect to the earth.

One way of determining these parameters is with the use of satellite data, information derived completely independently of the image content. Customarily, satellite data consists of (1) the satellite ephemeris for the three translational parameters, (2) measured and telemetered spacecraft attitude angles, and (3) calibration or autocollimation data to relate spacecraft attitude to image-sensor attitude. The space images obtained from meteorological satellites have been positioned exclusively from satellite data. A large body of knowledge has been developed in the performance of this positioning method, largely taken from missile and satellite guidance, control, and tracking technology.

A second way of positioning an image is with the use of ground control information derived using only image information content. Ground-control data consist of (1) the known locations of a few earth-surface features, and (2) the measured locations of these features in an image. This method of positioning, with various permutations, has been used for years in the precise mapping of the earth's surface from aerial photographs. The body of knowledge developed here has been taken largely from photogrammetry, surveying, and geodesy, disciplines considerably less familiar to NASA mission planners than those associated with satellite-data positioning.

The two image-positioning methods have been successfully combined recently in the Earth Resource Technology Satellite (ERTS) program. Satellite data initially are used to position all images obtained from the ERTS spacecraft. The attitude data are taken from horizon sensors and limit the positional accuracies obtained. Ground-control data are used to increase positioning accuracy for a selected number of images, and also to calibrate and monitor the offsets between the spacecraft attitude sensors and image sensors. (The ERTS combination should not be construed to mean that satellite-data methods are inherently inaccurate; the Orbiting Astronomical Observatory (OAO) program incorporates a stellar tracker to achieve very high (inertial-reference) attitude accuracies.)

From the ERTS experience, it is clear that both image-positioning methods have advantages and disadvantages. It is also apparent that a systems approach to the problem is preferable to one in which image positioning methods are incorporated after the rest of the program is complete. The question for EOS planning, then, is not, "which method is best for EOS?", but, "how should the two positioning methods be combined to give the best approach for EOS?" The combinations selected for this study may not necessarily be the best, although some effort was made here to select only the most promising. More extensive interaction between the two technology areas is needed. In fact, the major conclusion of the present study has been the recognition that the photogrammetry/surveying/geodesy technology and the control/guidance/tracking technology should work together to develop the best positioning scheme for EOS. Both areas have a specialized technical vocabulary and audience. It is not reasonable to expect a group well-versed in one area to master the other and at the same time conduct an adequate technical evaluation of a many-faceted problem. This conclusion is borne out not only by this report, but also in some of the references cited which were written from the opposite side of the technological fence.

1.2 SUMMARY OF FOLLOWING SECTIONS

Section 2 of the report presents a short description of the different positioning schemes that were considered in the study. In Section 3 the image sensors are discussed, in particular the internal geometry of the

sensors. This is an important subject, since the accuracy with which this geometry can be described is the limiting consideration in event registration Offset pointing is also considered, since it represents a departure from the ERTS geometry and carries with it certain geometric implications. Alignment between attitude and image sensors is important for satellite-data positioning, and is discussed in Section 3.4.1. The value of the RBV camera as an EOS sensor is discussed in detail in Section 3.4.2.

In Section 4, the central matters of satellite position determination, attitude control and measurement, and ground-control point principles and applications are discussed in some detail.

Section 5 is concerned with the accuracy attainable for the different positioning methods. Error analyses are presented based on the best values presently available for the different components. Finally, Section 6 presents the significant conclusions of the study. In most cases these conclusions also are stated in the relevant technical discussion. Recommendations for additional work also are presented in this section, following as logical extensions of one or more of the conclusions.

One problem in the discussion of internal sensor geometry was found to be a lack of knowledge about the geometry of a conical-scan Thematic Mapper such as that implemented in one design under consideration. Appendix A, written by T. A. Eppes, describes the analysis performed to better understand the detailed geometry of this sensor. In the course of the analysis, a Fortran simulation of the scanner geometry was programmed and exercised. The program and the results of the testing are given in this appendix.

Appendix B, written by R. J. Ouellette, presents the findings of a user requirements survey, performed to verify the ground-resolution needs of EOS image-data users. The survey summarizes many conversations with technical people in several Government agencies. The informality of these conversations was useful in obtaining user opinions under different circumstances from those used to compile published statements of agency needs, plans, and programs.

SECTION 2

POSITIONING TECHNIQUES

Two kinds of exterior orientation information are needed for positioning the EOS images: the three locational components of image-sensor position and the three angular components of attitude. For the RBV camera, this information is needed only for the moment of exposure. However, the Thematic Mapper and the HRPI require position and attitude data continuously over many minutes of uninterrupted image collection. The goals for position and attitude accuracies are commensurate with the highest-resolution image sensor. The 20-meter ground resolution of the HRPI for EOS is equivalent to 0.0012 degree.* These numbers indicate the magnitudes of interest for EOS position and attitude measurement.

Five components will be considered here in developing image-positioning techniques:

(1) Best-fit satellite ephemeris, for position

(2) Ground control points (GCP) for position and/or attitude

(3) Stellar absolute inertial attitude sensor

(4) Gyro short-term attitude measurement assembly

(5) Horizon-scanning earth-oriented attitude sensor

These components can be combined in several different ways to obtain the six image-positioning parameters required. Either (1) or (2) must present in any scheme to provide the three locational parameters. For the angular values, the situation is not so simple. Depending on the design of the attitude control system, no attitude information, a limited amount, or a great deal may be needed for positioning images.

Five main combinations of the components listed above were selected for detailed consideration. They are summarized in Table 2-1 and described in the remainder of this section. Extensive error analysis of the methods is postponed until Section 5, after additional discussion of the different components.

---

*During this study, angles have been seen specified in arc seconds, decimal parts of a degree, radians, and "milli-earth-rotation units". In this section, degrees and decimal parts of a degree are used throughout for uniformity, simply because the attitude control system specification is so expressed in reference (1). (Some standardization of angular measurement units seems as desirable for reports as the standardization of linear units.)

Table 2-1 - Positioning Methods

Method	Ephemeris Position Data	GCP		Components			Conditions
		Frequent	Occasional	Stellar Sensor	Gyro Package	Horizon Sensor	
SIMS-E	X			X	X		
GCP-E	X	X					Good fit of attitude angles to low-order curve within an image.
SIMS-EG	X(relative)		X	X	X		Good relative ephemeris accuracy.
GIMS-E-1	X	X			X		
GIMS-E-2	X		X		X		Smoothly varying ephemeris error; even gyro drifts.
GIMS-E-3	X		X		X		Good relative ephemeris accuracy; low and even gyro drifts.
HIMS-E	X				X	X	

P-51-367-3

2.1 STELLAR INERTIAL MEASUREMENT SYSTEM (SIMS) AND EPHEMERIS

This method, referred to hereafter as SIMS-E, represents a pure satellite-data positioning scheme, using components (1), (3), and (4) from Table 2-1. Ephemeris data define the three translational parameters of the image sensor. The gyros provide short-term attitude information. If the gyros are gimballed, this information is provided directly in some form of local-vertical attitude angles. If the gyros are strapped down, the rates must be integrated to give inertial attitude angles which are further processed from the ephemeris to give local-vertical attitudes. In either case, the gyros are subject to drifts and other anomalies which make them unreliable over some period of time which is short with respect to the operational life of the EOS satellite. The stellar sensor provides absolute inertial-attitude fixes at the time intervals required to update the gyro data.

This method further requires that the angular relationships between the star sensor, the gyro housing or platform, and the image sensor be defined to the same or higher accuracies than those needed for the stellar inertial-attitude fixes. This is called the attitude-transfer requirement here. The simplest conceptual way of meeting this requirement is to mount the three types of sensors directly to one another. This is possible for only one image sensor, and might well severely impact the design difficulties for both SIMS and the imager. If direct mounting is not feasible, SIMS attitude values can be referred to a calibration block mounted to one of the image sensors. This solution shifts the attitude-transfer problem to the sensor designer to ensure rigidity and parallelism between the block and the internal geometry of the imager. It also is suitable for only one of the image sensors, probably the one with highest resolution, HRPI.

The next simplest solution is to mount SIMS and the image sensors to a common rigid structure; the spacecraft would be the common structure, but it is difficult to thus maintain a calibrated attitude relationship to the one or two arc seconds needed. The remaining alternative is some form of "auxiliary-auxiliary" or tertiary attitude sensor which monitors the attitude between the image sensor and the stellar/gyro package. In reference (1)* a three-axis autocollimator is suggested for the tertiary sensor. This may take several forms, and is discussed in more detail in Section 3.4.1.

The SIMS-E method illustrates the strengths and weaknesses of the satellite-data technique for image-positioning:

- Image content is not considered at all for positioning.
- Ground processing of image data is completely automatic.
- Reliability of the three types of attitude sensors is of vital concern.

*References are listed in order of mention at the end of the report.

- Attitude transfer is needed to relate attitude and image sensors.
- Random ephemeris errors impose the ultimate accuracy limit, even with zero errors in attitude, attitude-transfer, and internal image geometry.
- Development costs are largely those associated with space-qualified reliable attitude and attitude-transfer sensors.
- More spacecraft weight and power are needed beyond that normally required for attitude control.

2.2 GROUND CONTROL POINTS (GCP) AND EPHEMERIS, METHOD GCP-E

This method represents a nearly complete ground-control positioning technique, using components (1) and (2) in Table 2-1. Ephemeris data are used for two of the three parameters, along- and across-track position. Ground control points are used for the other four unknown parameters, and also for other parameters associated with mean attitude rates and accelerations. The GCP positioning technique is such that errors in the ephemeris values are compensated by two of the angular parameters without significant error; the technique is described in detail in Section 4.3. The ephemeris data are not strictly necessary for the solution, but are normally available for the satellite anyway, and provide a modest statistical improvement in positioning accuracy.

This method is the only one of the five which does not require or use telemetered attitude data from gyros on the spacecraft. To achieve this freedom, some constraints are placed on the attitude behavior of the spacecraft, other than those originally specified in reference (1): attitude behavior must be known in advance to be such that deviations from some simple behavior model will not be in error over a 30-second period by more than 0.0005 to 0.001 degree in each axis. The magnitudes of the angles and rates are not of concern. Details are given in Section 4.2.

Method GCP-E shows the typical characteristics of the GCP method of positioning, constrained somewhat in this case by the non-framing EOS sensors:

- The primary component used for image positioning is the information within the image.
- Ground processing of image data requires some manual operations, supported by equipment and procedures designed to obtain highest production.
- The only spacecraft sensor of concern is the image sensor itself.
- Attitude transfer is not required.
- The accuracy limit is determined by image resolution and internal image geometry, and by the small irregular deviations in attitude from a smooth low-order curve.

- Development costs are those associated with an efficiently operating ground data-processing facility, including some manual steps.
- No extra spacecraft weight and power are needed.

2.3 STELLAR INERTIAL MEASUREMENT SYSTEM PLUS GROUND CONTROL POINTS, METHOD SIMS-EG

This method is the first of two hybrid positioning schemes which were selected for consideration in the study. Components (3) and (4) are used from Table 2-1, supported by shared limited use of components (1) and (2). Note from the table that the GCP are used infrequently, for one or perhaps a few images per orbital pass, rather than in each image to be positioned. They serve here primarily to detect and remove bias in the ephemeris. This bias is taken as representative, and applied ahead and back along the orbital arc to all other images to be positioned. If the spacecraft structure is suitably stable over a single imaging pass, the GCP will also solve the attitude-transfer problem.

There are several advantages to this sparing use of GCP over method GCP-E. First of all, the many fewer GCP to be selected and correlated mean much less difficulty in a high-production ground processing facility. This is especially true if a completely digital image processing scheme is to be used; the lengthy digital image correlation needs are much less significant than in a method where each image requires correlation of several GCP. Second, the GCP need be selected only in areas with highest image quality. Third, the ephemeris error effects are greatly reduced from what they were for method SIMS-E. Fourth, the need for some GCP processing also gives a back-up capability for use in the event of spacecraft attitude-sensor failure. Finally, attitude-transfer between attitude and image sensors can be achieved using GCP instead of pre-launch calibration.

Unfortunately, some of the negative aspects of methods SIMS-E and GCP-E also are incorporated in the hybrid SIMS-EG. Development costs are high, since both precision spacecraft attitude sensors and a ground processing facility for GCP are needed. Also, as is shown in Section 5, some of the errors of each method are added in this hybrid method, so that not much of an increase in accuracy is obtained. More spacecraft weight and power still are needed for attitude measurements than would be required only for attitude control. The reliability of the stellar and gyro attitude devices is of concern, too, although the GCP capability does provide some backup.

Table 2-1 shows that an additional condition is imposed on the use of method SIMS-EG: good relative ephemeris accuracy. Over orbital arcs of a few thousand kilometers, relative accuracy should be high enough (see Section 4.1) to make consideration of SIMS-EG worthwhile.

2.4 GROUND CONTROL POINTS PLUS GYRO DATA PLUS EPHEMERIS, METHOD GIMS-E

This hybrid positioning method removes the attitude-behavior condition imposed on method GCP-E by incorporating telemetered gyro data. There are three variations of this method to be considered, with a decrease in each variation of the amount of GCP needed.

The first, GIMS-E-1 uses ephemeris data for along-track and across-track position. Gyro data provide high-frequency relative attitude data. GCP define altitude and absolute attitude values for the three rotational axes. Gyro drifts are considered here to be less than 0.001 degree over 15 seconds. If this is not the case, mean attitude rates must be carried as three additional unknowns in the GCP image-positioning solution. This means either more GCP must be used to retain a given accuracy, or lower positioning accuracy for the same number of GCP per image.

The second variation is GIMS-E-2. In this case, GCP are not used in every image for positioning, but only at intervals along an imaging pass. Between GCP images, the attitudes and positions are interpolated, with bias-adjusted gyro and ephemeris data used for attitude and position, respectively. The variation requires fewer GCP operations than GIMS-E-1 and preserves much of the accuracy, but requires better gyro characteristics and low random error in the ephemeris.

The third variation is GIMS-E-3. Here, extrapolation is used instead of interpolation. GCP are used for a single image, together with ephemeris and gyro data. Values are obtained for the usual six parameters plus three mean attitude rates. These values are extrapolated forward and backward along the orbit using ephemeris differences and the angle- and rate-adjusted gyro data. Even fewer GCP are required here, in exchange for even better-defined gyro angles and ephemeris.

The three variations differ only in their trade of GCP frequency for ephemeris and gyro quality. Thus, they share these characteristics:

- Image content is used only to the extent necessary to overcome gyro and ephemeris deficiencies.
- Ground processing of image data requires some manual operations, but fewer than method GCP-E, and provides back-up for gyro failure.
- Reliability of the gyro device on the spacecraft is of concern.
- Attitude transfer is not required, if the attitude between the gyro reference and the different sensors remains constant between GCP updates.
- Ephemeris and gyro error effects can be traded with frequency of GCP use.
- Costs are in the development of a high-quality gyro package, as well as manually aided ground processing.

- Some spacecraft weight and power are needed* beyond that normally required for attitude control.

The variations of GIMS-E place somewhat greater reliance on GCP than does method SIMS-G, with a consequent decrease in concern over spacecraft components and an increase in the required manual processing. The accuracy is somewhat improved from SIMS-G as well, at least for variation GIMS-E-1. Accuracy for the other two variations can be traded with ephemeris/gyro quality and number of GCP needed.

2.5 HORIZON SCANNER WITH GYRO PACKAGE AND EPHEMERIS DATA, METHOD HIMS-E

This method is included to show back-up capability and a cost/accuracy benchmark. Method HIMS-E is a pure satellite-data positioning scheme, using components (1), (4), and (5) from Table 2-1. The method is functionally the same as that used to position the ERTS bulk images, although gyro performance is considerably improved. HIMS-E operates in the same way as SIMS-E, except that the horizon sensor replaces the stellar mapper or tracker of SIMS-E for attitude updates to be applied to the gyro data. The horizon data for HIMS-E will result directly (after some modeled adjustments) in true local-vertical attitude. This is different from the situation using SIMS-E, where the attitude derived is inertial and must be transformed to the local reference frame using accurate ephemeris data. The horizon sensor cannot approach the stellar sensor for attitude accuracy, although considerable improvements can be made in the raw data by proper oblateness-effect removal. The characteristics of this method are qualitatively the same as for SIMS-E, except that (1) spacecraft-component costs, reliability, weight, and power are somewhat less of a problem, and (2) the horizon-sensor error would be expected to impose the accuracy limit, not ephemeris errors. Overall, this method is probably the least expensive, and it is certainly the least accurate.

*It may be possible to use the ACS gyros for the required attitude information.

SECTION 3

IMAGE SENSOR CONSIDERATIONS

The following discussion is particularly concerned with the three high-resolution image sensors presently proposed for the EOS payload: the Thematic Mapper, the HRPI, and the RBV camera pair. Some of the material will be seen to apply also to image sensors and earth-resources missions in general.

The EOS orbit and ground-swath coverage parameters are those derived in reference (1):

(a) Altitude = 980 km above equator, circular orbit

(b) Period = 104.6 minutes

(c) Inclination = 99+ degrees

(d) Ground-swath width for high-resolution imagers = 185 km (100 nm), with 10 percent overlap at equator

(e) Revisit time = 17 days

(f) Local time of descending node = 8:39 AM

3.1 INTERNAL GEOMETRY

3.1.1 Thematic Mapper

In reference (1), a conical scan geometry is suggested for the Thematic Mapper. The conical scan results from an effort to increase duty cycle without severe weight penalty for a particular resolution. It is possible that this goal also can be met with an optical design which results in the more usual straight-line scan geometry, such as that employed by many aerial scanners. The simpler geometry may be preferable for ease of processing or some other considerations. Still, there is nothing in the use of conical scan which inherently limits the geometric use of the data.

The effect of one conical image-plane scanner implementation is shown in Figure 3-1. In this figure, the cone is vertical. The effective imaging geometry is based upon the text and the schematic diagram contained in reference (1), except that six catoptric probes are assumed instead of eight, as in reference (3). The six probes divide the cone base circle into six equal sectors, and 48 degrees of each sector are used for active scanning (80 percent duty cycle). Six high-resolution lines are swept out in each scan swath, with the detectors for a given spectral region arranged in a one by six array, as shown in the figure. To cover a strip 185 km wide on the earth with a 48-degree central angle of the base circle requires a cone vertex angle slightly

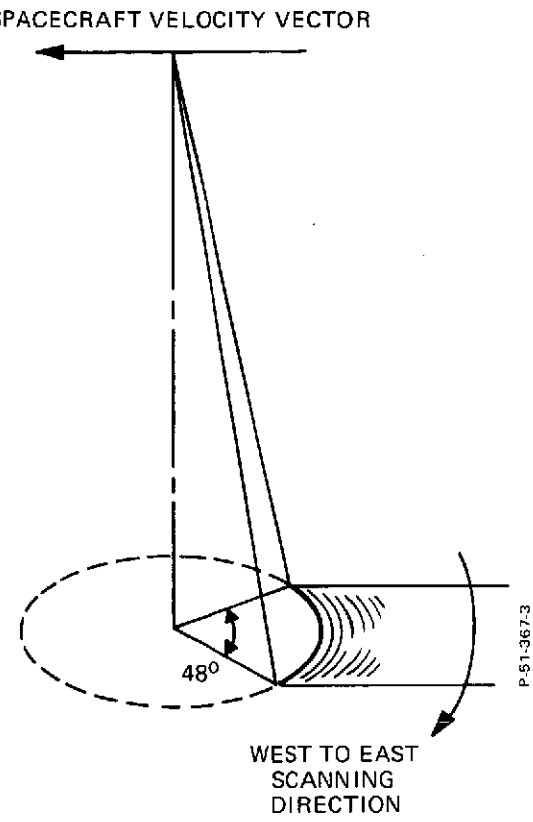

Figure 3-1 - Vertical or Circular Conical Scan

greater than 26 degrees. The chief characteristic of vertical-cone imaging is that all objects on the earth are scanned with the same nadir angle. This might appear to be advantageous for multispectral applications, since the spectral reflectance characteristics of many features change with viewing angle. However, the angle formed by the sun, ground feature, and the scanner detector also is important to spectral reflectance, and this angle changes during a single scan swath. Thus the fixed-nadir-angle scanning may not be of significant value.

In Figure 3-2, the scanner just described has been mounted in the spacecraft with a forward tilt of one-half the vertex angle. As a result, the arc formed on the earth by a single scan swath passes through the spacecraft nadir at the swath center, with increasing nadir angle toward the ends of the swath. This configuration supposedly results in a more "natural" viewing geometry, since it is more nearly that of a conventional scanner sweeping a straight line from side to side through the nadir (e.g., the ERTS MSS scanner). A more tangible reason for tilting the cone is to reduce the positional error caused by terrain relief variations. Figure 3-3 shows the projective displacement, dS, of a hilltop away from its orthogonal position. The displacement is equal to

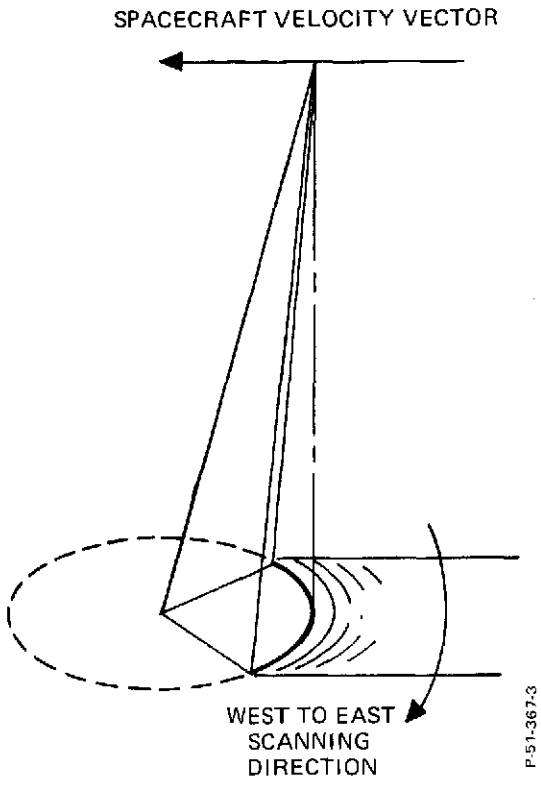

Figure 3-2 - Forward Tilted Conical Scan

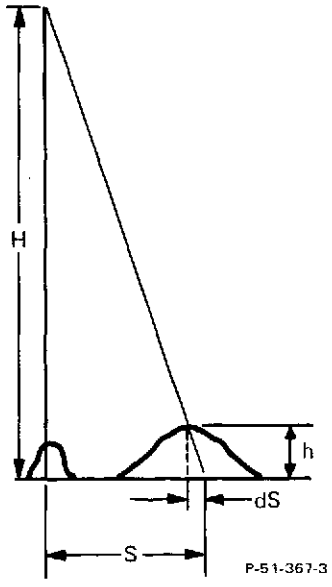

Figure 3-3 - Displacement Caused by Terrain Relief

h(S/H). For the vertical-cone EOS imager shown in Figure 3-1, the ratio of S/H is nearly one-fourth throughout each scan line, so that all points on the terrain are differentially displaced radially from the nadir by amounts equal to one-fourth their height differences. For the tilted-cone imager in Figure 3-2, no terrain relief displacements occur at the center of each scan line, where S/H is zero. Displacement effects increase away from scan center until, at the ends of scan, they are nearly as great as for the vertical-cone imager. But the near terrain displacements still are significantly less for the tilted-cone than for the vertical-cone imager. Such displacements are noticeable only in a positional sense, with respect to the map locations of image features; for either of the scanning cone configurations, any terrain displacements will repeat on subsequent imaging passes. Thus temporal registration will not be affected.

The instantaneous field of view (IFOV) for the Thematic Mapper was originally specified as 66 microradians for the six high-resolution channels described in reference (1). At the nominal EOS altitude of 980 km, a single high-resolution scan swath will contain 6 x 2,870 samples, and the swath thickness will be 388 m. As a result of the EOS Mission Review Group's conclusions, reference (2), the original IFOV will be reduced. The present goal is 44 microradians. If this is achieved, a single scan swath will contain 6 x 4,300 samples, and the swath thickness will be 259 m. The rotation rate of the wheel containing the six sets of scanning probes will be about 2.7 rps for the 66-microradian IFOV and 4.1 rps if the 44-microradian goal is achieved.

Details of the conical-scan image geometry, its interaction with earth-rotation effects, and the effects of attitude and altitude variations are described in Appendix A.

3.1.2 High Resolution Pointable Imager (HRPI)

This device presently is planned as a solid-state linear array of 1,800 detectors for each of 4 spectral bands, each detector with a 20 m square IFOV. The resulting geometry is that of a straight line 20 m wide and 36 km long, normal to the spacecraft velocity vector. The sensor can be rotated about the velocity vector to image any part of the 185-km wide Thematic Mapper coverage. If the Thematic Mapper is made capable of off-axis pointing, the HRPI may be required to follow; this requirement is not yet defined.

The extremely simple internal geometry of the HRPI has been aptly compared to a pushbroom. A straight line is scanned, with a fixed spatial relationship between all the detectors forming the line. As the spacecraft moves forward, this line is "pushed" ahead, covering the area of interest in a continuous swath.

3.1.3 Return Beam Vidicon Camera (RBV)

The RBV camera is familiar from its application as a multispectral imager in the ERTS program. For EOS no multispectral capability is to be used. The camera is proposed as a single-band (panchromatic in one reference) sensor to obtain reference images of higher resolution and greater locational accuracy than those provided by the Thematic Mapper. The RBV images also are to "aid greatly in achieving the desired location accuracy" for Thematic Mapper images, reference (2).

A pair of 2-inch RBV cameras have been recommended for EOS. Each has a focal length of 250 mm, twice that used for ERTS, and covers an area about 98 km on a side. The cameras must be tilted about 2.5 degrees, one to the left and one to the right of the ground track. Exposure and readout alternate between the two cameras.

A total of 4,500 television lines per image are to be scanned (the ERTS RBV tubes are scanning 4,125 lines), equivalent to a ground pixel (theoretical picture element) of 22 m on the earth. But image motion compensation will be required if effective resolution is to be at all commensurate with this pixel dimension.

Since the RBV cameras are basically analog television image sensors, the image distortion can be expected to change during any extended period. To enable the detection and correction of these random distortions, each of the RBV cameras for EOS will contain a reseau, a grid of marks etched on the camera faceplate. The measured locations of the reseau marks provide geometric calibration data. The same marks will appear in the RBV images and can be used to remove most distortions introduced during the readout sequence. For the ERTS cameras, the reseau array contained 81 marks in a regularly spaced 9 by 9 array. Some modifications to this pattern are recommended below.

3.2 GEOMETRIC DESIGN CONSIDERATIONS

In this discussion, the specific EOS image sensors are not so much of interest in their own right, but as examples of the geometric problems and potential in the design of image sensors. A great deal of geometric diversity is possible in designing image sensors to be used in earth-resources spacecraft. This stems from the different requirements to be satisfied by the sensors. Typically, high duty cycle, low weight, low volume, and low power requirements are sought. Under some conditions, by permitting "unusual" imaging geometry -- and any departure from a central perspective projection is sometimes considered unusual -- some of the other goals can be more nearly achieved. This is the rationale, for example, guiding the conical-scan geometry being considered for the Thematic Mapper design.

For image positioning and registration, there is nothing inherently "wrong" about incorporating unusual geometry in the design of an image sensor. However, it is important that the geometry be well known. Only with known internal geometry can the image data be effectively positioned.

Three methods can be considered for providing the image geometry information. The first is to correlate the image data point by point against a master image for which the geometry is known. The correlation process can be analog or digitial. The great advantage of this method is the lack of attention needed in image-sensor design. On the other hand, the method is quite slow (particularly when using digital methods), it requires continuous tracking to maintain the correlation process, and it will fail when adequate image detail is not present, references (27, 28), or when images from spectrally different regions are being matched, reference (26). It is clearly unsuited to high-throughput situations.

The second method is to provide advance calibration data on the image sensor geometry. This enables direct mathematical modeling of the sensor. The calibration data can be derived from grid images made in the laboratory, or from images collected over a test range containing a large array of ground control points. If this method is used, some care must be taken during image-sensor design to ensure geometric stability. Stability does not necessarily mean geometric simplicity, although data processing may be speeded if the geometry is simple. In any case, data processing proceeds quite rapidly using advance calibration data.

The third method of providing geometric information is to provide calibration data pertaining to each image. Typically, this is done by providing a reseau (grid) in the image. An intermediate amount of effort is required in both the sensor design and the image-data processing, compared with the first two methods. The image sensor must be geometrically "well-behaved" between adjoining reseau marks, so that some form of interpolation will adequately describe the image geometry. Also, the normal data processing operation must provide for the identification and measurement of the reseau marks in the image data, in order to properly calibrate the internal geometry for each image. This is a time-consuming operation, although much less so than point-by-point image correlation over the entire format.

In practice, the second and third methods often merge. The ERTS multispectral scanner (MSS) uses the second method, advance calibration. Even so, some analysis based on GCP residuals will be needed during the operational life of the MSS to detect possible changes in internal geometry. This analysis could be done easier using optional timing lines within each scan. The ERTS RBV camera array incorporates the third method of providing internal geometric information. Early ERTS data has shown that the random shifts in the internal geometry of the RBV cameras are smaller or slower than originally thought, reference (4).

If this behavior is characteristic, the reseau data from one image can be applied to a number of subsequent images, thus becoming a form of advance calibration.

Several points merit special consideration by image-sensor designers for EOS-type missions:

(1) An interrelationship exists between the attention paid to geometric properties during design and the attention that must be given to the geometric processing needed to process the image data obtained with the sensor.

(2) Stability is the most important geometric design consideration; adequate geometric stability should be provided in such form that only infrequent off-line methods need be used to monitor and update internal image geometry.

(3) Adherence to a particular geometric pattern for an imaging sensor is not always a necessity, provided the sensor gives the desired ground coverage and the geometry can be adequately described. This freedom in selecting geometry is greatest when extensive and complex processing must be applied to the image data for other reasons.

(4) Sensors with moving components require special calibration of their interaction with the spacecraft structure; depending on the frequencies involved, satellite attitude control may be degraded (Section 4.2), image-sensor geometry may be degraded, or image quality may be reduced.

3.3 OFFSET POINTING

One or more of the EOS image sensors is presently planned to have some capability for commanded offset pointing. Such capability has several advantages for data users, including avoidance of clouds or haze and the ability to image phenomena which are short-lived with respect to the normal 17-day repeat cycle.

At the equator, to center the Thematic Mapper on the adjoining ground swath to the east or west of the ground swath currently beneath the spacecraft, a roll angle of 10.7 degrees is needed. To center on the second ground swath east or west requires a roll angle of 20.5 degrees. The third swath requires 29 degrees of roll. These angles are maxima, decreasing with increasing latitude.

For purposes of data management it is most desirable to constrain the offset pointing capability to integral ground swaths. This is no hardship for users, since the coverage will be complete, and will correlate well with the normal images for the same ground swaths obtained in the normal downward-pointing mode. Since the overlap between successive ground swaths is a function of latitude, the amount of angular offset to be provided for the sensors must also be variable as a function of latitude, if offset imaging is to cover integral ground swaths.

Reference (1) shows that some misunderstanding of the offset pointing requirements may exist. The spacecraft motion supplies one dimension of a scanner image. This motion is quite rapid with respect to the

time-scale for earth-resource phenomena and cloud coverage. For example, by pitching a scanner in the EOS orbit ahead by 30 degrees, an image can be obtained only 1.5 minutes sooner than it would have been obtained by leaving the scanner vertical. Hence, there is no need to provide for a pitch offset. Gross yaw offset is not required either, at least for scanners which sweep rapidly compared to the earth's rotation effect. (There may be some rationale for a very small yaw offset to be provided by the spacecraft attitude control system as a function of latitude, in order to eliminate very small gaps in scanner coverage; this is discussed in Appendix A.) As a result, only a single axis is needed for offset pointing. One-axis pointing is considerably easier to design and implement than a three-axis offset.

Control of the pointing angle is the next item for consideration. Control can be provided in fixed large increments, such as five degrees, or in much finer increments. There is no need for extremely fine angular control here, since the image sensors cover several degrees. On the other hand, as mentioned above, efficient data management (cataloging, indexing, processing requests, retrieving image data) of the thousands of images which will be obtained dictate that the pointing be confined to integral ground swaths, referred to normal repeat cycle. The pointing precision should be about the same, too. For ERTS, repeat precision is ten percent. If the same figure is applied to EOS, the pointing increments need be no finer than about 0.5 degree. A stepper motor applying angular increments of this size would provide ground swath repeatability of about 6 percent, and 128 steps would cover the 60-degree range needed to step over 3 ground swaths to either side. To minimize the effects of disturbance torques on spacecraft attitude stability, it is necessary to implement the sensor offset pointing well in advance of any planned high-resolution image collection. The lead time depends on the attitude control system, the design of the pointing device, the moment of the pointing optics, and the placement in the spacecraft.

The accuracy with which the offset angle must be measured depends on the method used to position the image. For GCP techniques, measurement is not strictly needed at all, although some gross indication may be helpful in locating GCP for correlation. Satellite-data positioning methods require that the offset angles be measured with the same high accuracy as the spacecraft attitude angles. It may be desirable to avoid this high accuracy measurement by using only GCP for positioning off-axis images, even though the normal downward-looking images are positioned primarily with satellite data.

In regions of moderate terrain relief, some degradation in temporal registration accuracy must be expected when comparing off-axis images with the normal downward-looking images (Figure 3-4). The extent of misregistration caused by this effect depends on the height of terrain

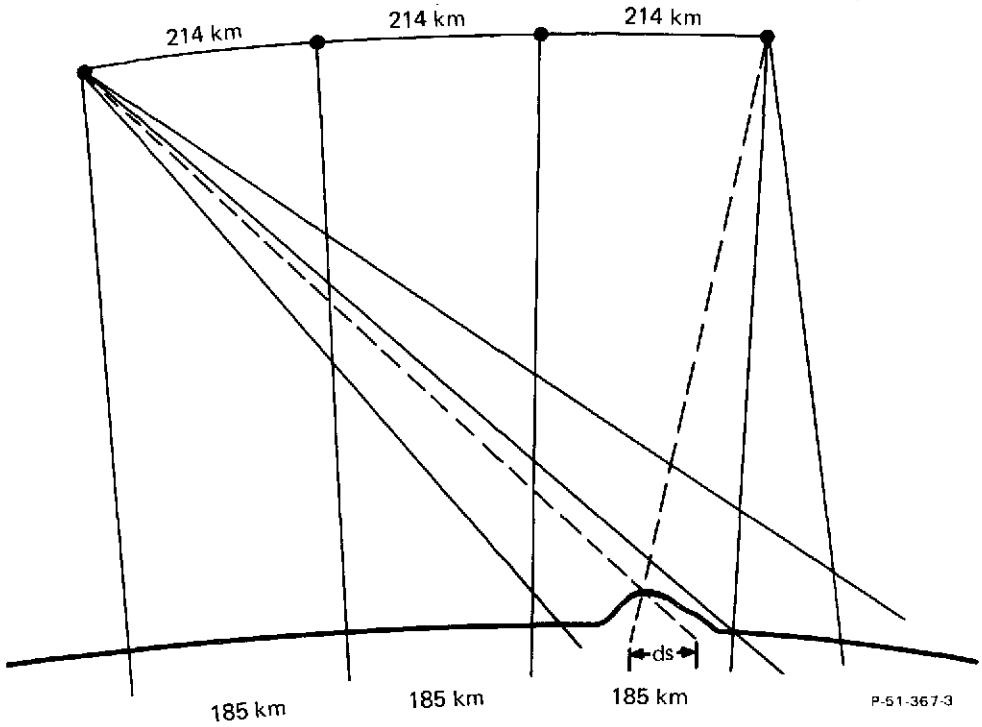

Figure 3-4 - Terrain Displacement from Offset Pointing

and the differences in the two imaging angles, and is given approximately by

$$ds = \frac{(214)}{(980)} N\ dh = 0.22\ N\ dh$$

where

ds = misregistration

N = number of ground swaths between the two images being registered

dh = terrain elevation

The terrain elevation dh is measured above mean terrain if GCP are used for positioning, or if spacecraft data are being used together with a world-wide mean terrain model. For spacecraft-data positioning without such a model dh is measured above mean sea level.

A positive way in which to consider terrain displacement is as a new capability for stereoscopic viewing. Even for a single ground-swath offset, an adequate stereo effect will be obtained. Terrain height determination can be performed under these conditions, with a relative error of

$$m_h = \frac{980}{214\ N}\, m_p = \frac{4.6}{N}\, m_p$$

where

m_h = standard error of relative height determination

m_p = standard error of position repeatability

3.4 OTHER SENSOR CONSIDERATIONS

3.4.1 Attitude Transfer

Some positioning methods depend on auxiliary data to determine the attitude of the imaging sensor. One of these methods may be used for EOS. If so, it is necessary to know the relative attitude between the auxiliary attitude sensor and each of the high-resolution image sensors. This is the attitude transfer requirement discussed in Section 2. The rms error with which this attitude should be known is commensurate with the rms error expected from the attitude sensor. To keep the effects of error to beneath significance in a root-sum-square error sense, the positional contribution of error normally must be held to one-third of the root-sum-square positional error from all other causes. For EOS, the rms error goal being used here is one HRPI resolution element, or 20 meters. The corresponding combined effect of attitude-transfer error goal then is 6.7 m/980 km or 0.00039 degree, about one-second of arc.

It is not necessary, or even desirable, to devote effort before launch to calibrating the attitude-transfer angles. They can be more meaningfully measured after launch using GCP in a single bias-removal calibration. However, some assurance of rigidity is needed so that these calibration values can be used with confidence.

The most straightforward way of achieving such rigidity would be to mount the image and attitude sensors together. This may not be possible for many reasons. But if the image and attitude sensors are mounted separately to the spacecraft structure, it appears to be very difficult to design the spacecraft with adequate rigidity to maintain such a high alignment accuracy. This leads to a tertiary-sensor method such as that suggested in Section 7.7-1 of reference (1). With this method, an additional optical device is used to measure and record the

three-axis misalignment between the external attitude sensor (a star mapper in this case) and one or more of the high-resolution image sensors. The alignment data obtained in this way would be telemetered to the ground receiving station along with the attitude-sensor data. This solution gives the greatest freedom to spacecraft design and to the placement in the spacecraft of the different sensor packages, and is undoubtedly feasible. However, it places another set of unknowns in the positioning problem, requiring additional reliability, cost, and care during system design to ensure adequate performance. It may be possible to combine the attitude alignment into either the auxiliary attitude sensor or the high-resolution image sensors, to either automatically maintain some fixed three-axis relationship or else record and compensate for deviations. Unfortunately, this solution simply shifts the problem to the image-sensor or attitude-sensor designers.

It must be noted again that a positioning method for which GCP are used with each image is not affected by these considerations. A gyro package may be needed for the scanning imagers, but such devices provide only attitude differences, over periods of time which are short enough to assume a constant angular alignment between gyro package and image sensor.

A second kind of sensor alignment concerns the different image sensors alone. To image the same area, these sensors must be boresighted before launch. Sometimes an array of imagers is intended to operate as a single composite image sensor; the array of three multispectrally filtered RBV cameras used for ERTS is an example. An inordinate amount of effort appears to be spent sometimes in the prelaunch boresighting of image sensors. For the relatively large areas typically being imaged, a misalignment of 0.1 degree is certainly permissible. This can be achieved with little effort. In general, the additional effort spent aligning image sensors more accurately could be more profitably devoted to designing ways to maintain constant alignment after launch.

3.4.2 Framing Camera Utility

In reference (2), the addition of the RBV cameras to the original EOS sensor complement was recommended for two reasons. The first is to provide higher spatial resolution than the Thematic Mapper (20 m for high-contrast and 50 m for low-contrast targets is quoted in reference (2)), with a corresponding capability for high location accuracy. The second is to somehow "relate the spectral and spatial data" of the Thematic Mapper, and so "aid greatly" in accurately locating Thematic Mapper image data (quotes are from reference (2)). Thus the advantages cited are (1) the effective resolution of the RBV camera versus other sensors, (2) the attainable positional accuracy for the RBV images, and (3) the ability to effectively use the RBV images as locational references for Thematic Mapper images. These three points will be considered in order.

First, the resolution advantage. Resolution is not a primary concern in this study, although it is unavoidably involved in some considerations. Resolution is not simply given by the theoretical pixel (picture element) size of the RBV camera, any more than by the instantaneous field of view (IFOV) of a scanner. Effective signal-to-noise ratio also must be considered. Initial ERTS images already have shown that the net image quality of the scanner with its 75 m IFOV is higher than that of the RBV camera with its 45 m theoretical pixel. Part of the reason for this may be the shading and mottling in the RBV images. A second point in connection with RBV resolution concerns image motion. During a nominal 0.010-second exposure, the camera moves over 60 m. Image motion already is blurring the ERTS 45-meter theoretical pixel size. There is no point in doubling the ERTS-camera focal length to obtain a theoretical 20-meter ground pixel unless some form of image-motion compensation is provided.

The second advantage cited for the RBV is that of locational accuracy. A framing camera is not necessarily of high geometric accuracy simply because it is a framing device. This is the very reason why simple amateur cameras are not used for photogrammetric mapping. The RBV camera is geometrically a framing sensor, but the reseau on the faceplate testifies to the need for extensive and continuous monitoring of the geometric stability. During data processing, each of the large array of reseau marks must be located and accurately measured, even in the presence of background imagery. This task cannot but add appreciably to the total data processing time necessary. At least some of the reseau marks must be checked in each image, reference(4), or series of images, to look for shifts in the distortion pattern. In fairness, early ERTS RBV images show rather good short-term stability of the image distortions.

The third stated advantage of the RBV camera concerns its ability to serve as a locational reference for Thematic Mapper images. The locational accuracy of the Thematic Mapper is discussed separately in Section 5. It is not in need of an RBV camera to be improved. For the present discussion, however, the accuracy of the Thematic Mapper image is not so much of interest as the mechanics of using one image to position another. Appendix G-3 of reference (2) recommends investigation of image correlation techniques to spatially relate the RBV and other images. Automatic image correlation techniques, both analog and digital, are well known, references (26, 27, 28, 29, 30), both for use in contouring and profiling the earth's surface and for simple image matching. The ERTS precision processing subsystem incorporates a modification of this electronic image correlation experience to precisely lock on selected ground control points. It must be emphasized, however, that there is a tremendous difference between correlating a few small areas specially chosen for their pattern and contrast and correlating continuously over the entire image. The problem is increased when attempting correlation between images from different spectral regions, reference (26). Experience gained at these laboratories and elsewhere has shown that image

correlation is a useful tool when used with discretion, human judgment, and manual back-up. This is true for digital as well as analog or hybrid applications. But correlation of all image details is extremely time-consuming; its wholesale application has no place in a high-production environment, and should not be considered further.

Summarizing the discussion above,

- Resolution: The RBV camera would need image-motion compensation and some other improvements before any comparison of net image quality is meaningful.
- Geometric accuracy: The reseaus require lengthy processing and periodic checking by methods ill-suited to automatic operations in order to maintain geometric quality; the quality is not demonstrably higher than that of the Thematic Mapper.
- Locational reference: The image correlation process is far too time-consuming and unreliable for high-production application in matching Thematic Mapper image detail to RBV images.

In conclusion, then, an RBV framing camera on EOS will not affect Thematic Mapper positioning or registration. With improvement, the RBV may have merits of its own in terms of resolution or as a backup sensor. Still, there may be other imagers with similar attributes and they merit equal consideration, in which cost, weight, power, and data processing complexity are balanced against usefulness of the images. Other use may be preferable for the weight and power entailed; an on-board data-filtering or compression package to cut transmission data rates is one possibility. A backup Thematic Mapper or Extended HRPI are others.

If, in spite of these arguments, the RBV camera is approved as an EOS sensor, some form of image-motion compensation device must be provided for the camera. In addition, the existing reseau pattern should be changed as follows:

(1) Reduce thickness of reseau crosses by at least 50 percent.

(2) Scribe crosses as X's rather than +'s, with respect to raster.

(3) Change spacing so reseau density is higher at edges and corners, but total number of reseaus remains the same.

3.4.3 Data Compression

Although it is not a subject for the present study, the high data rates associated with EOS cannot help but impress the observer. In the next few years, users can be expected to demand even greater spatial resolution, further increasing the data rate. One way of limiting the data rate is through onboard processing and filtering of meaningful

information. This approach is already being pursued. Another method is to sense and/or transmit data for only those spectral regions and resolutions currently of interest. There still appears to be some diversity of opinion as to the number of spectral bands necessary to detect the various phenomena under investigation, and the necessary amount of sensitivity within the bands. The numbers of bands needed, their wavelengths, and the resolution within the bands can be expected to change as functions of experience, data application, time of year, and geographic region, to name but a few variables. Thus ground-selected spectral regions and resolutions may satisfy the spectral needs of users, while permitting a more reasonable data rate. It has been noted from several user surveys, including the one carried out as a part of this study, that the need for multiple spectral bands to some extent complements the need for high spatial resolution. Thus, some advantages might be seen for an imager which could provide the same data rate by high resolution using a single panchromatic channel, or by decreased resolution but with several spectral channels.

SECTION 4

POSITION AND ATTITUDE

This section describes those aspects of geometric positioning which are not associated with the image sensors -- the external EOS geometry.

4.1 SATELLITE POSITION FROM EPHEMERIS

4.1.1 Selected Orbit

The basic requirements for the EOS orbit are nearly the same as for the ERTS orbit, and probably will remain so for most subsequent earth-resource satellites: a near-polar, nearly circular stable orbit, with regularly repeating continuous coverage of the earth's surface. For EOS and ERTS the orbit is also sun-synchronous, with the orbital plane precessing about the earth in inertial space at the same rate as the mean earth rotation about the sun. Within these constraints, the variables are altitude, repeat cycle in days, and right ascension of the ascending node. The latter variable determines the local time of transit and whether imaging will occur on the ascending (northbound) or descending (southbound) node. The various combinations were discussed in reference (1), and also in reference (9), and resulted in the EOS parameters shown in Table 4-1. The corresponding ERTS values also are shown in the table.

Table 4-1 - Orbit Parameters

	EOS	ERTS
Mean Altitude at Equator	980 km	920 km
Repeat Cycle	17 days	18 days
Imaging Node	Descending	Descending
Mean Local Time at Equator on Imaging Node	8:30 am	9:30 am
Inclination of Orbit	99+°	99°
Distance at Equator between Successive Orbits	685 km	2870 km
Distance at Equator between Adjacent Ground Traces	171 km	159 km

4.1.2 Discussion of Orbit Selection

In reference (1), the rationale governing the selection of the EOS orbit was discussed in some detail. Basically, the orbit was governed by the previous altitude selection of 1,000 km for the Thematic Mapper and another lower-resolution sensor. Many prospective users of earth-resources satellite image data claim they want higher image resolution. They naturally have asked why missions cannot be planned for a lower orbital altitude. From the mission-planning viewpoint, low altitudes are avoided for two reasons, increased air drag and decreased time above the horizon for transmission to ground receiving stations. With increased air drag, it is necessary to periodically carry out orbit maintenance with a small thruster. However, as reference (1) shows, the additional fuel weight required for this maneuver is quite low, at least for orbit maintenance intervals of about 20 days. Thus, it is at least feasible to discuss altitudes as low as the 570 km treated in reference (1).

Decreased above-horizon pass time is a severe limitation for satellite programs organized as was ERTS, with a very few stations acquiring data directly from the satellite. However, the higher data rates to be expected with future satellites, including EOS, raise the possibility of using a relay satellite to provide the link between imaging satellite and ground stations. Such a solution if adopted would have many advantages, only one of which is the removal of concern about above-horizon time for the imaging satellite.

So there are ways around the original limitations on lower altitudes. Other effects of lowered altitude now must be considered, and for these ground-swath width must be considered.

If ground swath-width in kilometers is kept constant and orbital altitude is decreased, the image sensors on the satellite must have a wider total angular field of view than at the higher altitudes. Since the image sensors are to maintain the same angular resolution, an increased data rate is needed to achieve the resulting higher spatial resolution over the same ground swath. Also, a larger maximum nadir angle will result when imaging from the lower altitude. Terrain relief displacements then will be larger. However, as long as the nadir angle remains within about 30 degrees very little terrain masking will result (conventional aerial cameras have half-field angles of over 40 degrees). Temporal registration between images made by successive passes over the same earth scene will not be affected as long as the ground-trace repetition is controlled properly.

A second matter of concern is the repeat cycle time. For any fixed altitude, the repeat cycle is determined solely by the selected ground-swath spacing, reference (1): the narrower the swath width, the more days needed for the repeat cycle. In general, a short repeat cycle is desirable to give more opportunities for cloud- and haze-free imaging of each area of interest. Thus, a wide ground swath is in

order. Figure 4-1 shows this relationship for two different orbital altitudes, 570 and 900 km. These altitudes are associated with 15 and 14 orbits per day, respectively, from reference (1). As the figure shows, a decrease in orbital altitude allows a choice between a modest decrease in either the repeat time or the ground-swath size. For any orbital altitude, a significant decrease in repeat time is possible only by increasing ground-swath size. Swath size can be much larger than the present 160-170 km and still result in a nadir angle of less than 30 degrees. The roll offset capability proposed for the EOS Thematic Mapper gives an effective shortening of the repeat cycle by increasing the available swath width on each pass.

Summarizing the discussion, a low orbital altitude can provide more spatial resolution and a slight decrease in repeat cycle time. These advantages must be compared against (1) the need for periodic orbit maintenance, (2) the possible need for relay satellites to provide adequate transmission to ground stations, and (3) larger nadir angles and data rates for a given ground-swath spacing.

Orbits other than circular can be considered for earth-resources missions. A highly elliptical orbit would allow imaging along a short arc near perigee without long-term air drag. The motion of perigee in the orbital plane would shift the imaging arc from one pass to the next. Earth rotation and orbital precession would shift the ground trace of the orbital plane. Such an orbit obviously is much more complex than the simple circular choice.

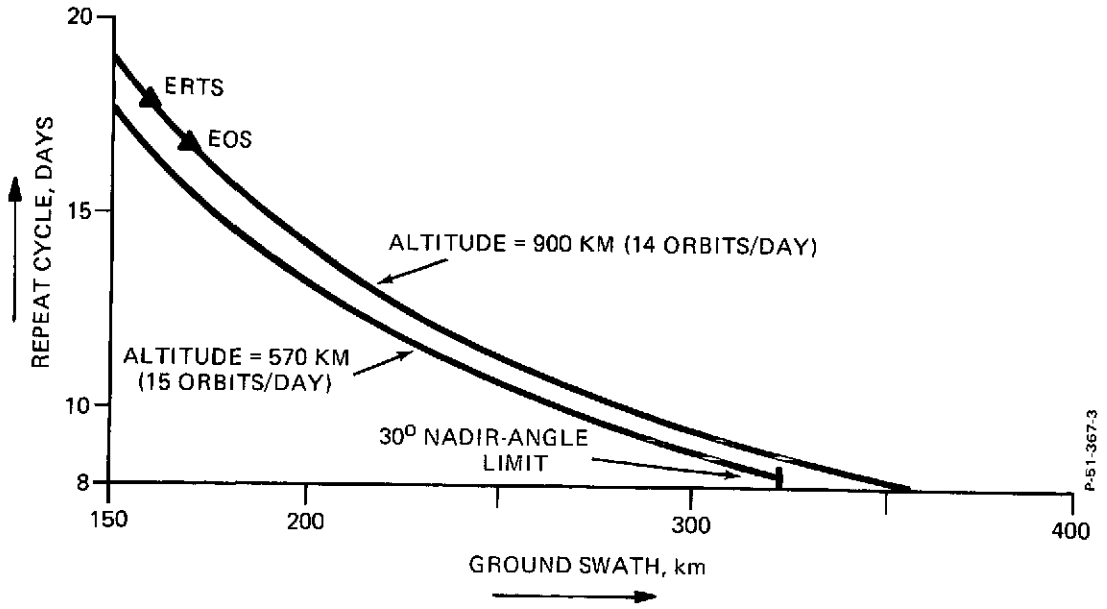

Figure 4-1 - Relation of Repeat Cycle and Ground Swath to Attitude

A circular orbit does not give constant altitude above the earth. As a result of the earth's oblateness, at the highest latitudes the satellite altitude is about 21 km greater than at the equator. The EOS images will have about a 2 percent range in scale as a result. This is a small but significant amount and will require additional work during digital image processing. The altitude range also causes an under- or over-scan condition with a fixed rate scanner, and a change to the number of scan swaths per image format. It would be desirable to use an orbit with an ellipticity which exactly matched the oblateness of the earth, thus giving constant altitude. For a sun-synchronous requirement, this orbit would have motion of perigee in the orbital plane, reference (7), so the earth and orbit ellipticity would match only occasionally. Hence, the circular orbit apparently is the best way to obtain nearly constant altitude above the earth.

4.1.3 Effects of Improper Orbit

For most imaging satellites, insertion into an incorrect orbit will significantly affect mission success. It is assumed here that departure from the planned orbit is too great for any small adjustment to be of much help. Then it is likely that sun-synchronism and a regular repeat cycle would be lost. The image scale, ground coverage, and ground resolution would depart from that designed, as would the sidelap between images.

These changes from design would have severe impact on image data processing. For efficient design, a high-production processing system requires that a relatively narrow range of parameters be assumed. This is true whether analog, digital, or hybrid processing schemes are being used. Digital-processing impact perhaps is not so obvious, but the special digital logic needed to obtain high production will constrain input geometry within narrow limits. The amount of high-speed memory provided for image-data shifting also will be only that needed for the planned orbit. Finally, any image printer producing a film output from a digital system will require special data modification to retain a uniform output scale or other pre-designed format, just as would the image printer used for any other method of processing.

The costs are very high to safeguard against improper orbit in the design of an image-data processing system. Past launch performances indicate that the risk of improper orbit insertion is quite small. If this is the case, it does not seem cost-effective to require the image-processing system to be designed for such an unlikely eventuality.

Incremental image sensors such as the Thematic Mapper and the HRPI collect image data as a function of time. If this time is a fixed pre-launch value, a bad orbit will cause along-track data gap or overlap. Only if the rotation rate of the Thematic Mapper or the integration and readout time of the HRPI can be adjusted by ground command

can the difficulty be corrected. A framing camera, collecting an entire image at once, has an advantage in this respect.

4.1.4 Ephemeris Accuracy

Some of the image positioning methods discussed in Section 2 require a very accurate value for the position of the EOS satellite in space at the time each image is being sensed. Since image positioning must be done in an earth-based coordinate system, satellite position must also be so defined. The usual positional reference is geodetic latitude, longitude, and altitude above the earth ellipsoid of reference. This information is provided by the satellite ephemeris, which is determined from tracking data. The ephemeris is frequently revised to incorporate the most recent tracking information. A best-fit ephemeris is determined for after-the-fact (past) satellite passes, and provides highest accuracy. A predictive ephemeris is used to extrapolate ahead in time with slightly lower accuracy.

Position uncertainty is caused primarily by lack of detailed knowledge about (1) the higher tesseral harmonics of the earth's gravity field, (2) air drag effects, and (3) tracking station location with respect to the earth's center of mass. Air drag effects are well in hand, and knowledge of the gravity field's fine structure is rapidly being augmented by reduction of data from many satellites. The center-of-mass distance also will be known more closely in the next few years. For the ERTS satellite, one sigma position uncertainty was estimated at 100 meters with the best-fit ephemeris. The along-track component is about 80 meters. For the 1976-78 time frame, a one-sigma estimate of 30-50 meters has been made by Cooley, reference (8), predicated upon improvements in knowledge of the three factors just listed. The lower figure is more likely to prevail over the United States, the higher outside tracking-station line of sight. One-sigma tracking station locational uncertainties with respect to mass center are expected to be considerably less than 10 meters. These estimates have proven to be somewhat conservative. ERTS-1 along-track ephemeris errors have been reported as 40 meters rms.

At least one-half the ephemeris uncertainty is estimated, reference (7), to be a systematic effect which will repeat for subsequent passes over the same subpoint vicinity. If this estimate is correct, repeatability uncertainty for EOS will be 20 to 30 meters, one sigma. Error as a function of time is said to take the form of a sine wave, with one cycle per orbit, reference (7). If this is the case, the positional ephemeris error over an arc of several thousand kilometers will change by only 5 to 10 meters.

Other opinions on accuracy differ somewhat from those cited above. Stansell, reference (5), states, "Today's [1971] geodesy permits determining a satellite orbit with an accuracy of 10-15 meters rms and predicting that orbit ... to an accuracy of 40 meters rms or

better." Stansell was writing about the U. S. Navy navigation satellites, whose typical altitudes and inclinations are similar to that planned for EOS.

Gaposchkin and Lambeck, reference (6), describe an extensive analysis which combined dynamic satellite analysis, simultaneous satellite photogrammetric triangulation, deep-space network tracking data (for relative longitude and distance from tracking stations to the earth's rotation axis), and surface gravity measurements. The combination solution provided a check with each of the individual data sources and showed generally good agreement. As a result, the geocentric positions of 15 stations are determined to 5-10 meters, one sigma, and the generalized geoid to 3-4 meters. Orbital residuals of 7-10 meters were obtained using a combination of laser and optical data.

Finally, a completely geometric solution of a global station network is nearing completion. This work, reference (11, 12), has used photogrammetric satellite triangulation [different observations from those described in reference (6)], combined with high-accuracy transcontinental baselines. One sigma position uncertainty for 45 stations is 4.5 meters, reference (10). When these results are combined with other data, even better results are expected, which will be of use in satellite orbit analysis.

A lower limit of 5 to 10 meters seems attainable for satellite positional uncertainty. The effort to achieve such accuracy and the time before it can be routinely obtained are not clear. Thus, the remainder of the analysis in this report has used Cooley's, reference (8), lower one-sigma repeatability error of 20 meters.

4.2 ATTITUDE DETERMINATION REQUIREMENTS

This section provides some additional details on the spacecraft attitude control system, inertial-attitude reference packages, and star sensors. The need for obtaining a more complete knowledge of EOS spacecraft attitude with time is stressed. Finally, in its admitted deficiencies and erroneous interpretations, the need again is emphasized for more communication and closer contact between the two areas of technology represented by the satellite-data and control-point methods of positioning images.

The section is divided into two parts, the actual attitude behavior of the spacecraft and the measurement of this attitude by auxiliary sensors.

4.2.1 Image Continuity Requirement

The EOS satellite must maintain a local-vertical or downward-looking attitude, at least during imaging. Yaw must be constrained to allow the Thematic Mapper and HRPI to scan normal to the orbital path. Any attitude corrections must be made slowly between the allowed

limits. These conditions are maintained by the attitude control system (ACS).

Attitude Error Amplitude

The baseline ACS is described in reference (1). Each of the three axes is allowed a bias of ±0.5 degree maximum, plus 0.2 degree rms about the bias. This implies maximum errors of 1.1 degree in any axis, with rms values of 0.7 degree. These limits appear to be adequate. No potential users are known who require closer tolerances than these for data collection. Even larger pitch and roll errors may be permissible. If lower attitude errors would prove of benefit, the greatest improvement with the least effort can be made by measuring and removing the 0.5-degree attitude biases. The high-accuracy attitude measurement technique to be used for image positioning (either stellar sensor or GCP) provides this information. By suitable ACS design, the measured biases could then be removed from the ACS using ground commands.

There are some opposing arguments concerning the allowable yaw error. On the one hand, the image displacements caused by yaw are at most only one-tenth those of either pitch or roll for the same angles, so it would seem less important to control yaw as tightly as the other two angles. On the other hand, a digital geometric correction of image data for yaw is troublesome for high-speed processing, since it entails more than the simple data translation which is needed for pitch or roll adjustment. It would be desirable to eliminate this adjustment, or at least reduce it as much as possible. Still, extensive geometric processing will be needed even with zero yaw correction, to adjust for scale change, map projection, internal sensor geometry, and earth-rotation effects. Finally, a conical-scan Thematic Mapper is somewhat sensitive to yaw angle in terms of continuous scan coverage. The optimum yaw angle differs with latitude (Appendix A); this adjustment could possibly be incorporated into the ACS. Adjustment precision of a few tenths of a degree would be adequate. To enforce such an adjustment might mean a tighter control for yaw than for pitch or roll.

In summary, the baseline yaw variation of ±0.2 degree rms is not obviously too large or too small for the imaging and processing requirements. In the absence of more critical considerations, it is recommended that the baseline control limits be retained.

A horizon sensor will collect the basic information used to control attitude. This sensor may be more precise than that used for the ERTS ACS. Telemetered horizon-sensor and torquer data will be used to develop approximate attitude values from ground processing. The after-the-fact attitude determined in this way is expected to be accurate to 0.1 degree rms in each axis. Some other high-accuracy attitude measurement obviously will be needed to suitably accurate image positioning.

It is possible that higher attitude accuracy may be obtainable from the telemetered ACS data by removing the earth-ellipticity horizon effects. These effects are believed to be responsible for much of the attitude error. One-sigma errors of 0.005 to 0.02 degree are thought to be feasible (20), using advanced horizon sensors and extensive ground data processing. More definitive information is needed, but there appears to be a potential for using ACS data as backup for a higher-accuracy independent attitude measurement system such as SIMS. For GCP positioning, such a capability would be of some limited usefulness in establishing initial absolute image locations. This would be of benefit when analyzing images from those areas of the world without suitable maps or other data from which to select GCP.

Attitude Error Rate and Acceleration

The baseline ACS specification defines dynamic attitude behavior with a single parameter of 0.05 degree per second maximum rate of change in any axis. This figure was chosen primarily to ensure that minimal overlap or underlap (less than one-fourth IFOV) between scan swaths would occur with the Thematic Mapper. There may be ACS designs with which improved positional accuracy for images could be attained by increasing the maximum allowable rate. If so, it is important to know exactly what rates are associated with what amount of over- or underlap. This relationship is summarized in Figure 4-2. The EOS altitude of 980 km has been assumed. Then the allowable rate depends only upon (1) the number of scan lines in a single scan swath, and (2) the fraction of a single IFOV allowed for overlap or underlap. As the figure shows, the present maximum rate is well within the limitations of six scan lines per swath and one-fourth IFOV lap.

ACS accelerations are not specified for EOS, and are of no concern for image continuity. However, in reference (23) a maximum value of 0.0114 degree/sec^2 is assumed. Acceleration durations are very short since the reaction wheels are acted upon by impulsive torques. Thus, the acceleration behavior over several seconds still is not specified.

The horizon-sensor/reaction-wheel ACS is basically of the type used for ERTS, with two main exceptions. The maximum attitude rate has been reduced by a factor of ten from ERTS. Three-axis gyros will be used for EOS, unlike the single gyro used with ERTS for roll/yaw conversion. Maximum accelerations are specified based on the maximum correcting torque applied to the inertia reaction wheels. When one of the wheels has reached maximum angular velocity, it is "unloaded" with a cold-gas impulse to nearly zero angular velocity. Based on experience gained from previous operational satellites, the frequency of wheel unloading will be very low, perhaps once every few days. During the brief time required for wheel unloading, the attitude rates are much greater than the operational maximum given above. Any EOS image data obtained during this time will not be usable, and it will be very difficult to

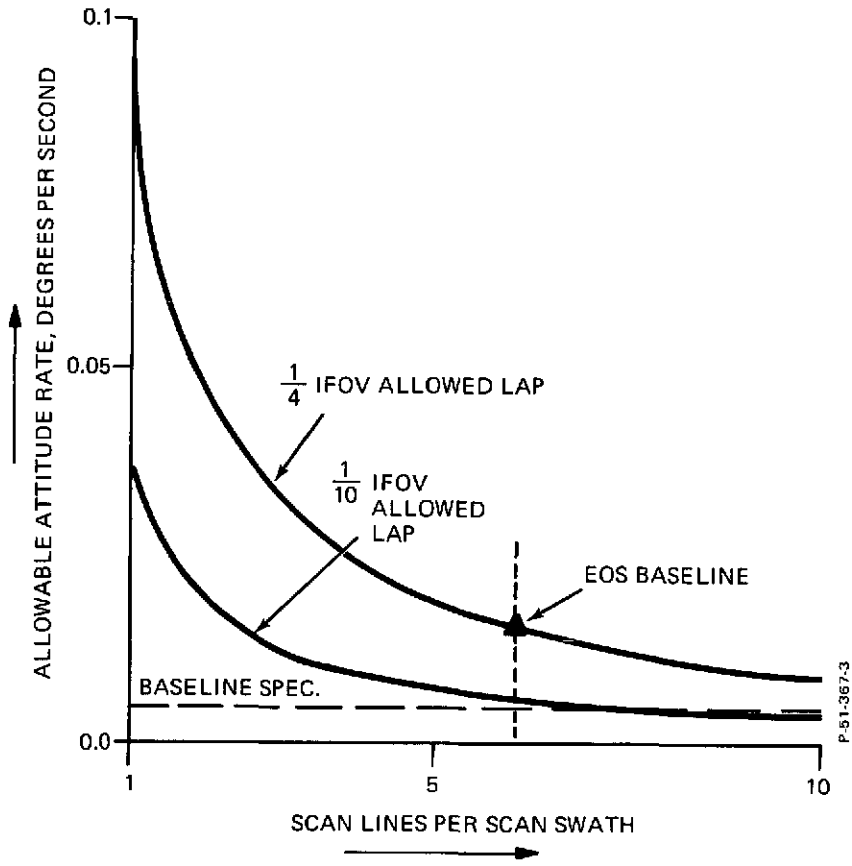

Figure 4-2 - Maximum Attitude Rate for Imager Considerations

accurately position the individual image frame collected over the 30 seconds during which unloading occurs. As a consequence, it is quite desirable that unloading not occur during imaging.

4.2.2 Image-Positioning Attitude Requirements

The influences of the ACS on image continuity are widely recognized and, as seen from Section 4.2.1, have been adequately addressed by the EOS specifications (1). Unfortunately, the influences of the ACS on image positioning methods apparently have not been recognized; this subject is ignored in the specifications. ACS design directly delimits the positioning methods which can be used for EOS images. This is an inescapable consequence of any orbital mission which uses any imagers other than high-speed frame cameras. It is particularly important when the image is acquired rather slowly, as is the case with the EOS line scanners which build up the image format over tens of seconds.

No single set of ACS requirements can be given for image positioning, unless only a single positioning method is being considered.

Such is not the case here. As a consequence, the costs, development time, and success probability of the ACS design become an integral part of the decision to be made on image positioning method. Several examples will quickly illustrate this fact.

Consider first an ACS design which makes no allowance for image positioning method, using only the requirements for image continuity developed in Section 4.2.1. Any of several designs will do for this case. Without any further conditions to be met, image positioning immediately requires addition of an independent gyro package for independent attitude angle measurement, and telemetry of the attitude values frequently enough to supply attitude changes of 0.001 degree in pitch and roll. (Yaw can be relaxed, if necessary, to several times this amount of change.) For the present study, such an ACS design would immediately eliminate method GCP-E from consideration. The only methods which could be expected to satisfy such conditions are SIMS-E, SIMS-EG, and GIMS-E-1.

Next, consider the opposite extreme, a high-accuracy ACS. This possibility has been discussed in Section 7.7.1 of reference (1). Essentially, this control system would be operated by closing the loop between a SIMS package and the control reaction wheels. There are several factors which argue against this scheme.* Disregarding these for the moment, such an ACS concept would leave very little to be done by either an auxiliary-sensor method or a GCP method. With attitude errors always 0.001 degree or less per axis, independent attitude measurement and telemetry would be needed on the spacecraft. An initial bias removal of attitude-transfer errors after launch would be needed, repeated occasionally during the operational life of the satellite. One image with only two GCP would theoretically suffice for this task (in practice, several more GCP probably would be used). The largest positioning error then would be caused by the ephemeris data. The systematic component of this error can be removed by positioning a single image with GCP on each pass. These minimal techniques do not correspond exactly to any of the 5 methods considered in this study, although the instrumentation includes some of the same components.

---

*The most significant probably is that users of EOS images do not need such absolute angular accuracy during data collection. Another reason is the inadequate accuracy, as given in reference (1): 175 meters is quoted,which is completely inadequate for temporal registration of images with 20-meter and 44-meter resolution elements. The onboard computer required to convert inertial to local-vertical attitudes is another difficulty with the concept in reliability, weight, and power requirements. The ephemeris developed by or transmitted to this computer from the ground would of necessity be a predictive ephemeris for real-time attitude control, with consequent lower accuracy than the best-fit ephemeris gives for after-the-fact determinations.

Between these extremes are a number of opportunities for ACS design which, considered along with the possible image-positioning methods, may well include the most cost-effective route for EOS. For all of these intermediates, the absolute attitude error amplitudes and rates are of no concern, in themselves. The behavior of interest is given by the time interval over which a straight line or second-order curve can be best fit in a least-squares sense to the attitude errors in each axis, with an rms error in the range 0.0005 to 0.001 degree per axis. The time intervals of interest range from 30 seconds to several hours. Obviously, the character of the error is important in this specification. Random errors of relatively high frequency can be removed with an independent gyro package used to measure short-term attitude errors. In this way, the achievable best-fit time intervals may be appreciably lengthened. However, the gyro package may be incorporated directly into the control loop of the ACS, in which case it no longer is an optional positioning-method component. As a consequence, it is recommended that the inclusion or non-inclusion of a gyro package, and whether it is a part of or independent from the ACS control loop, be left to the ACS design group. For the different image positioning methods, the time intervals and line-fittings of interest are as follows:

(1) 30 seconds, second-order (without gyro package)

(2) 30 seconds, first-order (with and without gyro package)

(3) 5 minutes, first-order (with and without gyro package)

(4) 5 minutes, second-order (with and without gyro package)

(5) 10 minutes, first-order (with and without gyro package)

(6) 100 minutes, first-order or second-order (with or without gyro package)

(7) Several hours, first-order or second-order (with or without gyro package)

There is probably little difficulty in an attitude system design which, with an independent gyro package, could meet the specified rms error requirements over 10 minutes. However, it is important in selecting positioning methods to know whether the same requirements can be met without the package, and what the costs would be. The intervals given are associated with angle updates once for each image, once for each landmass, and once for each orbital pass.

In summary, the image-positioning attitude requirements for EOS differ from the image-continuity requirements in being concerned with smoothness of angular changes, rather than rates or amplitudes of attitude angles. No single set of requirements can be made for the ACS; requirements should properly be based upon system considerations which include image positioning methods as well.

4.2.3 Accurate Attitude Measurement by Auxiliary Sensors

Present plans call for accurate measurement (0.001 to 0.003 degree) of EOS attitude to be performed by a technique which is independent of the attitude control system, reference (1). Continuous and highly accurate knowledge of attitude behavior is needed to properly position the line-scanning HRPI and Thematic Mapper image daga. It is possible that the ACS design could be such that quite smooth attitude behavior could be assumed. In this case, as mentioned previously, accurate measurement need be made only infrequently. In the following discussion, however, it is assumed that continuous high-accurate attitude measurement is needed. Gyros on the satellite would provide this data. The information is not truly continuous, but the sampling and telemetry interval can be made adequately small compared to the spacecraft attitude response. For EOS, the 0.1-second interval presently being considered is more than adequate.

Gyros must be updated occasionally to correct for drift. The frequency at which this update is required depends on the specific gyro design and the configuration. References (23), (24), and (25) give extensive consideration to gyro selection and configuration. This information would have been of greater value in the present study if (1) it had been available earlier in the program, and (2) the work described had not been optimized specifically for the SIMS technique. The gyros finally selected in reference (25) have performance matched to the update-frequency capability of the star-sensor.

Stellar-sensor and GCP methods are both candidates for use in attitude update. The following comments apply to the star-sensor method. GCP considerations are contained in Section 4.3.

Transformation of inertial attitudes to a local-vertical/velocity-vector reference requires detailed knowledge of the earth's orientation in inertial space and the location of the satellite with respect to the earth ellipsoid of reference. Small errors in the former reference frame result from polar motion and other effects. The errors in the latter stem from ephemeris errors, discussed in the previous section, and in accurately measuring the time of the stellar observations. Ephemeris errors will likely be the most significant. Their effect in positioning will be to replace the translational ephemeris errors by equivalent attitude errors. Additional care and complexity are required for the stellar-reference computations in defining the final image location in the geodetic coordinates used for geographic point positioning, instead of the geocentric or reduced coordinates normally used with satellite operations. The GCP method requires no such care on this account; the observations used for positioning are supplied in geodetic coordinates.

Some additional cautions in transforming from inertial to geodetic coordanates have been voiced by Schmid, reference (31), in connection with a photogrammetric triangulation using stellar control.

He found bias errors in his work which he ascribed to (1) lack of a rigorous connection between elevation and the reference ellipsoid which serves as the computational system for latitude-longitude determination, and (2) the fact that the latitude-longitude and right ascension-declination systems are related only insofar as the primary axes of the two systems are parallel to each other. Schmid removed the bias by allowing an additional spatial rotation in his baseline orientation.

Some estimates of stellar sensor costs, weights, and power requirements are given in reference (25). Power needs are very low; weights range from 3 to 16 kg depending on whether the sensor is a star mapper or star tracker. Page 6-29 of reference (25) comments on reliability: "None of the SIMS candidates has reached the development status that will support a comprehensive, quantitative assessment of reliability."

The need for an accurate attitude-transfer device in connection with an auxiliary attitude sensor has been commented on in Section 3.4.1. Such a measurement is needed to relate attitude data obtained by sensors which are independent of the image sensor. The reliability, power, weight, and telemetry requirements for such a device (or devices) probably could be designed to be quite satisfactory, but no detailed thought appears to have been given to such design.

4.3 GROUND CONTROL POINTS

4.3.1 Background

One basic method of positioning images with respect to the earth's surface is through the use of ground control points (GCP). The terms landmark points or geometric ground-truth points also are sometimes used for GCP. Such points are selected well-defined image details for which the earth positions are known. Positioning an image with GCP typically requires that several GCP be identified and measured on the image. The measured image locations and known ground positions of these points determine the geometric relationship of the entire image with respect to the earth's surface. For the procedure to be effective without requiring excessive GCP, internal sensor geometry must be well-defined.

GCP have been used for years in photogrammetric mapping using aerial photographs, where the method is almost universally applied. (Photogrammetric methods are used for virtually all original map compilation performed today.) The GCP used for this purpose typically must be specially surveyed to achieve the high accuracies required.

The mathematical GCP positioning process for a single photograph is called spatial resection, analogous to surveying resection on the earth's surface. The unique position and attitude of the aerial camera is determined as six orientation elements: three positional coordinates and three rotations. No auxiliary data from any other sensors

in the aircraft normally are used to determine these quantities, only the GCP.

Two separate equations can be written for each control point, one for the measured x and one for the y image coordinate of the point. The six unknown orientation elements appear in the same equations, along with the three positional coordinates of the control-point on the earth. Thus, three GCP with their six equations are adequate to solve for the six unknown orientation elements. Best accuracy is obtained if the points are well distributed throughout the photo; the solution is indeterminate if the GCP lie on a straight line. With the six orientation elements known, the ground-plane positions of all other photo images also are known. (If height differences in the photographed scene are a significant fraction of camera altitude, a two-photo technique is used, in which the intersection of conjugate image rays uniquely defines the ground position in all three coordinates. For satellite images from narrow-angle, downward-looking sensors, relief effects are small and potentially repeatable.)

In adapting the use of GCP from aerial photographs to the ERTS satellite images, some differences were noted. First, GCP accuracy for image positioning need not be nearly so high as that needed for conventional mapping. As a result, it usually is possible to select GCP from existing maps and other available sources without special field survey work. A second difference is in the large number of GCP potentially available for use, with the result that extra GCP can be used in the spatial resection. There are several advantages in using redundant data; these will be discussed later. A third difference is in the use of electronic image correlation to match GCP against a master image. Other implementation changes from usual mapping practice were incorporated. Finally, some form of auxiliary attitude-change information was recognized as desirable for positioning the ERTS MSS (scanner) images acquired. All of these differences apply to EOS as well.

The great advantage of ground control points for positioning is the elimination or great reduction in the reliance that must be placed on externally derived location and attitude data. In addition to the resulting economy and reliability increases that follow, the use of GCP usually results in higher positioning accuracy than can be attained using auxiliary data. As image resolution increases, the positioning accuracy typically increases accordingly.

Use of GCP has disadvantages. The major one is in implementation in what otherwise may be a more or less completely automatic processing scheme. For high-production programs with many images to be processed, implementation must be given careful consideration. Equipment must be selected to assist a trained specialist in GCP selection and accurate measurement, in as efficient a way as possible. However, although equipment and procedures are important, proper personnel are vital. Control-point selection requires a high degree of self-motivation

and job satisfaction, akin to mapping and some kinds of photo interpretation. It is not difficult to find people with these characteristics, provided the right kind of people are sought.

The main difficulty with GCP is in identification. In aerial photogrammetric practice, misidentification is the greatest problem associated with GCP. Work with space images cannot be expected to be immune from the same difficulty. The use of well-trained responsible personnel is the most effective way of minimizing the problem, but technology can be of considerably assistance as well; once the initial GCP selection has been made, automatic image correlation methods can be used to perform subsequent matching operations. Using extra GCP also helps greatly in detecting misidentified GCP. Initial results with ERTS-1 images indicate that these techniques work very well in reducing the incidence and effects of misidentified GCP.

4.3.2 Accuracy

The accuracy of positioning with spatial resection depends upon five main factors:

(1) Ground coordinate accuracy

(2) Pointing precision

(3) Image adjacency effects

(4) Internal sensor geometry

(5) Effective redundancy

The equipment errors associated with measuring image-detail location and producing the image to be measured are not treated here, since they concern implementation, not basic limitations. The other five factors are discussed in the following paragraphs.

Ground Coordinate Accuracy

Absolute and relative accuracy are important distinctions here. Absolute positional accuracy of the coordinates is defined with respect to the earth ellipsoid of reference. Elevation normally is taken as distance above sea level, although this differs from the reference ellipsoid by the separation between geoid and ellipsoid. Relative accuracy means that introduction of some bias into the absolute coordinates is permissible; repeatability is the important thing.

U. S. National Map Accuracy Standards require that the absolute positional accuracy of well-defined map features be within certain limits. These limits are equivalent to 0.3 mm rms at map scale. GCP for EOS should be selected from the standard U. S. map scales of 1/24,000, 1/50,000 (Alaska only), and 1/62,500. Additional high-accuracy positional information is available on highway structures and airfield runways. Some of the regular survey points in the second- and third-order

geodetic networks of the country lie at or are sufficiently close to features which can be identified on satellite images. In general, control-point accuracy need not be a problem, at least for positioning images in the U. S. or other nations with adequate surveying and cartographic activity. If smaller-scale maps are used for control-point selection, inaccuracies in the plotted map positions may significantly affect the final absolute position accuracy. But for many applications absolute position accuracy is less important than the repeatability needed for temporal registration. If the same GCP are used to position subsequent images of the same earth scene, the ground position errors will affect all images alike and good temporal registration will be achieved. Of course, it may not always be possible to use exactly the same GCP every time, because of cloud cover and seasonal changes. In this case, only that part of the ground coordinate error which is common to all GCP in the area can be ignored. One way of overcoming this problem and ensuring repeatability is some form of control intensification. The best available GCP are used to position the first image obtained of an earth scene. Auxiliary GCP then can be selected from this image to use in positioning subsequent images. Absolute accuracy will be no better than -- in fact, not quite as good as -- that of the first image, but temporal registration will be excellent.

Pointing Precision

When measuring the image location of a GCP, some form of measuring mark or cursor must be placed directly over the image detail which is to be used as the control point. This mark placement is called pointing.

Two kinds of pointing can be considered. The first is called descriptive pointing here, and occurs when a GCP is originally selected. Usually some written or graphic description of the GCP references the pointing operation. Pointing is done manually in this case, using optimum image illumination and magnification, together with the measuring mark of best shape and size. If the same GCP is used again on later images of the same earth scene, descriptive pointing may be repeated in the same way used initially. If possible, however, it is more efficient, reliable, and usually more accurate to use the second kind of pointing, called here image matching or correlative pointing. This is done by binocularly comparing two images. One is the new image in which the GCP is to be pointed; the other is a master image on which the GCP has previously been precisely located using descriptive pointing. Special optical devices may be needed for the image matching process to allow one or both of the images being viewed to be rotated and scaled so as to permit binocular superimposition. Image matching can be done automatically as well, using digital or analog image correlation techniques and appropriate equipment. The accuracies and times required to carry out pointing with such methods vary widely, depending on many factors.

The ability to precisely point at the correct image detail is affected by image quality, the type of mark used, and the ability to make fine adjustments to the mark. The latter two matters are considerations in equipment design and need not concern us here. Image quality is important. Several investigators, references (15, 14), have tried to quantize what is intuitively obvious: the higher the image quality the more precisely can one point to a selected image detail. In general, it is possible to center a measuring mark on a symmetric target within one to five percent of the target size. This ability depends upon the type, size, and contrast of the measuring mark and target, as well as such other factors as illumination and granularity in the displayed image.

From a limited amount of experience with ERTS images and photos from the Apollo 9 S065 experiment, it appears that when GCP are used which are asymmetric and poorly defined in the image, pointing error may be the principal factor in overall positioning error. As examples of this hypothesis the center of a nearly circular lake is better as a GCP than a peninsula extending into the lake; the center of a small regularly shaped island in the lake is still better. Similarly, the X intersection of two roads is better for pointing than a bend or corner in a road pattern. A Y intersection of two streams is a better GCP than a loop in a stream. Additional work is needed to confirm or refute this hypothesis, as well as on several other aspects of pointing to satellite images displayed in raster form.

The precision of descriptive pointing does not appear to have been explored for raster images. Thus, it is difficult to develop the errors associated with this process. The matter is further complicated by the quality of the ERTS-1 images, which has exceeded all prelaunch estimates. An extremely limited amount of data obtained from the ERTS MSS images indicates a standard deviation in pointing precision of about 20 m, or about one-fourth the IFOV. The Thematic Mapper then should give a precision of 11 m, and the HRPI 5 m. In light of the uncertainty in this value, a range of 10-20 m will be assumed here for the EOS precision.

Image Adjacency Effects

Some images are created using processes and materials which alter the position of a light-dark edge; photographic film is an example of a medium which exhibits these undesirable adjacency effects, reference (16). When it is necessary to measure GCP from such a displayed image, control points should be selected with special preference for symmetrical details, or at least details with low density difference from their background, in order to minimize the metric effects of edge migrations.

Internal Sensor Geometry

Spatial resection uses some mathematical model to represent the internal geometry of the image sensor. To a greater or lesser extent, this model errs in its representation, and so introduces image-location errors. For GCP, these errors adversely affect resection accuracy, resulting in positional inaccuracies for the image as a whole. Any image detail not used as a GCP also has an additional error associated with the internal sensor geometry error at that particular point.

For line scanners, the motion of the scanner platform provides the second dimension of the two-dimensional scanner image. To this extent, the description of the platform position and attitude as functions of time can be considered as vital parts of the scanner-image internal geometry. For a scanner on an orbiting satellite the platform-position changes can be modeled quite accurately as functions of time over arcs of hundreds of kilometers. For attitude behavior of the satellite, three courses are open: control the attitude precisely and continuously with respect to the local vertical so that modeling is extremely simple and needs no spacecraft data; design the spacecraft attitude control system such that attitude changes are suitably slow and regular as functions of time; or use telemetered changes in attitude over the imaging arc as auxiliary data in the spatial resection. These alternatives were discussed in Section 4.2. For any of these methods, the limitations on scanner internal geometry are those placed by the magnitudes of high-frequency attitude changes, for which no information is obtainable. The second alternative is particularly attractive. If the spacecraft control response to a disturbing torque is such that attitudes can change only slowly over the imaging arc, first- or second-degree attitude changes can be carried as additional spatial resection unknowns. A few more GCP then provide adequate observational data to determine these unknowns. This attitude control method results in the same virtue of the first method above: no need for auxiliary spacecraft data.

Effective Redundancy

If more than the minimum number of GCP are used in a spatial resection, a least-squares solution is used to determine the unknown orientation elements. By reducing the random effects of the four error causes discussed above, positioning accuracy of the image as a whole is statistically improved in accordance with the number of GCP and their locations within the image. The use of redundant control points has several operational advantages in addition to overall accuracy improvement. First, self-checking: the least-squares solution gives several accuracy indicators. These result from the residuals. (A residual is the distance of each measured GCP location from the best-fitting math-model location, as determined by the least-squares solution.) The residual for a single control point provides an accuracy indicator for that point, particularly useful in detecting misidentified GCP. Also, standard deviation of all residuals can be used as an overall

positioning quality indicator for each individual image. This is useful as a single-number value index. Residuals also are helpful in long-range analyses of operator ability, equipment performance, and sensor calibration, to name some additional applications.

The GCP's used for satellite images are not specially surveyed points, but selected map points. Thus the cost per point is very low, making redundancy more attractive than is the case for normal aerial photomapping. For maximum benefit, the GCP should be selected in particular image areas. In general, the best image areas are those which (a) allow uniform GCP distribution within the image, and (b) are located in image areas of greatest sensitivity to orientation-element errors. In general, greatest sensitivity is found at the corners and edges of the images, where yaw and altitude changes have their maximum effects. If the GCP placement does not cover a large portion of the image, positioning accuracy will be lost.

A mathematical analysis can be performed to show the redundancy advantage for any number and distribution of GCP. Such an analysis was done for the RBV (17) and MSS (18) ERTS images, based upon earlier work carried out during the ERTS Phase B/C study, reference (19). Figure 4-3, taken from reference (19), shows the decrease in relative positioning error associated with the placement of GCP in the image and the number of GCP used.

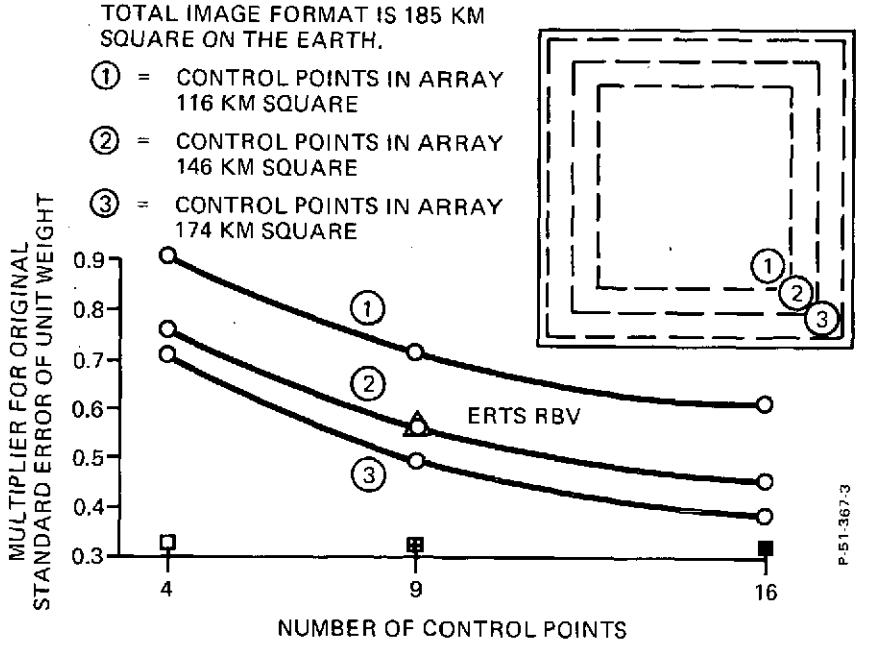

Figure 4-3 - Example of Decrease in Positioning Error with Increasing Image Coverage and Numbers of GCP, Taken from Reference (19)

Additional analysis along these lines was carried out during the present study. Of interest was the effect of an increase in the number of unknown attitude parameters on the accuracy of the spatial resection. The method is described in reference (19). Several different GCP configurations were considered in the analysis, which neglected some minor effects. The results are summarized in Table 4-2. Maximum array size used for the GCP was 146 km square (Case 2 in Figure 4-3). The table shows that a requirement to determine mean attitude angles, rates, and accelerations with GCP need not degrade results significantly from a determination of angles and rates alone. The number in the body of the table represents a multiplier to be applied to the standard error of unit weight for a single GCP image point. The multiplied value becomes the rms positioning error as a result of the spatial resection. The values range from about 0.35 for an angle-only solution, (three unknowns) to about 0.60 when angles, mean rates, and mean accelerations (nine unknowns) must be found. The results of the analysis accrue to the advantage of method GCP-E, and place in sharper focus the need for an ACS with predictably smooth behavior characteristics.

4.3.3 Applications

The GCP positioning method can be adapted for many different applications. Some of the applications discussed in this section are common in aerial photogrammetric practice. Others are of interest primarily to multi-sensor satellite programs.

Perhaps the most obvious application of the GCP method might appear to be as an independent check on attitude (determined from other spacecraft sensors) and position (taken from the spacecraft ephemeris, itself determined by tracking the satellite). This is not necessarily a valid application. In general, the wider the image-sensor field of view, the better determined are the six orientation elements. For downward-looking narrow-angle images, such as the ERTS RBV and MSS, it is not possible to isolate the effects of pitch from along-track translation. The effects of a change in either orientation element on the image are virtually identical. The same is true of roll and across-track translation. Such a lack of determinacy does not affect the accuracy with which images can be positioned with respect to the earth, only the accuracy in isolating the two parameter pairs which are highly correlated.

The correlation between orientation elements can be used to some advantage for EOS images, as is being done for the ERTS program. The satellite ephemeris gives along-track and across-track position to within 100 m rms for the ERTS-1 satellite. By considering the ephemeris along-track and across-track values to be errorless, the spatial resection computation can use two fewer unknowns. In this way the degrees of freedom are increased for a given GCP redundancy, resulting in a formal improvement in the statistical positioning quality. The small errors that are actually present in the ephemeris positions are

Table 4-2 - Relative Position Error After Thematic-Mapper Spatial Resection, Using Different Error Models

Number of Unknowns	GCP Configuration					
			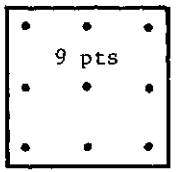	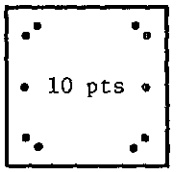		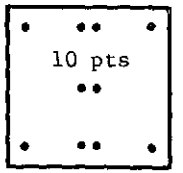
3, Angles only	0.41	0.42	0.41	0.38	0.36	0.38
6, Angles and Mean Rates	0.53	0.59	0.58	0.49	0.50	0.61
9, Angles, Mean Rates, and Mean Accelerations	*	0.60	0.58	*	0.51	0.61

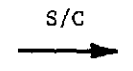

(1.00 = Standard Error of Unit Weight for a Single GCP Observation)

*Insufficient data using this configuration.

P-51-367-3

compensated almost perfectly in the solution by slight increments in the computed pitch and roll angles. The maximum error, dS, introduced by this approximation occurs in the image corners of a framing sensor or along the edges of a scanner. For a downward-looking framing imager, dS is given by the usual photogrammetric differential, references (21, 22):

$$dS = \frac{S^2}{H} d\theta = \frac{S^2}{H^2} dE$$

where

S = maximum ground-distance from the nadir which appears in the image, ≈ 130 km for EOS

H = spacecraft altitude, ≈ 1,000 km for EOS

$d\theta$ = angle increment to correct for ephemeris error

dE = position error from ephemeris, ≈ 20 m rms for EOS

so that dS is much less than one meter rms. Even a 200 m ephemeris error would be acceptable, giving a maximum error of 3 meters.

As the image sensor is tilted farther away from the nadir, the correlation between the angular and translational orientation elements decreases in the direction of tilt. Even for an image rolled 30 degrees off the vertical, the ERTS resection technique -- carrying ephemeris position fixed in the solution -- can be used for offset-pointed EOS sensors as well.

The high correlation just discussed between angular and positional errors is an example of an important characteristic of GCP positioning: the composite nature of the results. Any error component which has the same image displacement effect as an angular or positional orientation element will be removed as a part of that orientation element. For example, the yaw of the image sensor may be determined with high accuracy, but without further information it is not possible to separate the component caused by spacecraft yaw from that caused by yaw misalignment between the image sensor and the spacecraft yaw axis. Similarly, changes in spacecraft altitude, camera focal length, film dimensions, or voltage in the image-sensor power supply all may have the same net effect in the image: a simple scale change. This compositing effect has both advantages and disadvantages. On the one hand, it automatically reduces the number of unknowns to only those necessary and sufficient to position the image on the earth's surface. On the other, it requires some care when attempting to use GCP to isolate a particular error component. Nevertheless GCP are very useful in several special applications of concern for EOS operations. Four of these are discussed here.

Detailed Sensor Geometry

Assume that more than the minimum number of GCP are used in a spatial resection. The image-coordinate residuals after the resection represent geometric errors which could not be compensated by the spatial resection unknowns. Part of each residual is random, associated with errors in pointing, ground-coordinate measurement, and some kinds of internal sensor geometry. The other component is systematic, typically resulting from uncompensated sensor behavior. It is this systematic component which shows the extent to which the mathematical model being used for the imaging geometry is deficient. If the random components can be detected and removed from the residuals, the systematic components remaining will show how the imaging geometry model should be modified. Incorporating these changes will improve the accuracy of all subsequent spatial resections for that image sensor, providing the systematic errors do not change.

The random effects of the GCP residuals are removed by making an error anlysis which sums the effects of a great many residuals. The random components (with the normal-distribution zero-mean conditions which usually prevail) tend to cancel, and the systematic components reinforce one another. Residuals may be accumulated from only one or a few resections, each with many redundant GCP, or from the results of many resections, each with only slight redundancy.

Examples of typical image-geometry errors detected in this way include lens distortion effects in cameras and sweep-angle nonlinearity in scanners. Sometimes the systematic errors are in the image processing equipment, not the original sensor, and the corrections may take the form of polynomial functions of the x and y image coordinates. Analysis of residuals can be done graphically or computationally. If computational, some a priori model usually is assumed for the error form, although this may be revised in the course of the analysis.

Analysis of GCP residuals is a very powerful technique, and can be expected to see much use in satellite image analysis. This application is particularly useful for checking on slow changes in sensor geometry, such as can be expected from the MSS scanner on the ERTS satellites.

Alignment of Two Image Sensors

This application has already been used operationally with the ERTS-1 RBV three-camera array to precisely measure the angular alignment of the cameras. Such alignment accuracy was needed to produce event-registered multi-spectral color composite images. For this application, true GCP are not needed, only conjugate image details which are sharply defined on both images being aligned. The measured locations from one image serve as "ground coordinates," and a modified spatial resection provides the alignment of the second image sensor with respect

to the first. For the ERTS application, the "red" RBV camera was the reference to which the other two were aligned.

This application of GCP positioning can give very accurate results, since a great many common points -- 20 or more -- can be easily located and used in the resection, and very small and sharp micro-details can be selected which do not appear on any map.

Alignment Between Image Sensor and Auxiliary Attitude Sensor

This application of GCP is useful for several different programs. A few examples are:

- Determination of initial alignment angles after launch
- Measurement of changing alignment angles caused by spacecraft flexure or attitude-sensor drift
- Performance check on autocollimator or other device used to enforce the attitude-transfer requirement
- Removal of initial bias component in gyros used as inertial measurement devices.

For this kind of application the positional ephemeris error acts as an error in the procedure. This is once again a consequence of the high correlation between the pitch/along-track and roll/across-track orientation elements. The angular error, $d\theta$, as a result of ephemeris error, dE, is simply $d\theta = dE/H$, where H is spacecraft altitude. With position fixed at ephemeris values, the error from a single spatial resection cannot be less than $d\theta$. For the EOS ephemeris, $d\theta$ will be about 20 m/1,000 km rms, or about 0.001 degree. Interestingly, the spatial resection does not give the true local-vertical attitude with this precision, but an attitude which is locally repeatable from the bias errors in the ephemeris. The effective error in measuring angular alignment can be reduced further by performing several spatial resections, selecting the locations in such a way that the ephemeris errors can be taken as truly random. This may require some care, since it was seen in Section 4.1.4 that ephemeris errors have an associated periodicity.

Update of Gyro Drifts

This application is sufficiently important that it forms the basis for one of the positioning methods being investigated in this study. GCP can be used for this purpose. Problems can occur if it is necessary to update the gyro data at some regular time interval. Clouds and irregular land-mass distribution prevent any guarantee of control-point acquisition at a desired interval. Also, the method loses much of its attraction if it is necessary to perform a GCP update simply to provide smoothing-data continuity. To be of most benefit, an update

should be necessary only when in the vicinity of a series of images for which positioning is desired.

There are two cases where GCP may be advantageous for providing gyro updates. The first would result from selection of gyros with very low drifts. If a regular update is required only once every several orbital passes, or only once per day, GCP could dependably provide the data at very low system cost. In assessing the gyro potential, the work on gyro selection in references (24) and (25) would have been more valuable to the present study had it not been so closely connected with the SIMS concept, as mentioned in Section 4.2. Of considerably more interest here is the selection of a gyro which requires the least frequent update, even at some greater penalty in cost or weight.

The second case applies if it is necessary to use GCP gyro updates only for those passes in which image data is to be positioned. Methods GIMS-E-2 and GIMS-E-3 in Section 2 are based on this situation. One image may be positioned with GCP in the center of an imaging sequence; the updated gyros at that point then would supply attitude data in both directions along the arc. If extrapolation of attitude data in this way is not possible, it may be feasible to use two sets of update GCP at the ends of an image sequence, interpolating attitude data between the resected end images. This interpolative scheme is outlined in Section 6.2 of reference (25) as feasible for one particular gyro selection.

Any of the implementations discussed here has the virtue of greatly reducing the number of GCP required to position EOS images, for a given required accuracy. This is important, since the biggest difficulty foreseen in applying a GCP-positioning method to EOS is in implementation of the great number of descriptive and correlative points required. However, more work is needed to properly assess the potential for this application of GCP to positioning EOS images. In reference (25), the potential advantages of the GIMS-E method "landmark-inertial" method were recognized. But the existence of a considerably body of knowledge based on "landmark" techniques is not recognized. This shows once again the need for close contact between "landmark" and "inertial" disciplines.

SECTION 5

ANALYSIS OF POSITIONING METHODS

Section 5.1 provides an error analysis for each of the five positioning methods defined in Section 2. The information developed in previous sections was drawn upon for the numerical values attached to each error contribution. Section 5.2 develops the significant points of difference for the methods, and identifies the area in which further work is needed to give a clear choice.

5.1 ERROR ANALYSIS

In all the analyses which follow, several simplifying assumptions have been made. The accuracy indicator of concern has been defined as the rms positional error in the Thematic Mapper image which is not repeatable from one pass to the next. Errors introduced by film printers or other data processing equipment have been ignored, as have the effects of computational simplification and round-off. Mechanical errors such as reference-mark mismatch also have been ignored for all methods. Components for which no data are available have been estimated; where uncertainty exists, an effort was made to be liberal for satellite-data accuracy and conservative for GCP accuracy.

Once again, a cautionary note: the values below do <u>not</u> represent the entire error budgets.

5.1.1 Method SIMS-E

The component error contributions for method SIMS-E are shown in Table 5-1. This completely satellite-data method uses ephemeris data for position, a gyro package for short-term attitude behavior,

Table 5-1 - RMS Positional Errors, Method SIMS-E

SIMS Attitude Determination: 0.001° each axis, or 17 m $\sqrt{2}$	24 m
Attitude Transfer, Gyro Package to Imager: 0.00028° to 0.00056° each axis	7 - 24 m
Ephemeris Repeatability:	20 m
Internal Sensor Errors: 0.25 to 0.5 IFOV	11 - 22 m
Root Sum Square Error	34 - 41 m

and a star sensor to be used occasionally to correct gyro drifts. The error contributions show that there is no particular pacing error; to that extent the system is well-balanced. The attitude-transfer estimates assumed that some form of recording autocollimator is attached to the different sensor packages. Internal Thematic Mapper geometric errors are taken as one-fourth to one-half the IFOV. This value -- repeated in the other analyses -- represents the root sum square total of detector misalignment, scan-wheel wobble, timing errors, and any other effects which are not mathematically modeled in the solution and are unlikely to be determined and calibrated out during the mission.

5.1.2 Method GCP-E

The component error contributions for method GCP-E are shown in Table 5-2. This completely ground-control method uses approximate ephemeris data for position, and ground control points for all other attitude errors needed to represent the spacecraft attitude behavior over a 30-second image frame. The computed attitudes also remove the effects of ephemeris errors. The method also assumes the spacecraft attitude control system is functioning such that attitude behavior over 30 seconds can be represented by at worst a second-order curve in each axis, with deviations from this behavior of 0.001 degree rms.

Table 5-2 - RMS Positional Errors, Method GCP-E

Spatial Resection: (0.51 - 0.61) (16 - 35 m)	8 - 21 m
Internal Sensor Errors:	11 - 22 m
Attitude Departure from Second Order Model: 0.001 degree each axis, or 17 m $\sqrt{2}$	24 m
Root Sum Square Error	28 - 39 m

The error contribution from the spatial resection is determined from (1) the standard error of unit weight in a GCP before the resection, and (2) a multiplicative weight factor determined by the number and distribution of GCP within the image. The positional standard error of unit weight is determined from the error contributions of ground coordinates, descriptive pointing, and internal image geometry. The effects of correlative pointing and equipment have not been included; by proper design of the processing system, these effects can be made beneath significance. The errors from ground coordinates are those associated with the selection of points from 1/24,000 and 1/62,500 maps.

The descriptive pointing error was developed in Section 4.3. The standard error of unit weight, μ_p, in a GCP before resection then is computed as:

From Ground Coordinates: (0.3 mm at map scale, rms)	7 - 19 m
From Descriptive Pointing:	10 - 20 m
From Internal Sensor Errors	11 - 22 m
Root Sum Square = μ_p	16 - 35 m

Note that it is not assumed here that the same GCP will always be used for positioning successive images. (If this could be done, the ground-coordinate error contribution could be deleted from considerations.)

The weight factor with which to multiply μ_p is taken from Table 4-2 in Section 4 assuming that angles, rates, and accelerations all must be determined for the image. Depending on GCP numbers and distribution, the values range from 0.51 to 0.61 for the weight factor.

5.1.3 Method SIMS-EG

The component error contributions for method SIMS-EG are listed in Table 5-3. This method incorporates occasional GCP to remove ephemeris bias errors, together with the star-sensor and gyro attitude measurement of method SIMS-E. It is assumed that the use of GCP will also remove the attitude transfer error between the gyro package and the imager. For this method, the spatial resection errors replace the ephemeris errors.

Table 5-3 - RMS Positonal Errors, Method SIMS-EG

SIMS Attitude Determination: 0.001° each axis	24 m
Residual Position Errors from Spatial Resection:	8 - 21 m
Internal Sensor Errors:	11 - 22 m
Root Sum Square Error	28 - 39 m

5.1.4 Method GIMS-E-1

The component error contributions for method GIMS-E-1 are listed in Table 5-4. This method incorporates a spacecraft gyro package with method GCP-E. The gyros are needed if spacecraft attitude behavior

Table 5-4 - RMS Positional Errors, Method GIMS-E-1

Spatial Resection: (0.36 - 0.42) (16 - 35 m)	6 - 15 m
Internal Sensor Errors:	11 - 22 m
Gyro Errors: 0.00028° to 0.00056° each axis (one to two arc seconds) or (5 - 10 m) $\sqrt{2}$	7 - 14 m
Root Sum Square Error	14 - 30 m

cannot be characterized to the precision required for GCP-E. For this method, only the attitude angles must be found in the spatial resection to update the gyro data. The multiplicative weight factor from Table 4-2 can be taken as 0.36 to 0.42. The same gyro performance will be used here as was applied to methods SIMS-E and SIMS-EG. Attitude transfer will be done as part of the spatial resection composite angle determination. Error estimates for variations GIMS-E-2 and GIMS-E-3 cannot be included because of present uncertainty as to the effects of interpolated and extrapolated gyro attitudes.

5.1.5 Method HIMS-E

The component error contributions for method HIMS-E are listed in Table 5-5. This satellite-data method incorporates the lower-accuracy attitude sensors associated with the attitude control system, together with ephemeris data for position. One attitude-transfer is shown for this method, reflecting the possibility that the horizon sensor and gyros may be hard-mounted to the same structure. However, the attitude transfer between the control-system package and the

Table 5-5 - RMS Positional Errors, Method HIMS-E

Attitude Determination: 0.005 to 0.02° each axis, (87 - 350 m) $\sqrt{2}$	120 - 480 m
Attitude Transfer of Gyros to Imager: 0.0017° each axis	70 m
Gyro Errors: 0.001° each axis	25 m
Ephemeris Repeatability:	20 m
Internal Sensor Errors	11 - 22 m
Root Sum Square Error	135 - 480 m

image sensor is taken as 0.0028 degree (ten arc seconds) instead of the smaller values used for the other methods. It is unlikely an autocollimator would be used with the HIMS-E method and as is seen in the table, there would not be significant improvement using such a device. Finally, the gyro performance is not assumed to be as high quality as for the other methods above, again with little effect in the overall error.

Unlike the situation for the previous methods, method HIMS-E shows an obvious pacing error component. The values for attitude error assume some additional data processing to achieve these accuracies.

5.2 COMPARISON OF POSITIONING METHODS

The five positioning methods can be compared in many ways. Some of the criteria mentioned in the previous sections of this report are listed in Table 5-6. Even if the proper information were available,

Table 5-6 - Possible Comparison Criteria to Apply to Different Positioning Methods

1. Accuracy
2. Cost
3. Equipment Reliability
4. Speed
5. Impact on Spacecraft Weight and Power
6. Self-Checking Operation
7. Ability to Upgrade Accuracy During Mission Life
8. Personnel Requirements
9. Lead Time for Design
10. Capability for Future Improvement
11. Monitoring Behavior of Other Equipment Components
12. Constraints on Spacecraft Structural Configuration and Component Placement
13. Attitude Control System Requirements
14. Computational Load of Ground Data Processing
15. Previous Experience

and it certainly is not, it would be futile to rank each of the methods studied according to this or any other list of performance trades. The weights to be attached to the criteria are missing; these can only be

supplied by NASA, and only with consideration of all aspects of the EOS program. Any method or methods recommended by BRL would be meaningless. What can be done in the way of comparison is to attempt to draw together the different characteristics of the different methods and summarize them.

The five methods differ primarily in their reliance upon the different potential information components given in Table 2-1. A qualitative expression of this reliance, from zero to ten, is given in Table 5-7. Also shown is the reliance upon the spacecraft attitude

Table 5-7 - Reliance of Positioning Methods on Different Components

	METHOD						
COMPONENT	SIMS-E	GCP-E	SIMS-EG	GIMS-E-1	GIMS-E-2	GIMS-E-3	HIMS-E
GCP	0	10	5	10	10	10	0
Ephemeris (beyond that needed for tracking)	10	0	5	0	3	5	10
Gyro Package	10	0	10	5	10	10	10
Stellar Sensor	10	0	5	0	0	0	0
Horizon Sensor	0	0	0	0	0	0	10
ACS	0	10	0	0	0	0	0

control system, which was used only for method GCP-E of those examined. As the ACS designers respond to the requirements given in Section 4.2.2, the methods of interest may have to be modified accordingly. The intermediate values result for those cases where only relative accuracy, low error rate, or near-linear error rate is demanded, or where some back-up is available in case of failure.

SECTION 6

CONCLUSIONS AND RECOMMENDATIONS

The discussion in Section 4.2 on ACS design has shown that control-system performance capabilities must be more extensively considered before deciding on the recommended image-positioning method for EOS. It is significant that, of the five methods selected for detailed analysis, the most attractive from the cost-accuracy aspects appear to be those which impose some conditions on ACS or gyro-package performance. The most important conclusion of this study thus is considered to be that ACS design must be considered as a part of the image positioning problem for EOS, along with image sensor design and ground image processing system design.

The second major conclusion applies only to the methods analyzed in detail for EOS. For these five methods, when all reasonable criteria are considered, the use of ground control points shows either equality or clear advantages over satellite-data methods in every area but one: speed of ground data processing. Here there is not a clear disadvantage, but a concern over the need for human decision-making in a high-production data-processing environment. The hybrid positioning methods SIMS-EG and GIMS-E-2 and -3 manifest this concern; the less frequent use of GCP with these methods means less emphasis is placed on speed in the manual operations and man-machine interface. The ability of the ACS to provide smooth attitude data enters directly into this controversy. The longer the interval needed between attitude updates, the more attractive the GCP method looks in comparison with a stellar sensor. The efficiency of GCP selection and matching can only be evaluated for a specific design implementation including equipment costs, personnel requirements, training, and so on. Experience being gained with the ERTS Precision Processing Subsystem has been and will continue to be of value in assessing GCP problems and potential; some modifications that would be of benefit for EOS have already been seen. Thus, the second conclusion: with suitable efficiency for GCP selection and matching activities during data processing, extensive reliance should be placed on ground control points for positioning the images obtained for EOS and similar programs. Part of this efficiency can be attained from implementation of the operations to be performed in the ground image processing. ACS design can also contribute to the efficiency by requiring only infrequent GCP updates of attitude values. The extent to which auxiliary gyro data are required follows from the attitude behavior characteristics in the ACS design.

In addition to these major conclusions, a number of other findings from the previous sections are summarized in the following list:

1. Some GCP will always be needed in a satellite image program requiring positioning or registration. Applications include (a) measuring angular misalignment of image and attitude-measurement sensor at intervals after launch, (b) monitoring internal sensor geometry distortions, (c) measuring angular bias in inertial attitude reference devices, and (d) periodically assessing overall positioning/registration accuracy. These operations should not be done by an outside agency or investigator, but as an operations-dedicated part of the processing facility.

2. Offset pointing offers a potential for radically decreasing the interval between EOS image collection for selected areas. This capability should be implemented so that pointing is done by integral ground-swath stepover. These is no need to effect extremely precise pointing; accurate measurement of the pointing angle may be necessary, depending on the image positioning method. Stationary pointing to a single ground location is not needed. During and immediately after any image-sensor offset pointing motions, no imaging should occur for any high-resolution imager on the spacecraft until transients have decayed suitably.

3. Reaction-wheel unloading should never be permitted during imaging.

4. No special effort should be made before launch to boresight the image and attitude sensors; a higher-accuracy and more meaningful determination can be made after launch using GCP. The effort saved here should be spent on designing adequate stability in the spacecraft structure to support more dependable alignment of the various sensors.

5. To assist users of EOS images as much as possible, all film images generated should as a minimum be corrected for all known internal geometric error; to the extent practicable, absolute positioning and registration are desirable.

6. The sole justification for including RBV cameras on any EOS mission which includes either the Thematic Mapper or the HRPI is in one particular failure mode of the attitude control system. The RBV cameras will not improve Thematic Mapper positional accuracy.

7. User agencies should be asked to define the extent of the coverage they will require, in addition to the ground resolution and frequency. When these indicate operationally impossible amounts of information for processing, the users should be so advised.

8. Determined efforts should be made to better define the necessary sensor IFOV for different ground resolution requirements; the ERTS MSS is expected to be useful in this regard.

9. For image sensors requiring extensive digital or analog geometric manipulation for other reasons, stability of internal sensor geometry is of more concern than simplicity.

10. In evaluating image-sensor designs for satellites, the costs for the geometric processing needed for the image data should be one of the factors considered.

11. The need for attitude-transfer techniques, with consequent weight, power, telemetry, and reliability impact, should be given more detailed consideration for high-accuracy image-processing schemes involving auxiliary attitude sensors.

12. For satellites carrying line-scanning imagers, smooth attitude behavior is more important that high-accuracy verticality; control-system designs should more fully reflect this requirement.

13. An attitude control system with high absolute accuracy is not needed for EOS.

APPENDIX A

SIMULATION OF CONICAL SCAN GEOMETRY

T. A. Eppes

A.1 SENSOR DESCRIPTION AND CONFIGURATION

In an effort to examine the geometry of the conical scanner, a simulation of its sensing operation was developed during this study. The model was designed with as much flexibility as required to adequately explore various sensor-spacecraft configurations. For the purposes of describing the geometry of the sensor, it was assumed ideal in that no internal distortion was allowed, hence the simulation provided an external geometric treatment of conical-scan sensors.

Figure A-1 illustrates the basic operation of a conical scanner. It is characterized by some cone angle γ_o and active scan polar angle η. Data is collected only during the period when the scanner is "looking" at targets in the active scan region. This region is interrogated sequentially in time by the stack of detectors within the sensor. Figure A-2 illustrates the track of the detectors in sensor coordinates as one swath is scanned. This figure is typical of all but one of the seven spectral bands. Six detector elements are shown, indicating a six line scan swath. For the seventh (far-infrared) band, the resolution cells are three times as large, hence each swath consists of only two scanning detectors.

There are basically three sensor-spacecraft configurations: (1) forward scanning, (2) aft scanning, and (3) circular scanning. Forward scanning involves mounting the sensor such that the central axis of the cone lies in front of the spacecraft while the active scan region passes directly under the spacecraft. Aft scanning is identical to forward scanning except that the cone axis is now behind the spacecraft and the swath curvature is opposite. Circular scanning means that the central axis of the cone passes through the nadir while the active scan area is located behind the spacecraft. Data is collected by sampling the output of the detector array at some rate that produces near adjacency in the resolution elements. Since the rotational motion of the scanner is constant, sampling is performed in terms of equal time or equal polar angle increments. Each data point is stored with enough binary bits to adequately represent the reflectivity of one instantaneous field of view (IFOV), the ground coverage of each data point being determined by the IFOV which is a function of the imaging optics and the physical size of the detector array. Data from each stack of six (two for infrared) detectors, although obtained at essentially the same time, are stored sequentially.

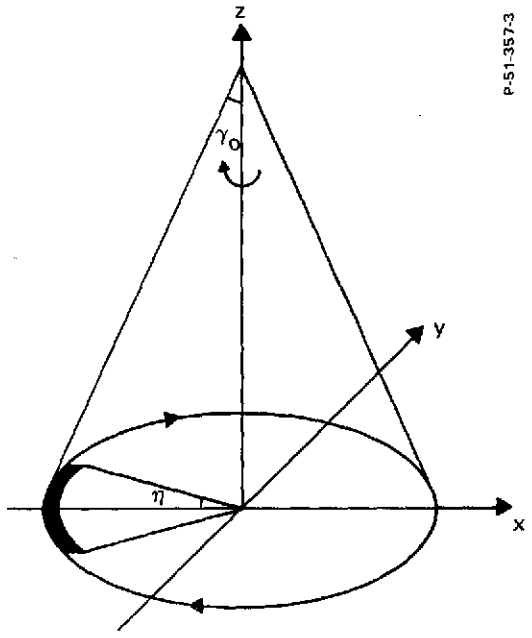

Figure A-1 - Illustration of the Operation of the Conical Scanner in Sensor Coordinates

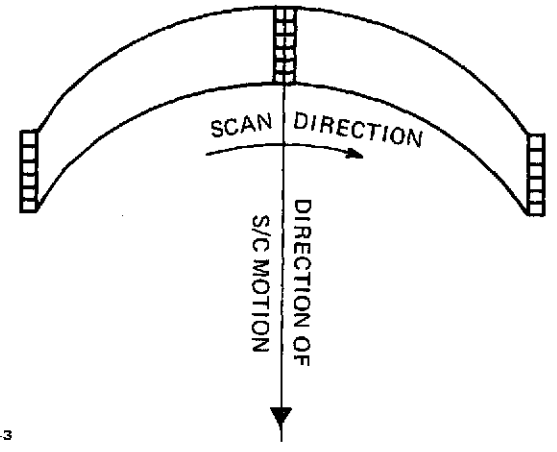

Figure A-2 - Orientation of Detector Array During One Swath

Because of the forward motion of the spacecraft, subsequent swaths interrogate new areas on the ground. These data form the basis for the final image which is composed of data from many differnt swaths. The required image format is assumed to be 185 km by 185 km which at a nominal equatorial altitude of 1000 km forces the scanner to have a cone angle of 13.23 degrees if the active polar angle is $\pm$24 degrees. For the purpose of discussion, all specifications are based upon the use of a forward scanning sensor-spacecraft configuration. With a detector element angular field of view of 44 μrad square, each image consists of approximately 720 swaths. Correspondingly, each swath consists of about 4200 by 6 IFOVs. In order to produce adjacency at swath center for a latitude of 30 degrees, the sample period between stacks is 3.8 μsec. Hence, the time required to scan one swath is 0.032 second, and with a duty cycle of 80 percent, the time between identical points in subsequent swaths is 0.04 second.

The following sections outline procedures whereby points in sensor space or earth coordinates may be mapped from one to the other. For the above-mentioned numerical data, examples of IFOV lay-out and swath structure are shown. In addition, latitude-longitude grids are mapped into sensor coordinates. Section A.5 at the end of this appendix provides a listing and operational explanation of the Fortran routines that were used to generate the data.

A.2 SENSOR-TO-EARTH DEVELOPMENT

This section describes the basic equations associated with transferring points in sensor space to their locations on the ground. Geometrically, points in image or sensor space will be defined in terms of some scanner polar angle and swath number, measured from some reference swath number. No attention is given to the problems of geometric scanner distortion, detector array sampling, radiometric error due to IFOV distortion, or digital tape format. Hence, the problem entails the projection of the IFOV of the scanner characterized by some swath number, polar angle, and spacecraft location to corresponding points on the earth's ellipsoid. Because the numerical values of the sensor parameters depend upon which sensor-spacecraft configuration is used, the treatment was developed for an arbitrary system configuration.

For the purpose of this derivation, the conical scanner may be thought of as emanating "rays" that vary in space as a function of time. This convention in no way reflects an attempt to represent the physical operation of the sensor. Figure A-3 illustrates the sensor coordinate system where origination of the rays occurs. Based on the direction cosines of the ray projected from the scanner, and since the scanner position and orientation at future times are known, the intersection of that ray with the earth may be computed.

To achieve this end, however, the direction cosines must be transformed through several coordinates systems beginning in sensor space and ending in geocentric coordinates. The earth is assumed to be an ellipsoid

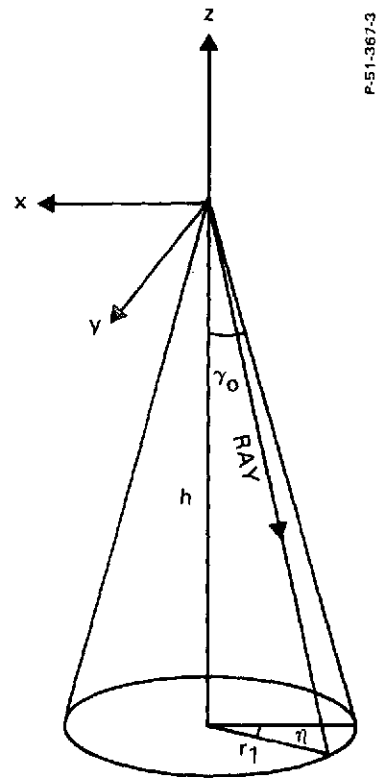

Figure A-3 - Definition of Sensor Coordinate System

rotating at constant rate and with shape unperturbed by surface features. The spacecraft position at time t is given in addition to the orbital parameters necessary to define its location at any later time. Orientation elements (i.e., attitudes, attitude rates, and attitude accelerations) are given at some reference swath center, and all values needed prior to or after this time are calculated by extrapolating these values and assuming them constant over the time frame of interest.

The development begins by defining the equation of the ray leaving the conical scanner in sensor coordinates shown in Figure A-3. The equation of this line is

$$\frac{x\left[1 + \cot^2 \gamma_o\right]^{1/2}}{\cos \eta} = \frac{x}{A'} = \frac{-y\left[1 + \cot^2 \gamma_o\right]^{1/2}}{\sin \eta} = \frac{y}{B'} = \frac{z\left[1 + \cot^2 \gamma_o\right]^{1/2}}{\cot \gamma_o} = \frac{z}{C'} \tag{A-1}$$

The polar angle η may be expressed as a function of time by

$$\eta = C_1 (t - t_o) \tag{A-2}$$

where

η = polar angle

C_1 = rotational rate of scanner

t = time

t_o = time required to scan 1/2 swath

The sensor coordinate system (x, y, z) must be rotated to account for spacecraft attitudes or built-in sensor offsets manifested as attitudes. The rotated coordinate system will be labelled (x', y', z') coupled to sensor coordinates by a transformation matrix consisting of Eulerian derived matrix elements. Hence

$$\begin{bmatrix} x \\ y \\ z \end{bmatrix} = \tilde{A} \begin{bmatrix} x' \\ y' \\ z' \end{bmatrix} \tag{A-3}$$

where

$\tilde{A}$ = transformation matrix

and

$$\tilde{A} = \begin{bmatrix} \cos\phi_e \cos\kappa_e - \sin\phi_e \sin\omega_e \sin\kappa_e & \cos\phi_e \sin\kappa_e + \sin\phi_e \sin\omega_e \cos\kappa_e & -\sin\phi_e \cos\omega_e \\ -\cos\omega_e \sin\kappa_e & \cos\omega_e \cos\kappa_e & \sin\omega_e \\ \sin\phi_e \cos\kappa_e + \cos\phi_e \sin\omega_e \sin\kappa_e & \sin\phi_e \sin\kappa_e - \cos\phi_e \sin\omega_e \cos\kappa_e & \cos\phi_e \cos\omega_e \end{bmatrix}$$

where

ϕ_e = pitch at some time t

κ_e = yaw at some time t

ω_e = roll at some time t

Two of the attitudes, roll and pitch, may be broken up into separately derived components. The pitch may be considered as consisting of a pitch offset and a space platform error. The pitch offset is used to generate forward, aft, or circular scanning. The space platform error is time-varying and may be expressed as a function of pitch at reference swath center, pitch rate, and pitch acceleration. Likewise, roll may be thought of as both offset and platform derived. The roll offset is used to generate scanning of ground swaths to the right or left of the present ground swath. The platform-derived roll is, of course, identical in nature to that of the pitch component. Consequently, the angles necessary to compute the transformation matrix of (A-3) are

$$\begin{aligned} \phi_e &= \phi_t + \beta_o \\ \omega_e &= \omega_t + \theta_o \\ \kappa_e &= \kappa_t \end{aligned} \tag{A-4}$$

where

$$\phi_t = \phi_o + \dot{\phi}_t (t - t_o) + \frac{1}{2} \ddot{\phi}_t (t - t_o)^2$$

$$\omega_t = \omega_o + \dot{\omega}_t (t - t_o) + \frac{1}{2} \ddot{\omega}_t (t - t_o)^2$$

$$\kappa_e = \kappa_o + \dot{\kappa}_t (t - t_o) + \frac{1}{2} \ddot{\kappa}_t (t - t_o)^2$$

t_o = time required to scan 1/2 swath

t = time when platform attitudes are required

ϕ_o = pitch at time $t = t_o$

$\dot{\phi}_t$ = pitch rate at time $t = t_o$

$\ddot{\phi}_t$ = pitch acceleration at time $t = t_o$

ω_o = roll at time $t = t_o$

$\dot{\omega}_t$ = roll rate at time $t = t_o$

$\ddot{\omega}_t$ = roll acceleration at time $t = t_o$

κ_o = yaw at time $t = t_o$

$\dot{\kappa}_t$ = yaw rate at time $t = t_o$

$\ddot{\kappa}_t$ = yaw acceleration at time $t = t_o$

ϕ_t = platform pitch at t

ω_t = platform roll at t

κ_t = platform yaw at t

β_o = pitch offset of sensor

θ_o = roll offset of sensor

ω_e = total roll at t

ϕ_e = total pitch at t

κ_e = total yaw at t

Substituting the transformation of (A-4) into (A-3) and rearranging terms yields

$$C_1 x' = C_2 y' = C_3 z' \qquad \text{(A-5)}$$

with

$$C_1 = \left(\frac{\frac{a_{11}}{A'} - \frac{a_{21}}{B'}}{\frac{a_{23}}{B'} - \frac{a_{13}}{A'}} \right) - \left(\frac{\frac{a_{11}}{A'} - \frac{a_{31}}{C'}}{\frac{a_{33}}{C'} - \frac{a_{13}}{A'}} \right)$$

$$C_2 = \left(\frac{\frac{a_{22}}{B'} - \frac{a_{12}}{A'}}{\frac{a_{23}}{B'} - \frac{a_{13}}{A'}} \right) - \left(\frac{\frac{a_{32}}{C'} - \frac{a_{12}}{A'}}{\frac{a_{33}}{C'} - \frac{a_{13}}{A'}} \right)$$

$$C_3 = C_1 \frac{\left[\frac{\left(\frac{a_{33}}{C'} - \frac{a_{23}}{B'} \right)}{\left(\frac{a_{32}}{C'} - \frac{a_{22}}{B'} \right)} - \frac{\left(\frac{a_{23}}{B'} - \frac{a_{13}}{A'} \right)}{\left(\frac{a_{22}}{B'} - \frac{a_{12}}{A'} \right)} \right]}{\left[\frac{\left(\frac{a_{21}}{B'} - \frac{a_{31}}{C'} \right)}{\left(\frac{a_{32}}{C'} - \frac{a_{22}}{B'} \right)} - \frac{\left(\frac{a_{11}}{A'} - \frac{a_{21}}{B'} \right)}{\left(\frac{a_{22}}{B'} - \frac{a_{12}}{A'} \right)} \right]}$$

where

a_{ij} = element of $\tilde{A}$ corresponding to the i'th row and the j'th column

A', B', C' = direction cosines of line in sensor coordinates defined by (A-1)

The rotated (x', y', z') coordinate system must be translated to an earth-based system (x_e, y_e, z_e). The system (x', y', z') is defined as one whose z' axis coincides with a perpendicular from the earth's ellipsoid. Since (x_e, y_e, z_e) will be defined as a system tangent to the ellipsoid at the origination of the perpendicular, (x', y', z') and (x_e, y_e, z_e) are related by

$$x' = x_e \qquad y' = y_e \qquad z' = z_e - H_{se} \tag{A-6}$$

where

H_{se} = spacecraft altitude measured along perpendicular to ellipsoid

Figure A-4 illustrates the next transformation, that is, from local (x_e, y_e, z_e) to geocentric (U, V, W) coordinates. The U-axis coincides with the meridional plane associated with the spacecraft longitude at time t. The origin of the (U, V, W) system is located at the center of the ellipsoid. The (x_e, y_e, z_e) and (U, V, W) systems are related by

$$\begin{bmatrix} x_e \\ y_e \\ z_e \end{bmatrix} = \begin{bmatrix} \cos\alpha_{se} \sin\Phi_{se} & -\sin\alpha_{se} & -\cos\alpha_{se} \cos\Phi_{se} \\ \sin\alpha_{se} \sin\Phi_{se} & \cos\alpha_{se} & -\sin\alpha_{se} \cos\Phi_{se} \\ \cos\Phi_{se} & 0 & \sin\Phi_{se} \end{bmatrix} \left\{ \begin{bmatrix} U \\ V \\ W \end{bmatrix} - \begin{bmatrix} U_x \\ 0 \\ W_x \end{bmatrix} \right\} \quad \text{(A-7)}$$

where

α_{se} = instantaneous heading or azimuth of spacecraft measured from the south.

Φ_{se} = latitude of spacecraft measured at origin of local coordinate system (x_e, y_e, z_e)

$U_x = E \cos\Phi_{se}$

$W_x = E (1 - e^2) \sin\Phi_{se}$

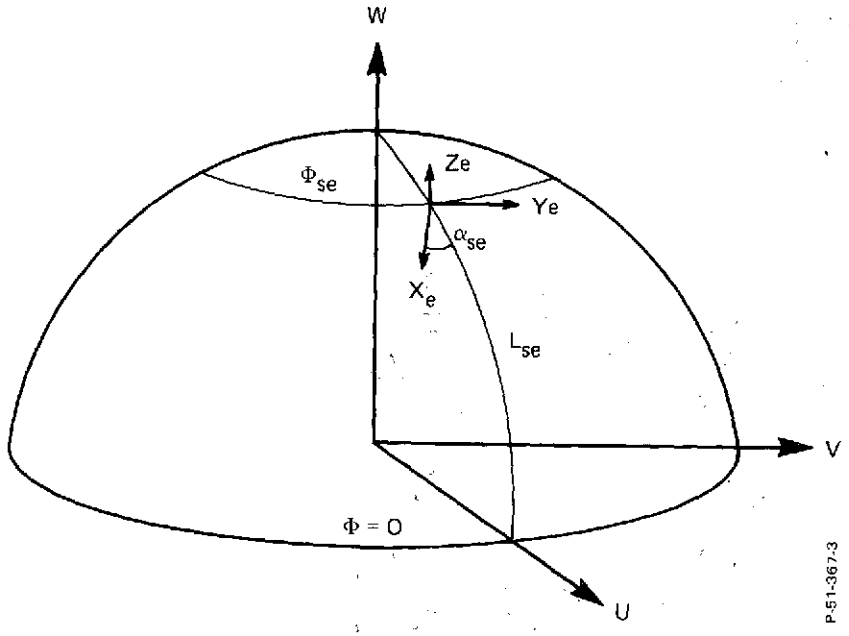

Figure A-4 - Transformation Between Geocentric and Local Coordinates

$$E = a \cos \Phi_{se} \Big/ \left[1 - e^2 \sin^2 \Phi_{se}\right]^{1/2}$$

e = eccentricity of the earth

a = semi-major axis of the earth

Substituting (A-6) and (A-7) into (A-5) and rearranging terms yields

$$R_1 U + R_2 = R_3 V + R_4 = R_5 W + R_6 \qquad \text{(A-8)}$$

where

$$R_1 = \left(\frac{\bar{A}_1 - \bar{A}_2}{\bar{C}_2 - \bar{C}_1}\right) - \left(\frac{\bar{A}_1 - \bar{A}_3}{\bar{C}_3 - \bar{C}_1}\right)$$

$$R_2 = \left(\frac{\bar{D}_1}{\bar{C}_2 - \bar{C}_1}\right) - \left(\frac{\bar{D}_1}{\bar{C}_3 - \bar{C}_1}\right)$$

$$R_3 = \left(\frac{\bar{B}_2 - \bar{B}_1}{\bar{C}_2 - \bar{C}_1}\right) - \left(\frac{\bar{B}_3 - \bar{B}_1}{\bar{C}_3 - \bar{C}_1}\right)$$

$$R_4 = \left(\frac{\bar{D}_2}{\bar{C}_2 - \bar{C}_1}\right) - \left(\frac{\bar{D}_3}{\bar{C}_3 - \bar{C}_1}\right)$$

$$R_5 = R_1 \frac{\left[\left(\frac{\bar{C}_2 - \bar{C}_1}{\bar{B}_2 - \bar{B}_1}\right) - \left(\frac{\bar{C}_3 - \bar{C}_1}{\bar{B}_3 - \bar{B}_1}\right)\right]}{\left[\left(\frac{\bar{A}_1 - \bar{A}_2}{\bar{B}_2 - \bar{B}_1}\right) - \left(\frac{\bar{A}_1 - \bar{A}_3}{\bar{B}_3 - \bar{B}_1}\right)\right]}$$

$$R_6 = R_1 \frac{\left[\left(\frac{\bar{D}_2 - \bar{D}_1}{\bar{B}_2 - \bar{B}_1}\right) - \left(\frac{D_3 - D_1}{B_3 - B_1}\right)\right]}{\left[\left(\frac{\bar{A}_1 - \bar{A}_2}{\bar{B}_2 - \bar{B}_1}\right) - \left(\frac{\bar{A}_1 - \bar{A}_3}{\bar{B}_3 - \bar{B}_1}\right)\right]} + R_2$$

$$\bar{A}_1 = C_1 b_{11} \qquad \bar{B}_1 = C_1 b_{12} \qquad \bar{C}_1 = C_1 b_{13} \qquad \bar{D}_1 = -C_1 (b_{11} U_x + b_{13} W_x)$$

$$\bar{A}_2 = C_2 b_{21} \qquad \bar{B}_2 = C_2 b_{22} \qquad \bar{C}_2 = C_2 b_{23} \qquad \bar{D}_2 = -C_2 (b_{21} U_x + b_{23} W_x)$$

$$\bar{A}_3 = C_3 b_{31} \qquad \bar{B}_3 = C_3 b_{32} \qquad \bar{C}_3 = C_3 b_{33} \qquad \bar{D}_3 = -C_3 (b_{31} U_x + b_{33} W_x + H_{se})$$

b_{ij} = element from the i'th row and j'th column of the transformation matrix of (A-7)

C_1, C_2, C_3 = coefficients associated with (A-5)

Rewriting (A-8) in parametric form gives

$$U = \frac{1}{R_1} (R_5 W + R_6 - R_2)$$

$$V = \frac{1}{R_3} (R_5 W + R_6 - R_4) \qquad \text{(A-9)}$$

The equation of the ellipsoid is

$$\frac{U^2 + V^2}{a^2} + \frac{W^2}{b^2} = 1 \qquad \text{(A-10)}$$

where

a = semi-major axis of the earth

b = semi-minor axis of the earth

Since the equation of the line projected from the sensor is given by (A-9), and the equation of the ellipsoid is given by (A-10), the intersection of the two may be computed. Substituting (A-9) into (A-10) and solving for W gives

$$W_o = \frac{-B'' \pm [B''^2 - 4\ A''\ C'']^{1/2}}{2\ A''}$$

where

$$A'' = \frac{1}{b^2} - \frac{R_5^2}{a^2}\ \frac{1}{R_1^2} + \frac{1}{R_3^2}$$

$$B'' = \frac{2\ R_5}{a^2}\ \frac{R_6 - R_2}{R_1^2} + \frac{R_6 - R_4}{R_3^2}$$

$$C'' = \frac{(R_6 - R_2)^2}{a^2\ R_1^2} + \frac{(R_6 - R_4)^2}{a^2\ R_3^2} - 1$$

In general, two values of W_o will be found; only one is of interest. Since that point is the one directly beneath or in the neighborhood of the sensor, the value of W which is positive in sign will be selected. This forces calculations to be done only in the northern hemisphere for the present mode. A small modification would allow operation over the entire ellipsoid.

Using (A-9), U_o and V_o may be calculated; thus the point of intersection at time t in geocentric coordinates is known. If terrain height variations are ignored, the latitude and longitude of the point are given by

$$L = L_{se} - \tan^{-1}\ \frac{V_o}{U_o} \qquad \text{(A-12)}$$

$$\Phi = \sin^{-1}\left[\frac{U_o^2 + V_o^2 - a^2}{(U_o^2 + V_o^2)\ e^2 - a^2}\right]^{1/2}$$

In order to express the point in some tangent-plane coordinate system (x_e, y_e, z_e), (A-7) may be used. The values used for Φ_{se}, L_{se} α_{se} must be the same for all points to be expressed in that system. The above values are usually chosen as those corresponding to reference swath center. In any event, the transformation of points in sensor space to their locations on the ground is now complete if all matrix elements are known at time t.

To evaluate the transformation equations presented above, it is required that spacecraft latitude and longitude be known at all times. They are given at some initial reference point, and the orbital equations may be used to extrapolate those values to some other time. Figure A-5 is a diagram of the orbital motion of the spacecraft in two coordinate systems. It is seen that the orbit is retrograde with the sensor imaging during the descending mode. If the orbit is assumed circular, the orbital angle will vary linearly with time. The orbital angle is taken here as that angle subtended by two lines passing through the center of the earth (also the orbital center). One line passes through the terminator, or point of maximum latitude. The other passes through the spacecraft position at time t. The orbital angle may be expressed as

$$\theta = \theta' + \frac{V_o}{R_o} (t - t_o) \qquad \text{(A-13)}$$

where

θ' = orbital angle at reference swath center

V_o = tangential velocity of spacecraft

R_o = radius of spacecraft orbit

t = time when θ is desired

t_o = time required to scan 1/2 swath

The longitude of the spacecraft at time t is then

$$L_{se} = L'_{se} + C_o (t - t_o) + L_{seo} \qquad \text{(A-14)}$$

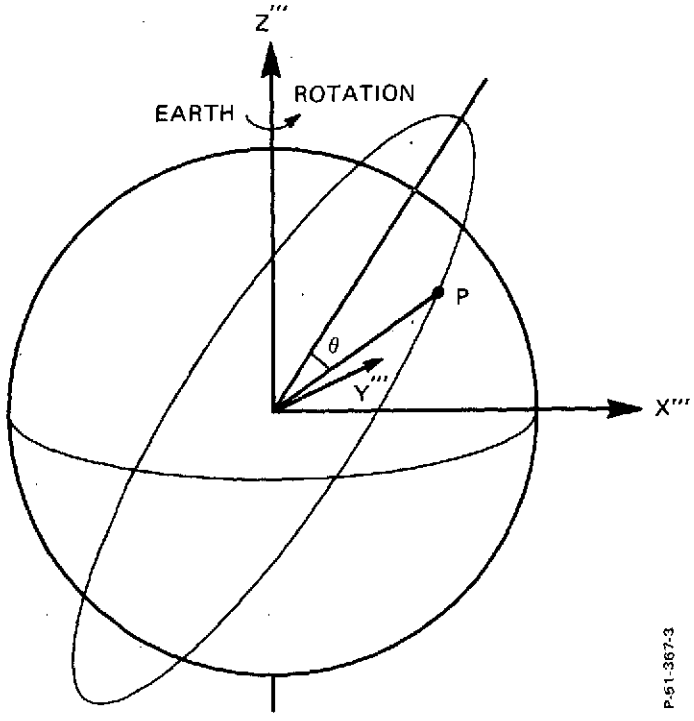

Figure A-5 - Configuration of Spacecraft Orbit

where

$$L'_{se} = \tan^{-1}\left[\frac{\tan\theta}{\sin\alpha_{seo}}\right]$$

C_o = earth rotation rate

L_{seo} = longitude of spacecraft at reference point

α_{seo} = inclination of orbit measured from the poles

Because of the transcendental nature of the equations, Φ_{se} and H_{se} cannot be computed directly and must be found iteratively. Nevertheless, convergence is rapid and excellent accuracy is attainable. Inserting some nominal value for H_{se}, Φ_{se} is estimated by

$$\Phi_{se} = \tan^{-1}\left[\left(\frac{a^2 + a\,H_{se}}{b^2 + a\,H_{se}}\right)\left(\frac{\cos\theta\,\cos\alpha_{seo}}{\left[\sin^2\theta + \cos^2\theta\,\sin^2\alpha_{seo}\right]^{1/2}}\right)\right] \qquad \text{(A-15)}$$

A new value of H_{se} is computed from

$$H_{se} = \frac{R_o \cos\theta \cos\alpha_{seo}}{\sin\Phi_{se}} - \frac{a(1-e^2)}{\left[1 - e^2 \sin^2\Phi_{se}\right]^{1/2}} \qquad \text{(A-16)}$$

If the increment in H_{se} from the previous value is excessive (>1 meter), a return to (A-15) is in order and a new Φ_{se} is generated. This process continues until the increment in H_{se} is acceptable.

The only remaining quantity required in the transformation equations is the spacecraft heading α_{se}. This is computed as the dot product of two unit vectors tangent to the ellipsoid at spacecraft nadir at time t. One vector denotes the velocity neglecting earth rotation while the other lies in the meridional plane or longitudinal plane of that point and is tangent to the ellipsoid.

The velocity vector components in the coordinate system shown in Figure A-5 are

$$x_t = \cos\Phi_{se} \sin\psi \frac{\partial E}{\partial t} + E \cos\Phi_{se} \cos\psi \frac{\partial\psi}{\partial t} - E \sin\psi \sin\Phi_{se} \frac{\partial\Phi_{se}}{\partial t}$$

$$y_t = \cos\Phi_{se} \cos\psi \frac{\partial E}{\partial t} - E \cos\Phi_{se} \sin\psi \frac{\partial\psi}{\partial t} - E \cos\psi \sin\Phi_{se} \frac{\partial\Phi_{se}}{\Phi t}$$

$$z_t = (1 - e^2) \sin\Phi_{se} \frac{\partial E}{\partial t} + E \cos\Phi_{se} \frac{\partial\Phi_{se}}{\Phi t}$$

where

$$\frac{\partial E}{\partial t} = \frac{a e^2 \sin\Phi_{se} \cos\Phi_{se} \frac{\partial\Phi_{se}}{\partial t}}{\left[1 - e^2 \sin^2\Phi_{se}\right]^{1/2}}$$

$$\frac{\partial\psi}{\partial t} = \frac{V_o}{R_o} \frac{\sin\alpha_{seo}}{\cos^2\theta \sin^2\alpha_{seo} + \sin^2\theta}$$

$$\frac{\partial \Phi_{se}}{\partial t} = \frac{V_o}{R_o} \frac{(C13 - C23\ C11/C21)}{(C12 - C22\ C11/C21)}$$

$$C11 = C22 = 1$$

$$C12 = \frac{R_o \cos\theta \cos\alpha_{seo} \cos\Phi_{se}}{\sin^2 \Phi_{se}} + \frac{a\,(1 - e^2)\, e^3 \sin\Phi_{se} \cos\Phi_{se}}{\left[1 - e^2 \sin^2 \Phi_{se}\right]^{1/2}}$$

$$C21 = \frac{1}{1 + URG^2} \frac{a\,(a^2 - b^2)}{\left(b^2 + a\,H_{se}\right)^2}$$

$$C13 = - \frac{R_o \sin\theta \cos\alpha_{seo}}{\sin\Phi_{se}}$$

$$C23 = \frac{a^2 + a\,H_{se}}{b^2 + a\,H_{se}} \cdot \frac{1}{1 + URG^2} \cdot \frac{\cos\alpha_{seo} \sin\theta}{\left[\sin^2\theta + \cos^2\theta \sin^2\alpha_{seo}\right]^{3/2}}$$

$$URG = \frac{a^2 + a\,H_{se}}{b^2 + a\,H_{se}} \cdot \frac{\cos\theta \cos\alpha_{seo}}{\left[\sin^2\theta + \cos^2\theta \sin^2\alpha_{seo}\right]^{1/2}}$$

The meridional vector components may be expressed as

$$x_m = -CC1 \cdot CC2 \cdot \sin\psi$$

$$y_m = -CC1 \cdot CC2 \cdot \cos\psi$$

$$z_m = -CC2$$

where

$$CC1 = - \frac{a^2}{b^2} \frac{z}{x \sin\psi + y \cos\psi}$$

$$CC2 = \frac{1}{\left[1 + CC1^2\right]^{1/2}}$$

$$x = E \cos \Phi_{se} \sin \psi$$

$$y = E \cos \Phi_{se} \cos \psi$$

$$z = E \left(1 - e^2\right) \sin \Phi_{se}$$

$$\psi = \tan^{-1} \left[\frac{\sin \theta}{\cos \theta \sin \alpha_{seo}} \right]$$

$$E = \frac{a}{\left[1 - e^2 \sin^2 \Phi_{se}\right]^{1/2}}$$

The above components are not normalized to unity; hence the dot product of the two vectors has to be divided by the two vector lengths. The azimuth is then expressed as

$$\alpha_{se} = \cos^{-1} \left[\frac{x_m x_t + y_m y_t + z_m z_t}{\left[\left(x_m^2 + y_m^2 + z_m^2\right)\left(x_t^2 + y_t^2 + z_t^2\right)\right]^{1/2}} \right]$$

Figure A-6 is a plot of azimuth (although it includes earth rotation) as a function of latitude. Consequently, given some time t measured from the beginning of some reference swath, the orientation elements at that swath center, and the spacecraft position at that swath center, the projection of the line corresponding to the IFOV of the scanner at that instant on the ground may be computed.

The only additional requirement analytically is providing a means of projecting all four corners of the (assumed square) IFOV for a given resolution element size and sample interval. That is, the input to the projection equations will be a lateral resolution element number and a corner number for the six-element detector array. Figure A-7 illustrates the requirement of a new cone angle and polar angle as a function of lateral resolution element number and IFOV corner number. It also establishes the numbering convention for the detector array corners. The relationship between cone angle and polar angle changes for the case of "longitudinal" incrementation (in the along-track dimension) is shown.

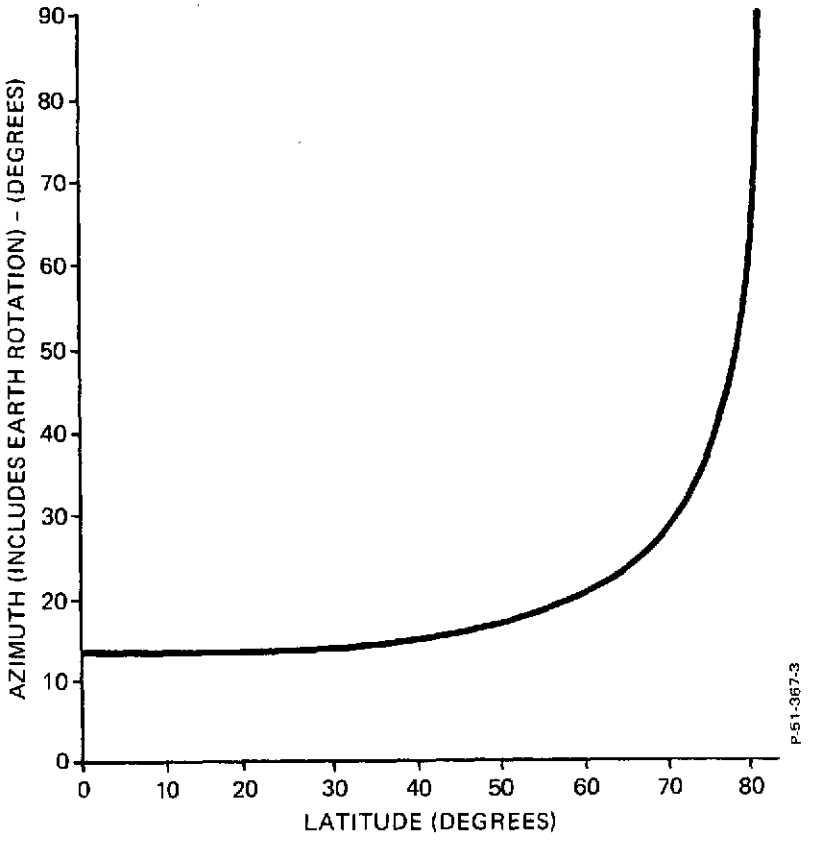

Figure A-6 - Azimuth as a Function of Latitude

A similar diagram could be drawn to show angular IFOV width in the transverse dimension. The relations between the cone and polar angle of corners 1 and 3 are

$$\gamma_o' = \cos^{-1}\left\{\cos\gamma_o\left[\cos\Delta_1 + \frac{\sin\gamma_o\cos\eta\sin\Delta_1}{\left[1-\cos^2\eta\sin^2\Delta_1\right]^{1/2}}\right]\right\} \quad \text{(A-17)}$$

$$\eta_o' = \sin^{-1}\left[\frac{\tan\gamma_o\sin\eta}{\tan\gamma_o'}\right] \quad \text{(A-18)}$$

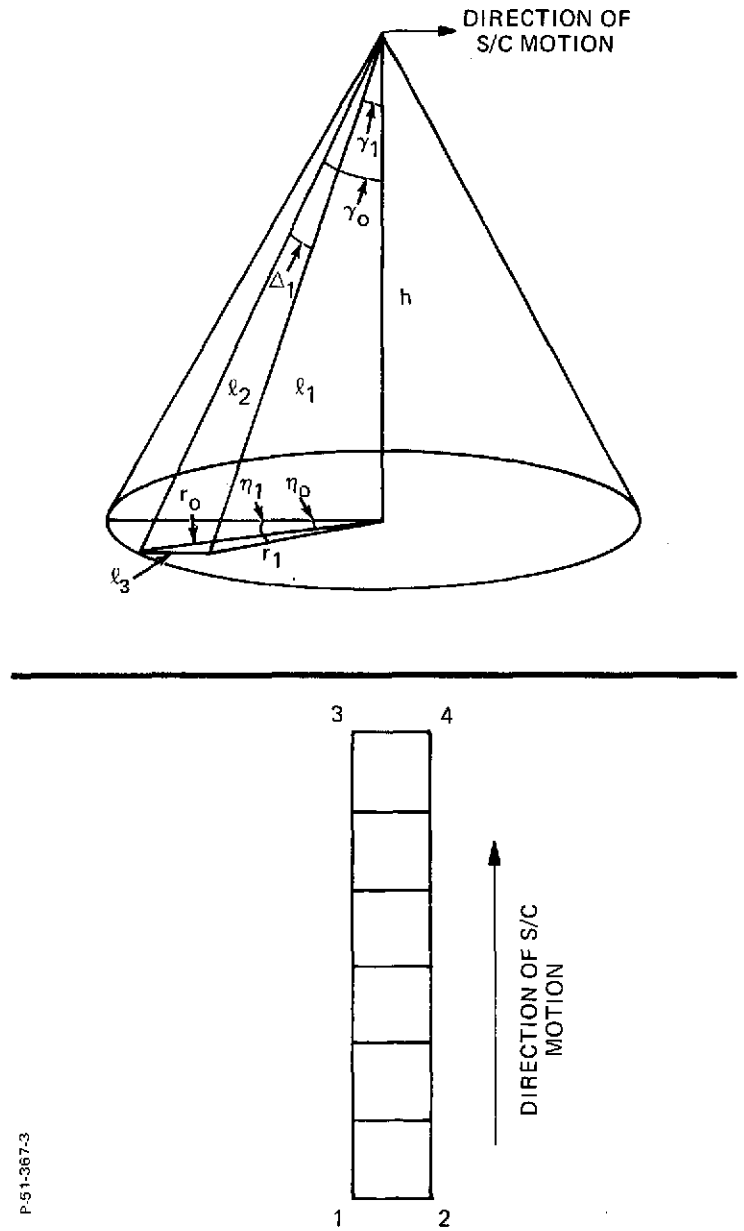

Figure A-7 - Change in γ_o and η as a Function of Detector Array Number

The relationship between corners 3 and 4 or 1 and 2 is

$$\gamma_o' = \cos^{-1}\left\{\cos\gamma_o'\left[\cos\Delta_2 - \frac{\sin\gamma_o'\sin\eta_o'\sin\Delta_2}{\left[1-\sin^2\eta_o'\sin^2\Delta_2\right]^{1/2}}\right]\right\} \quad \text{(A-19)}$$

$$\eta_1' = \cos^{-1}\left[\frac{\tan\gamma_o'\cos\eta_o'}{\tan\gamma_1'}\right] \quad \text{(A-20)}$$

With respect to (A-1), the values substituted for γ_o and η vary depending on which corner of the stack is of interest. Equations (A-17) through (A-20) represent only small changes in η and γ_o since Δ_1 and Δ_2 are the angular dimensions of the detector array (typically 44 μrad by 264 μrad). The input value of η for (A-17) or (A-19) is determined by the lateral resolution element number while γ_o is always the cone angle.

A.3 EARTH-TO-SENSOR DEVELOPMENT

This section describes the equations and procedures associated with mapping points from the ground to sensor coordinates. The objectives are to determine (1) when a point was sensed, (2) after how many swaths from some initial swath did this occur, (3) what is the lateral resolution element number, and (4) what is the detector number within the array. The position of the spacecraft is given for some time t = 0. The latitude and longitude of the point to be projected are known. The unknowns mentioned above are determined using an iterative procedure whereby estimates of spacecraft location at sensing time are generated. Based on the errors in these estimates, new time increments are incorporated which eventually produce convergence to the time when the point was sensed.

Initially, the location in sensor coordinates is computed for t = 0. The transformation is performed using the given location of the spacecraft at that time. The point is transferred for two times, the beginning and ending of the swath connected with the initial spacecraft position shown in Figure A-8(a). Assuming a linear velocity in sensor coordinates, the necessary number of swath increments is calculated and the spacecraft is advanced accordingly. This process continues with varying degrees of refinement until the swath number where detection occurred is located. At that point, the lateral resolution element number and detector number are easily found by a successive iteration over some nominal range.

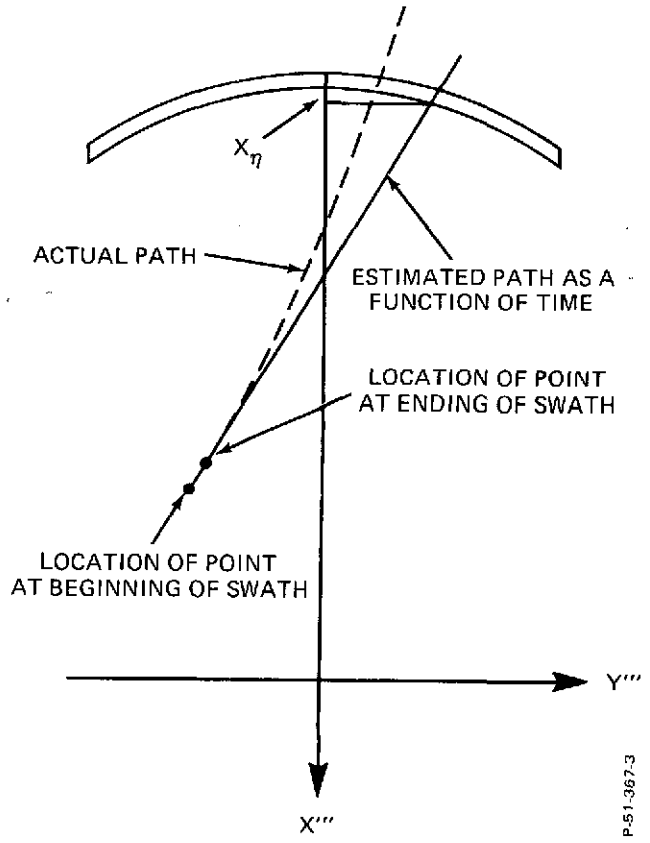

Figure A-8(a) - Ground Point Mapping Into Sensor Coordinates

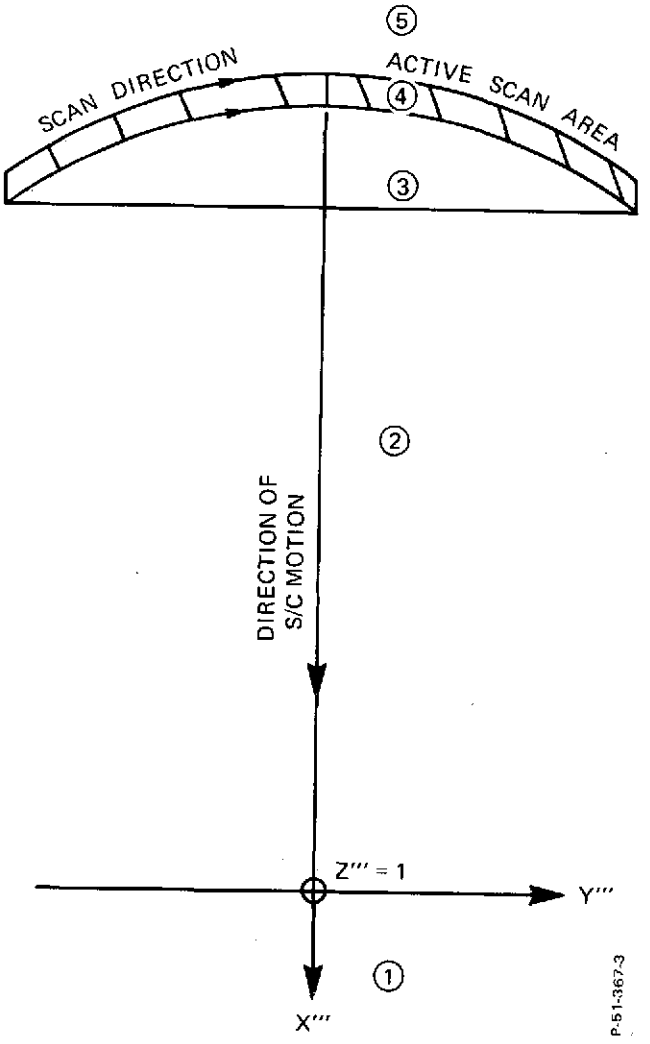

Figure A-8(b) - Designation of Zones With Respect to the Determination of Time of Detection

To begin, the point of known latitude and longitude is expressed in geocentric coordinates where the U axis passes through the meridional plane corresponding to the spacecraft location at that time. Hence

$$U_p = E'' \cos \Phi \cos (L_{se} - L)$$

$$V_p = E'' \cos \Phi \sin (L_{se} - L) \qquad \text{(A-21)}$$

$$W_p = E'' (1 - e^2) \sin \Phi$$

where

$$E'' = \frac{a}{[1 - e^2 \sin^2 \Phi]^{1/2}} + H$$

a = semi-major axis of the earth

e = eccentricity of the earth

H = height of point above reference ellipsoid usually zero

L_{se} = longitude of spacecraft at time of interest

Φ = latitude of ground point

L = longitude of ground point

(U_p, V_p, W_p) = position of ground point in geocentric coordinates

A transformation identical to that of Figure A-4 which expresses the point in local coordinates which are tangent to the ellipsoid at spacecraft nadir may be written as

$$\begin{bmatrix} x_e \\ y_e \\ z_e \end{bmatrix} = \tilde{G} \left\{ \begin{bmatrix} U_p \\ V_p \\ W_p \end{bmatrix} - \begin{bmatrix} U_x \\ 0 \\ W_x \end{bmatrix} \right\} \qquad \text{(A-22)}$$

where

$$\tilde{G} = \begin{bmatrix} \cos \alpha_{se} \sin \Phi_{se} & -\sin \alpha_{se} & -\cos \alpha_{se} \cos \Phi_{se} \\ \sin \alpha_{se} \sin \Phi_{se} & \cos \alpha_{se} & -\sin \alpha_{se} \cos \Phi_{se} \\ \cos \Phi_{se} & 0 & \sin \Phi_{se} \end{bmatrix}$$

and

$$U_x = E \cos \Phi_{se}$$

$$W_x = E (1 - e^2) \sin \Phi_{se}$$

$$E = \frac{a}{\left[1 - e^2 \sin^2 \Phi_{se}\right]^{1/2}}$$

α_{se} = instantaneous azimuth of spacecraft measured from the south

(x_e, y_e, z_e)= local coordinates components of the ground point.

A transformation must now be performed to arrive at a sensor-based coordinate system. This is accomplished by translating the local system by H_{se} (spacecraft altitude) and incorporating the Eulerian attitude elements. Hence,

$$\begin{bmatrix} x''' \\ y''' \\ z''' \end{bmatrix} = \tilde{B} \left\{ \begin{bmatrix} x_e \\ y_e \\ z_e \end{bmatrix} - \begin{bmatrix} 0 \\ 0 \\ H_{se} \end{bmatrix} \right\} \qquad \text{(A-23)}$$

where

$$\tilde{B} = \begin{bmatrix} \cos \phi_e \cos \kappa_e - \sin \phi_e \sin \omega_e \sin \kappa_e & \cos \phi_e \sin \kappa_e + \sin \phi_e \sin \omega_e \cos \kappa_e & -\sin \phi_e \cos \omega_e \\ -\cos \omega_e \sin \kappa_e & \cos \omega_e \cos \kappa_e & \sin \omega_e \\ \sin \phi_e \cos \kappa_e + \cos \phi_e \sin \omega_e \sin \kappa_e & \sin \phi_e \sin \kappa_e - \cos \phi_e \sin \omega_e \cos \kappa_e & \cos \phi_e \cos \omega_e \end{bmatrix}$$

H_{se} = spacecraft altitude along perpendicular

(x''', y''', z''') = sensor coordinate system components

The Eulerian angles required in evaluating $\tilde{B}$ are obtained by extrapolating the orientation elements from the initial spacecraft location as in (A-4). In addition Φ_{se}, H_{se}, L_{se}, and α_{se} are computed in the same way as in the previous section.

As previously stated, the ground point is projected for the beginning and end of a swath where detection is suspected. To facilitate handling in sensor coordinates, the values obtained by (A-23) are normalized in the z-direction. The two points found in sensor coordinates appear separated in space and time. Since, in general, the initial swath will not be the one in which detection occurred, some form of swath incrementation using the above space and time separation must be devised.

The normalized sensor coordinate plane of z = 1 is divided into five zones as shown in Figure A-8(b). Zone one will consist of all areas where $x \geq 0$. Zone two will be that area where $X \leq 0$ and $X \geq XMAX$ where XMAX is the x-coordinate of the foremost portion of the active scan area. It may be expressed as

$$XMAX = \sin \gamma_o \cos \eta_{max} + del$$

where

$$del = \sin \gamma_o - \sin (\gamma_o - \Delta_1)$$

Δ_1 = angular size of detector array in along-track direction ($\Delta_1 = 6\Delta_2$)

γ_o = cone angle

η_{max} = maximum polar angle ($\sim$24 degrees)

If the initial transformation produces points which lie in zone 1, the swath increment is computed assuming a linear velocity in sensor coordinates. The swath increment is such that the time advance it produces causes the points to lie in zone 2. The increment may be calculated from

$$\text{No. Swath Increm.} = \frac{x_2'''}{V_x \cdot t_{oo}}$$

where

$$V_x = \frac{x_2''' - x_1'''}{2t_o}$$

t_{oo} = time between identical points in subsequent swaths

t_o = time required to scan 1/2 swath

x_2''' = sensor x-coordinate for point projected at the end of the swath where detection is suspected

x_1''' = sensor x-coordinate for point projected at the beginning of the swath where detection is suspected

Because the velocity is not linear and the estimate of the velocity is made over a small interval compared to the necessary incrementation, the point will not appear where it was predicted at the new times. However, the increment needed to place the point in region 2 is not critical and over-incrementing by adding some fixed number of swaths to the calculated value is desirable. Since the motion of the spacecraft is in the $+x'''$ direction, the time increment will be positive, and the point at the times will be closer to the active scan region.

If the point is found to be in zone 2 either initially or because of action taken by the above discussed procedure when zone 1 is encountered, a different equation for swath incrementation is needed. In this case the swath increment is

$$\text{No. Swath Increm.} = \frac{x_{max} - x_2'''}{V_x \cdot t_{oo}} \qquad \text{(A-24)}$$

Since the estimate of the velocity is in error, care must be taken to ensure that if the point tends toward a swath end, over-incrementation does not force the spacecraft past the true sensing time. For this reason, (A-24) is scaled to about 0.95. If this new time forces the point to again lie in zone 2, a swath incrementation of 1 is suggested. In this way, the point will not be passed over accidentally.

If the point is found in zone 3, a similar equation to the above is used. In this case, the polar angle is estimated by projecting the line connecting the two points and finding its intersection with the foremost edge of the active scan area as shown in Figure A-8(a). The

polar angle η is estimated using the above procedure, and the required number of swath increments is

$$\text{No. Swath Increm.} = \frac{x_\eta - x_2'''}{V_x \cdot t_{oo}}$$

where

x_η = x-coordinate of the point in the active scan area where detection is suspected, from Figure A-8(a).

To avoid over-incrementation, the above estimate is reduced by up to 3 swaths. Each time beyond this stage when the point projects into zone 3, the swath increment is made 1.

As soon as either the beginning or end of a swath falls within the active scan area, the interswath mode is begun. The polar angle is easily estimated by computing it from the average point projection which corresponds to swath center. The lateral resolution element number is then known. To ensure detection, these numbers are decreased and "stepped" in equal time samples. Each time, the ground point is projected to sensor coordinates. At this stage, the point is projected at only one time, that time corresponding to the lateral resolution element number. At each resolution stack, the point is checked to see if it lies in the region bounded by the 6 detectors. If not, the element number is increased by one (with a maximum search range of 20) and the above test is reapplied. Since it is possible to lie within the active scan area and not be sensed during that swath, once the point is not detected using resolution-element searching, the swath number is increased by 1, and the above procedure is repeated. After three interswath mode attempts, the point is assumed not to have been sensed as a result of combined yaw/earth-rotation. During this period, the point is also checked to ensure that the y-coordinate is within the bound of the active scan region.

To facilitate overall procedure, all points found to lie behind the spacecraft initially are forced into zone 2 by retreating the spacecraft sufficiently. This is done to prevent the need for equally elaborate convergence schemes for these points since convergence time could not be decreased sufficiently. Once the point is placed in zone 2, normal operation toward true detection time applying the procedure discussed above is resumed.

In general, the point will have been detected by this time, therefore the time from initial spacecraft location, the lateral resolution element number, and the total number of swath increments are known. The only remaining unknown parameter is the detector number, 1 through 6.

Since all six are interrogated essentially simultaneously, the center of the detector lying closest to the sensor coordinate of the ground point at the instant of detection will be the detector number. In conclusion, all parameters necessary to determine the location of some point on the ground in the sensor data format are known.

A.4 CHARACTERIZATION OF CONICAL SCANNER GEOMETRY

This section graphically illustrates the geometry associated with the conical scanner in terms of swath curvature, IFOV projection, and ground-point grid mapping. Based on the information provided previously and with the aid of the Fortran programs in Section A.5, numerical examples of conical scanner operation are shown for various spacecraft-ground-point configurations.

To meet the above objectives, the spacecraft or sensor parameters that must remain fixed are listed. It is required that the swath width on the ground be 185 km wide. The orbit is fixed at a radius of 9799 km and is circular. In addition the maximum active polar angle is 24 degrees. The spacecraft will also be operated in a forward scanning mode since this configuration minimizes overall terrain effects and requires a lower duty cycle. Based on the above data, all other adjustable parameters will be determined.

From the altitude, maximum polar angle, and required swath width, the cone angle is found to be 13.23 degrees. If the angular IFOV of each detector is 44 rad (design goal), the polar angle sampling interval to produce adjacency at swath center must be 0.1923 mrad at 30 degrees latitude. In order to match adjacent swaths at 30 degrees latitude, the time between identical points on subsequent swaths is 0.040225 second. With a scanner duty cycle of 80 percent, the time required to scan one swath is 0.032084 second. Since the maximum polar angle is 24 degrees, the sample interval of the detector array is 7.4 μsec. Hence there are 4340 samples per swath with each sample requiring 6 addresses to the detector array. At this point all adjustable scanner parameters have been specified.

The immediate point of interest is the macroscopic structure of one swath. Figure A-9 is a plot of the swath as it appears in a plane tangent to the ellipsoid at the reference swath center. The error in the z-direction varies radially from the spacraft nadir and is maximum at each end of the swath at a value of -720 m. This value is representative of the earth drop-off at swath end points. The swath thickness is 262 m, which is approximately that of the width of the plotted line at the scale of the figure.

In addition to overall swath geometry, an important feature of the scanner, both radiometrically and geometrically, is its IFOV projection. Figure A-10 illustrates the layout of adjacent resolution-element stacks for two subsequent swaths at three regions in the swath. The spacecraft latitude was approximately 30 degrees. There are four

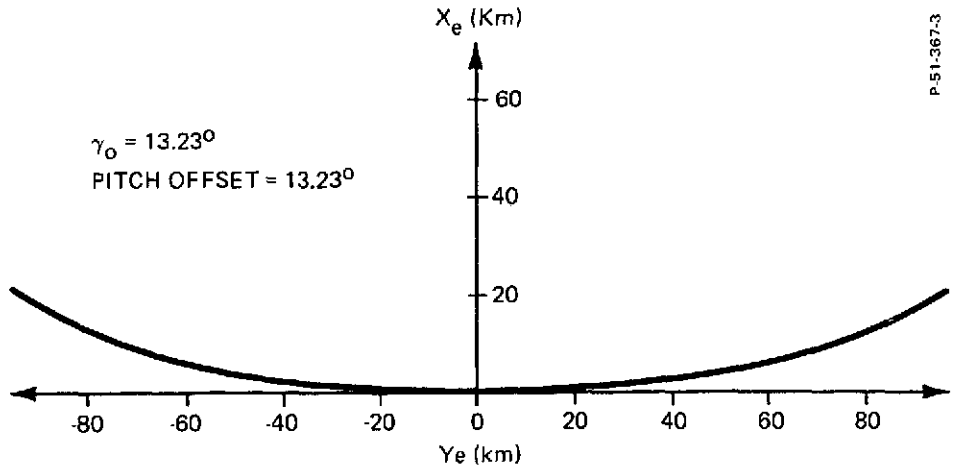

Figure A-9 - Swath Geometry in Local Coordinates

possible situations which might arise with respect to the IFOVs: (1) no coverage, (2) single element coverage, (3) two-element coverage and, (4) three-element coverage. In Figure A-10, only four detector IFOV are annotated to illustrate the above categorized phenomena. It is apparent that the greatest single difference between the western and eastern ends is the effect of earth rotation which produces overlapping and underlapping, respectively. With increasing slant range, the constant angular-width IFOV projects a larger area on the earth. Since the sampling interval was picked to provide adjacency at swath center, there will be overlap at all other points with the most severe at swath ends. This effect is manifested by the four small rectangular areas of two-element coverage on the eastern and western sides. Note that the swath center is affected only by earth rotation which produces a shear of the detector arrays with no overlap. A unique effect caused by earth rotation on the western side is the appearance of small areas where three-element coverage occurs.

Figure A-11 illustrates the layout of IFOVs at the terminator of 81 degrees latitude for the same portions of the swaths. Comparison with Figure A-10 reveals that earth rotation perpendicular to the spacecraft motion is not present, which is to be expected since the heading is due west. Nonetheless, overlap due to increased slant range is the same. However, since the earth rotation is parallel to but opposite spacecraft motion, an increase in along-track IFOV overlap is present. This effect is present at swath center as well, while the earlier shear is missing.

Figure A-12 illustrates the layout of IFOVs at the equator for the three sections mentioned previously. It may be contrasted with Figure A-10; most phenomena are present, but to a greater or lesser degree.

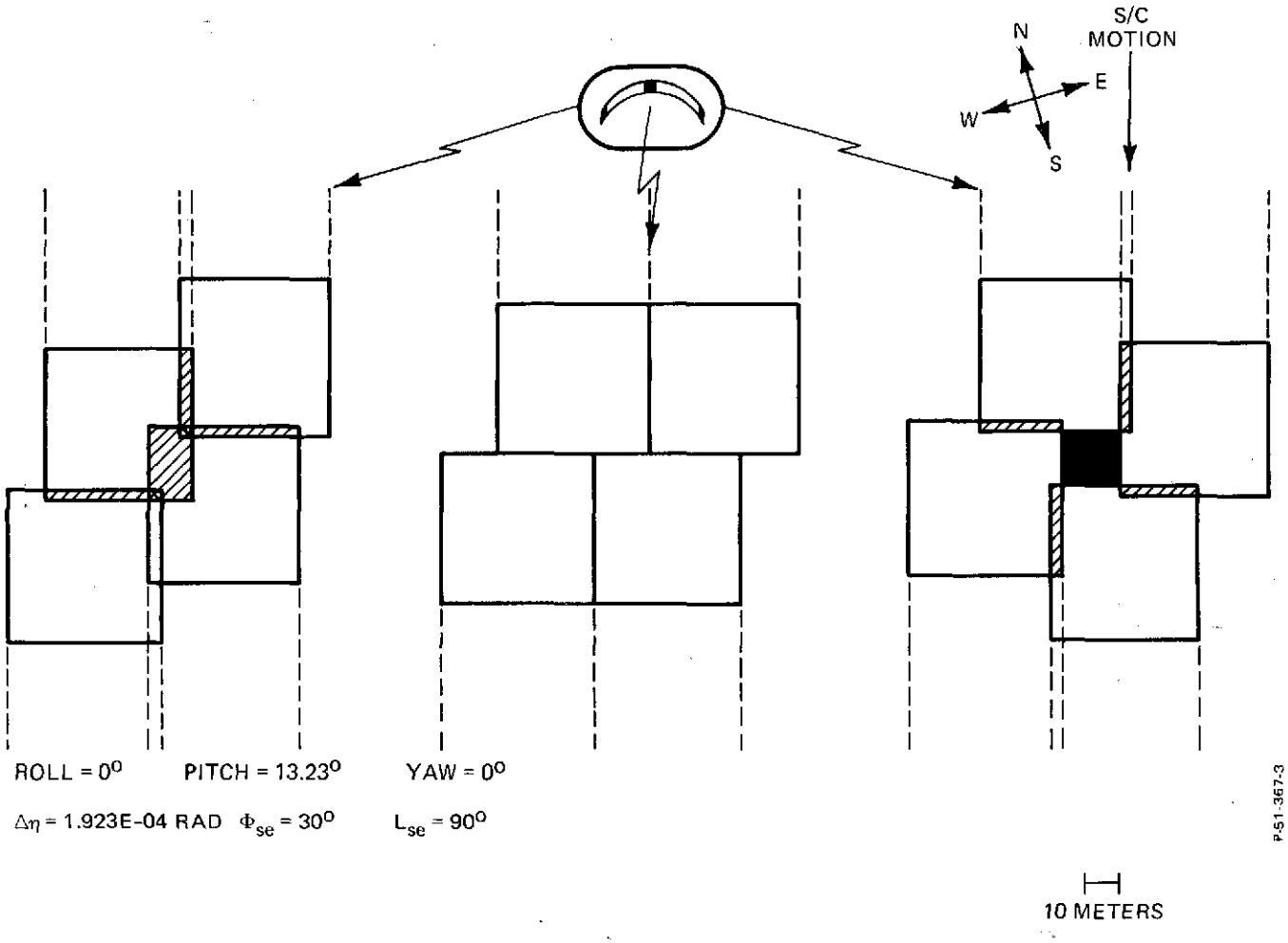

Figure A-10 - IFOV Geometry at 30° Latitude Under Normal Operation

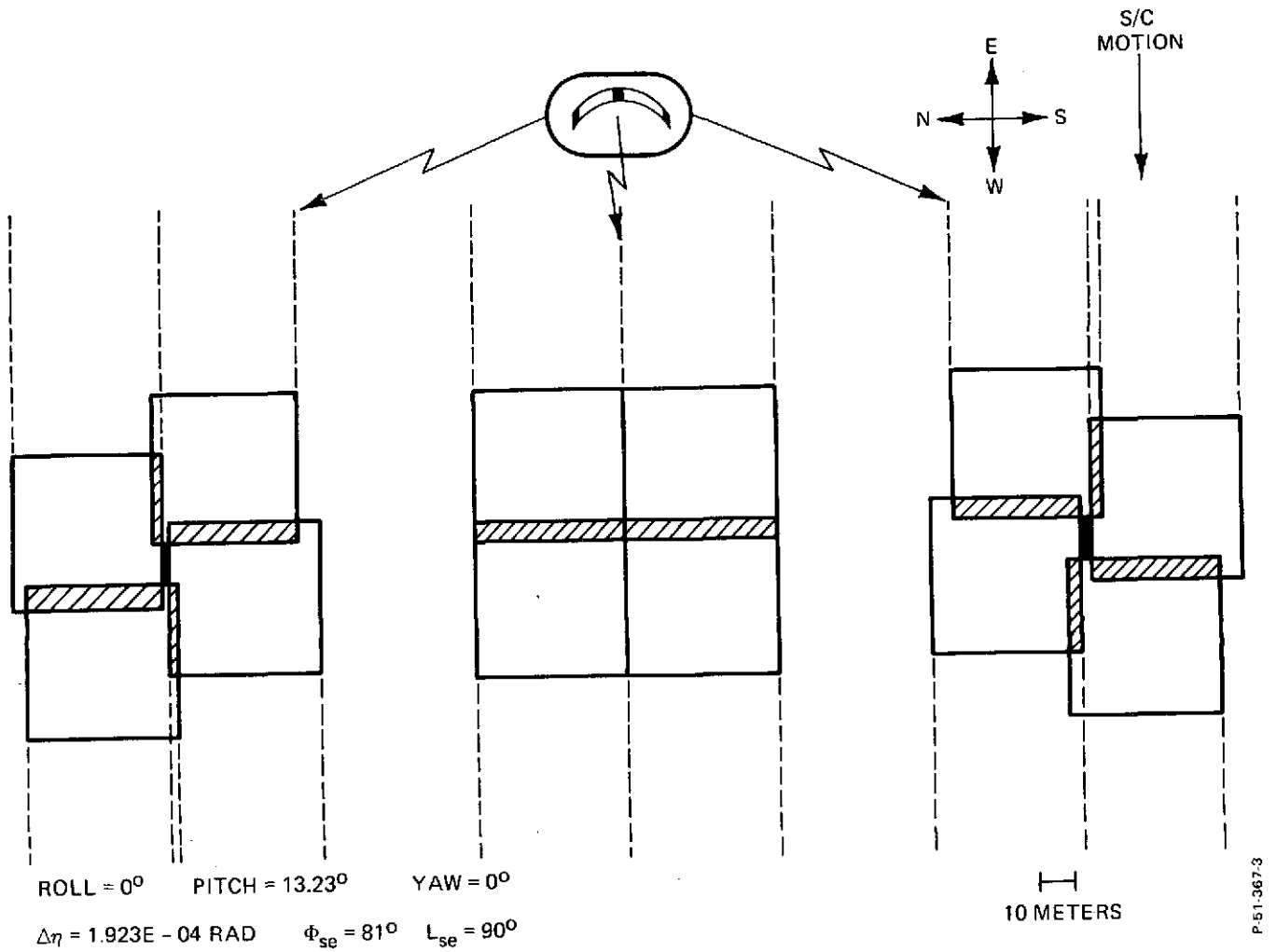

Figure A-11 - IFOV Geometry at Terminator Under Normal Operation

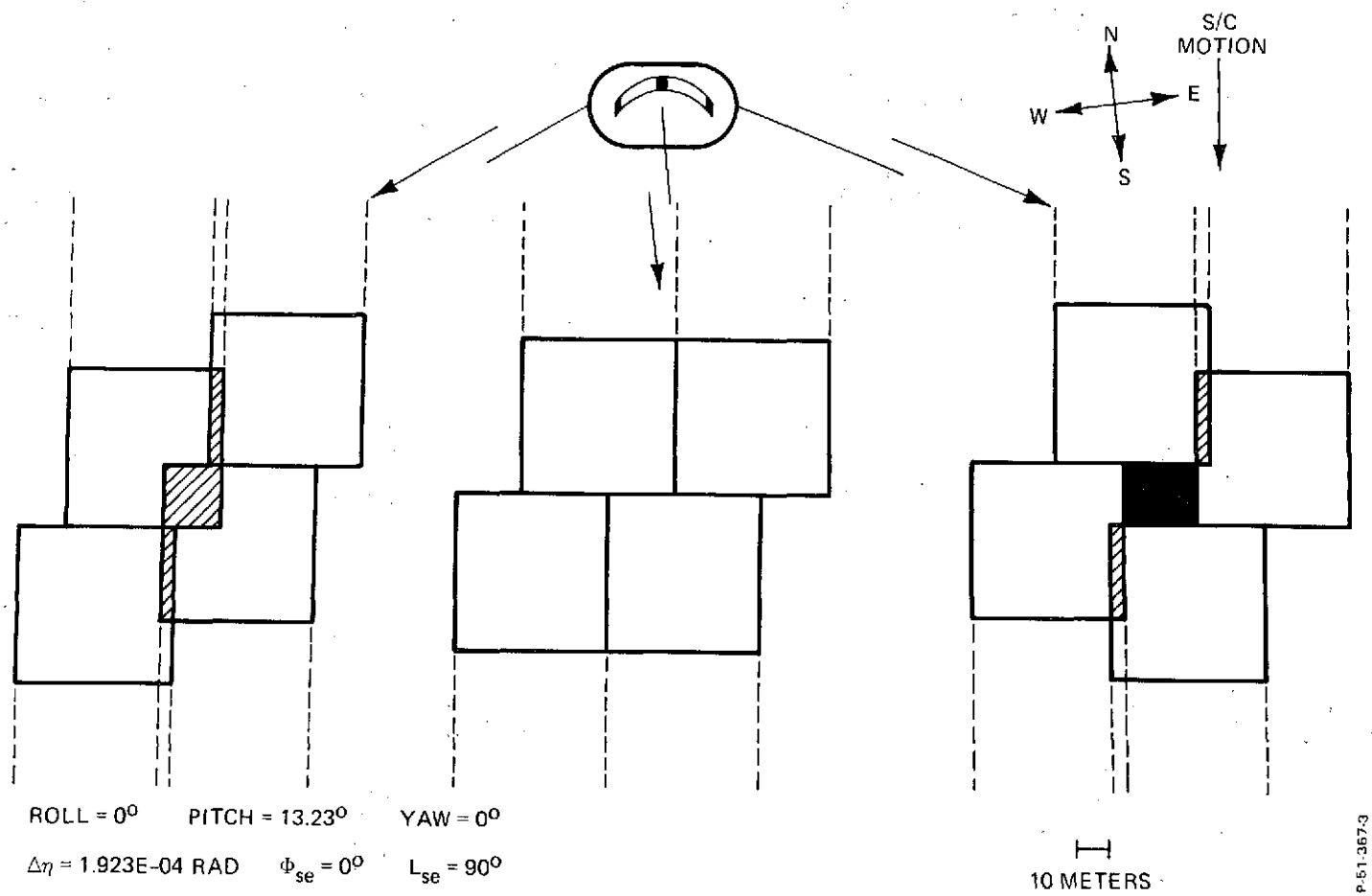

Figure A-12 - IFOV Geometry at Equator During Normal Operation

The major feature lacking in Figure A-12 is the cell overlap along the horizontal edges of the IFOVs caused by earth rotation. Since the normal component to earth rotation is minimum at the equator, the disappearance of the overlap is expected. This figure represents a worst case insofar as earth-rotation shear effects are concerned.

As a means of minimizing earth rotation effects, the sensor may be yawed to produce a more southerly heading. The required yaw varies with latitude and the effects cannot be eliminated at all points in the swath. Figure A-13 illustrates the effect of a 3.5-degree yaw which is that value required at 30 degrees latitude. The ends still exhibit earth rotation effects although the situation at swath center is ideal. Maintaining the yaw at 3.5 degrees, the IFOV layout at 81 degrees latitude was explored to see what adverse effects would occur. Figure A-14 illustrates what amounts to an overcorrected yaw since no transverse earth rotation components exists for the spacecraft at that latitude. At the equator, the 3.5 degree yaw compensation would reduce the over- and underlap, but not to the same extent as for 30 degrees latitude.

As a final check of IFOV geometry, a 20 degree eastward roll offset was incorporated at 30 degrees latitude. Figure A-15 illustrates the three sections of the swaths used in the previous figures. Earth rotation and slant-range expansion are severe in the far eastern side and at swath center with only moderate distortion at the near eastern side. Note that the near eastern side has more three-element coverage compared to Figures A-10 and A-14.

Another area of investigation of conical scanner geometry on ground point mapping was the projection of two latitude-longitude grids to sensor coordinates. The analytical procedure developed in the previous sectionwas used in performing the transformation. Figure A-16 shows how a grid of latitude-longitudeliness would appear if the sensor data were to be printed sequentially in time across the swath and sequentially in swath number in the along-track direction. The grid is centered at 30 degrees latitude, with equal spacing of about 28 minutes of arc in latitude and longitude. Figure A-17 is a representation of a grid mapping at 81 degrees latitude where latitude lines are much further spaced in distance than longitude lines, although the spacings are equal in arc minutes. It is apparent that the spacecraft heading has changed by about 75 degrees. The swath curvature still produces a bowed distortion in the grid as it would be printed.

This section has discussed the basic imaging geometry of the conical scanner as well as providing graphical illustrations of swath structure, IFOV projection, and grid mapping. The overall interaction of the rotating earth with the conical scan sensor has been characterized. It is hoped that this information will serve as an aid in estimating the degree of geometric correction required, and in understanding the problem of the geometric relationship between sensor and earth.

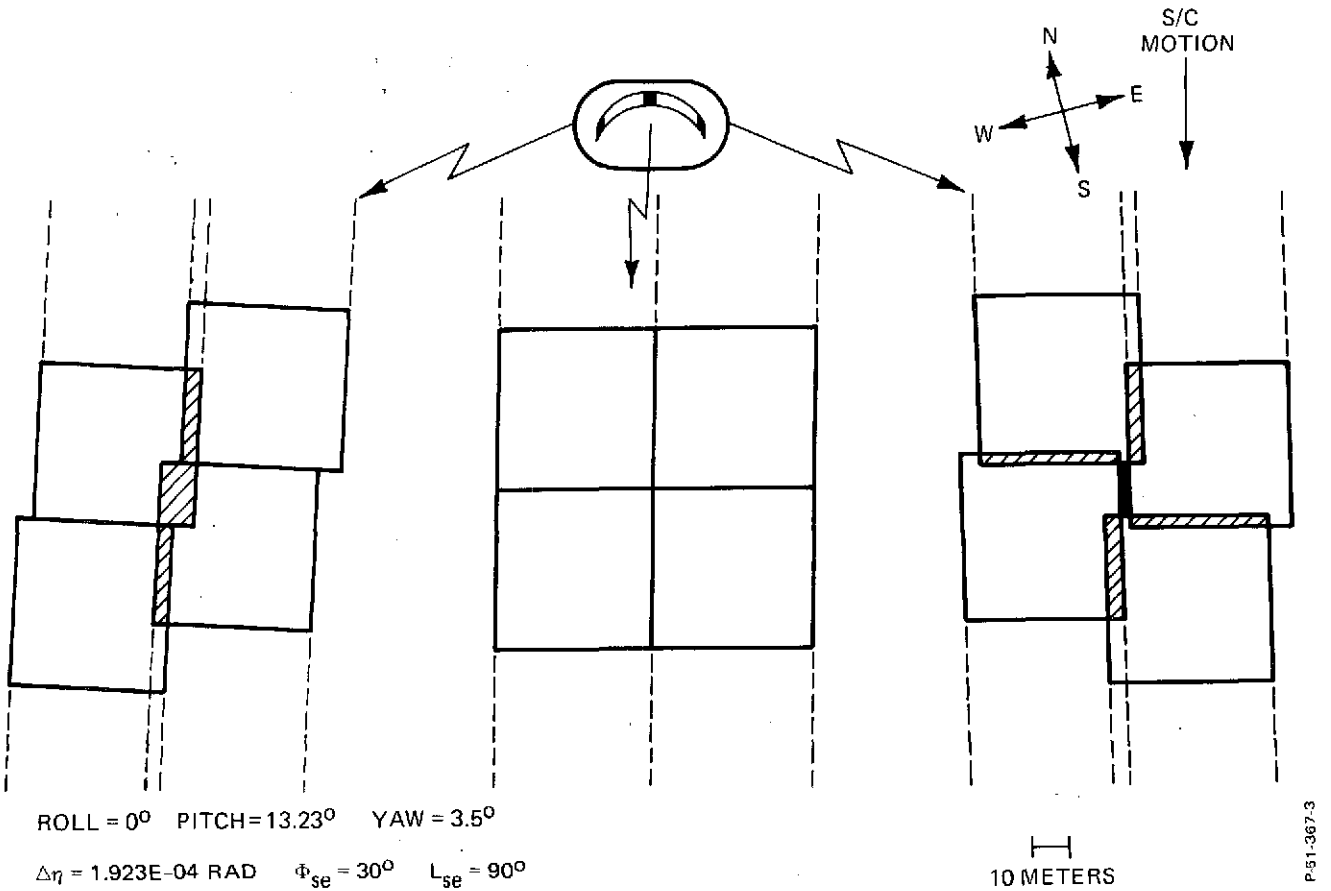

Figure A-13 - IFOV Geometry for Yaw Compensation at 30° Latitude

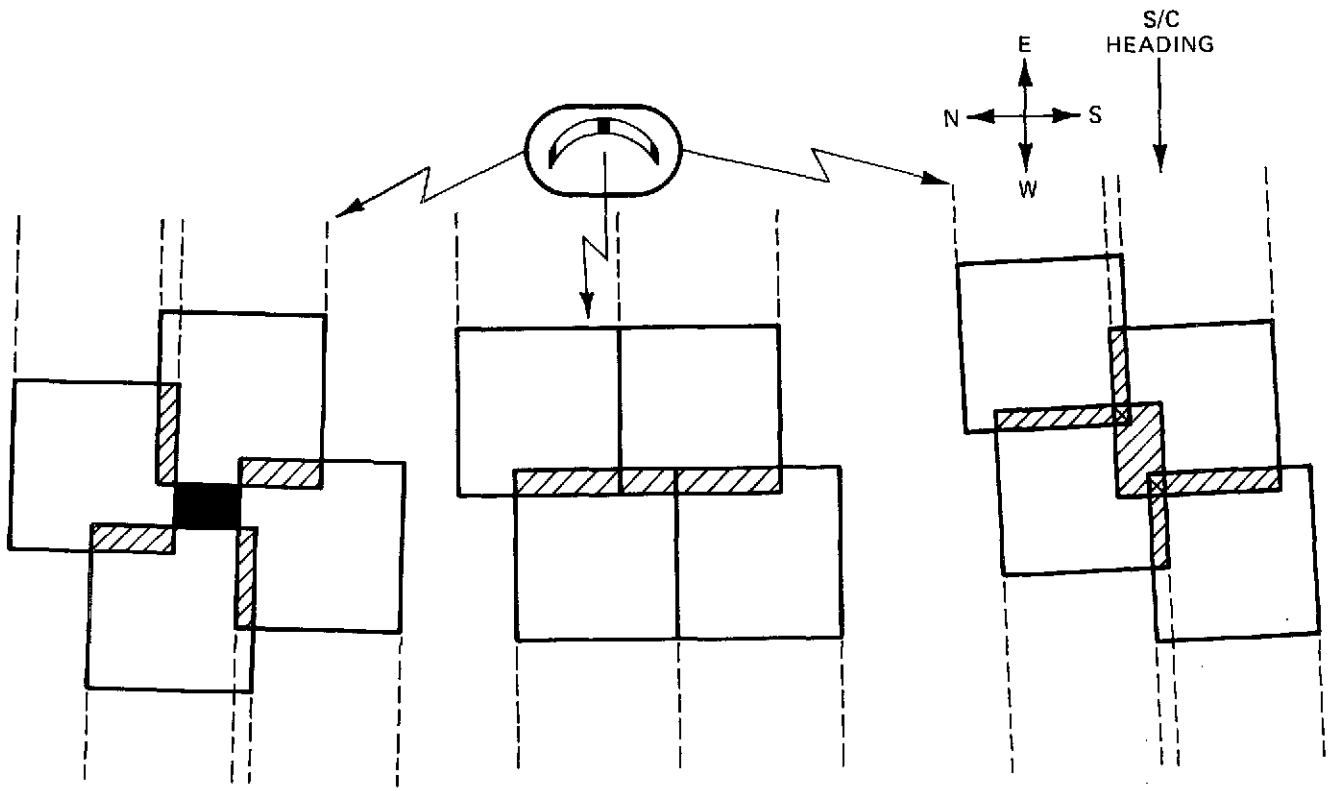

Figure A-14 - IFOV Geometry at Terminator for Yaw Compensation at 30° Latitude

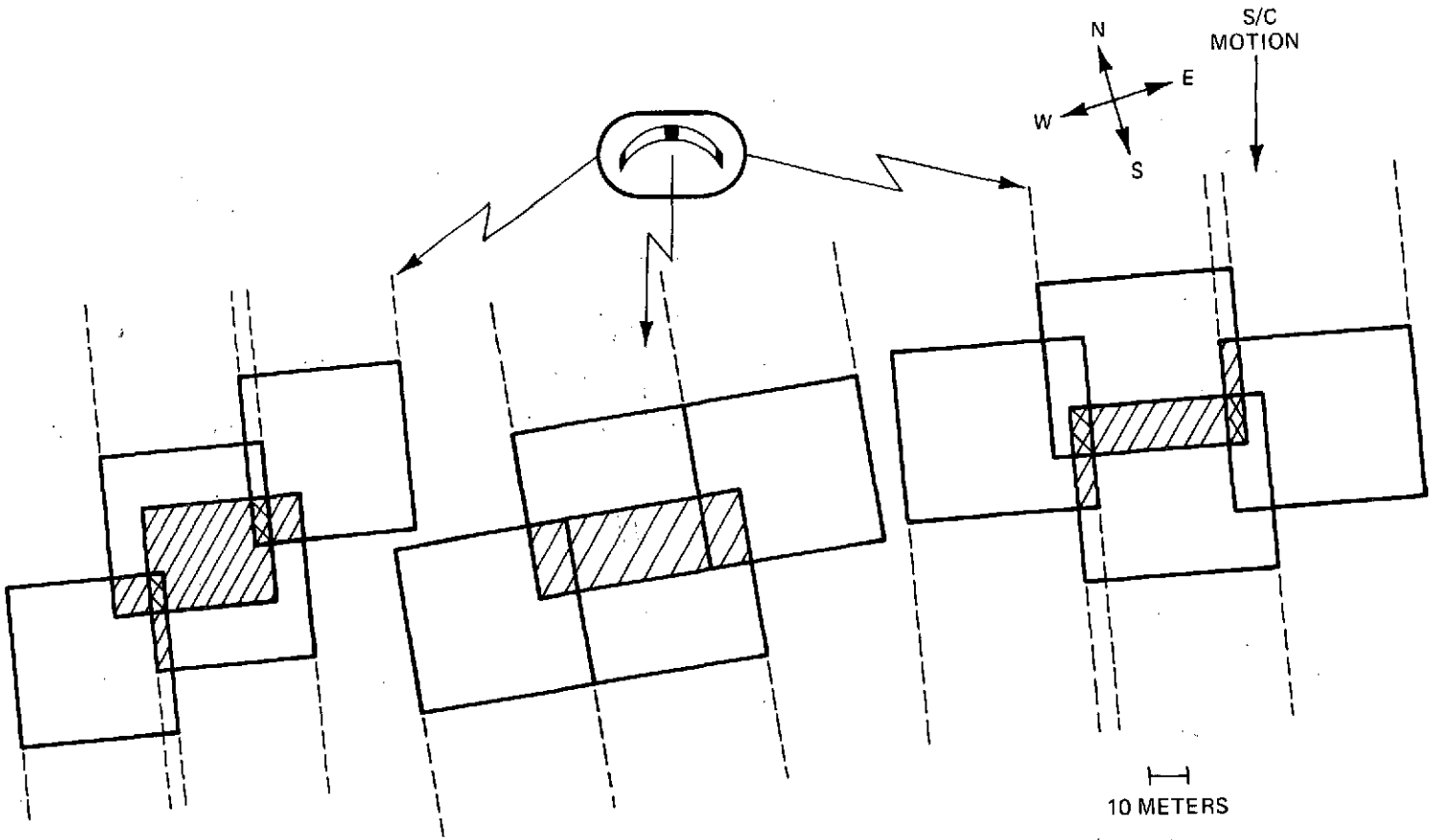

Figure A-15 - IFOV Geometry for a Roll Offset at 20°

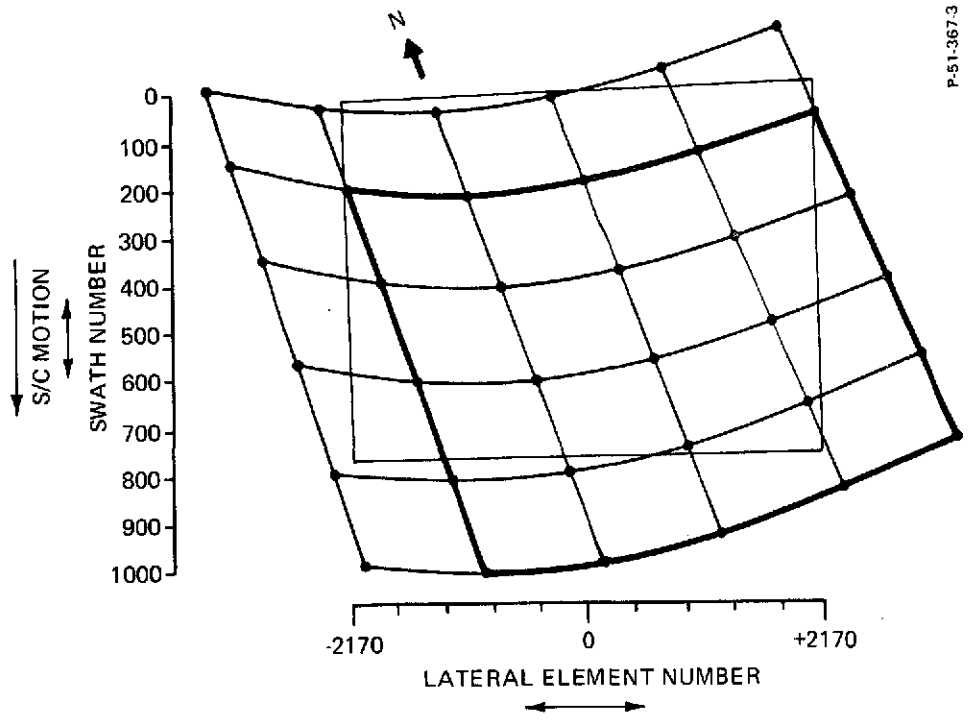

Figure A-16 - Latitude-Longitude Grid Mapping at 30° Latitude

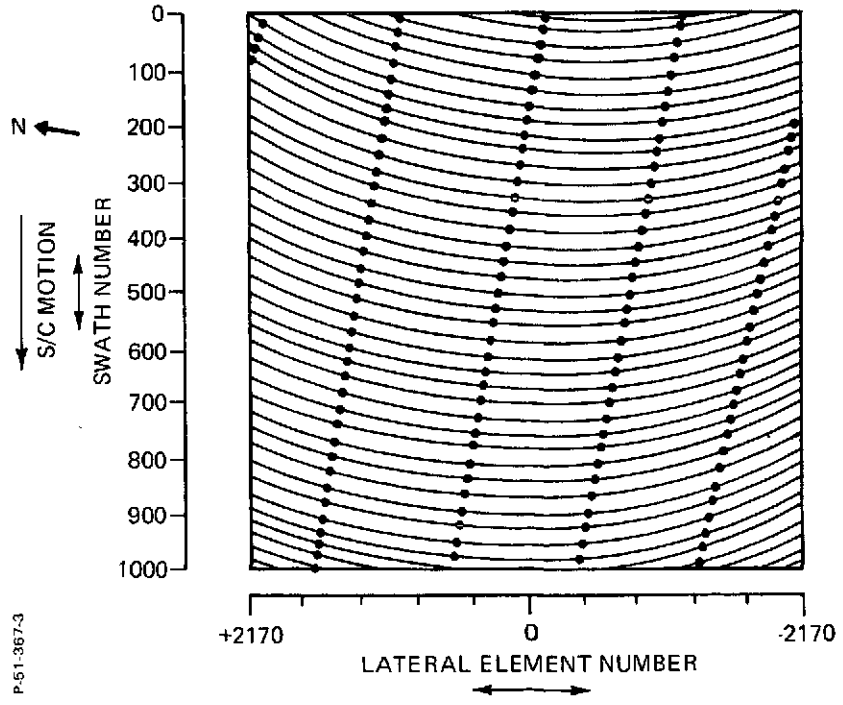

Figure A-17 - Latitude-Longitude Grid Mapping at 81° Latitude

A.5 PROGRAM LISTINGS

Printed teleprinter listings of the image-to-earth and earth-to-image computer programs are presented on the following pages. Each program is prefaced by a long explanatory paragraph. The program was written in Fortran for the SBC "Call 370" time-sharing service.

```
100 "      THIS SUBROUTINE CALCULATES THE INSTANTANEOUS LOCATION
110 "ON THE EARTH OF THE FOUR CORNERS OF THE IFOV OF A CONICAL
120 "SCANNER.  IN ORDER THAT THESE POINTS BE LOCATED, ALL S/C
130 "ORIENTATION ELEMENTS (ATTITUDES, ATTITUDE RATES, AND ATTI-
140 "TUDE ACCELERATIONS, AND ALTITUDE) MUST BE KNOWN AT SOME
150 "TIME AND THE NUMBER OF SWATHS AND RESOLUTION ELEMENTS LATER
160 "OR EARLIER AT WHICH THE IFOV LOCATION IS DESIRED.  THE PRO-
170 "GRAM WAS DEVELOPED FOR A SPECIFIC SET OF ORBITAL PARAMETERS
180 "ALTHOUGH THEY MAY EASILY BE ALTERED INTERNALLY.  GIVEN THE
190 "GEOMETRIC BOUNDS ON THE EARTH, THE CONICAL SCANNER PARAMETERS
200 "WERE DERIVED USING THE ASSUMED ORBITAL DATA BY ITERATION WITH
210 "THE PROGRAM.
220 "      AS PRESENTLY ARRANGED, THE ORBIT IS CIRCULAR WITH AN
230 "ORBITAL RADIUS OF 7358288 M MOVING AT A CONSTANT TANGENTIAL
240 "VELOCITY OF 7400 M/SEC.  THE ORBITAL INCLINATION WAS ASSUMED
250 "TO BE 81 DEG WITH THE S/C HEADING AT THE EQUATOR BEING EITHER
260 "SW OR NE.  THE EARTH WAS ASSUMED TO BE A ROTATING ELLIPSOID
270 "WITH A PERIOD OF 23 HR, 56 MIN, 4 SEC AND A SEMI-MAJOR AXIS
280 "OF 6378388 M.  THE CONICAL SCANNER CURRENTLY HAS A HALF-
290 "CONE ANGLE OF 13.23 DEG YIELDING A SWATH OF 185 KM ON THE
300 "EARTH FOR AN ACTIVE SCAN ANGLE OF + OR -24 DEG WITH THE
310 "ORBITAL DATA GIVEN ABOVE.
320 "      FOR EACH OF THE VISIBLE BANDS, THERE ARE SIX DETECTORS
330 " WHICH SIMULTANEOUSLY SENSE THE EARTH, CONSEQUENTLY, EACH
340 "SWATH IS COMPOSED OF SIX RESOLUTION ELEMENT TRACKS.  THE
350 "ANGULAR WIDTH OF THE ELEMENTS IN THE ALONG TRACK DIRECTION
360 "WAS ASSUMED TO BE 44 MICRORAD WHICH AT THE ASSUMED MEAN
370 "ALTITUDE YIELDED A CELL 43.4 M LONG.  THE CELL WIDTH IN
380 "THE CROSS TRACK DIRECTION WAS DETERMINED BY THE SAMPLE RATE
390 "OF THE DETECTOR ARRAY.  THE SAMPLE RATE CAN ONLY BE DETER-
400 "MINED IF THE TOTAL SWATH SCAN TIME IS KNOWN AND THE DUTY
410 "CYCLE OF THE SCANNER IS GIVEN.  THE TIME BETWEEN SWATHS WAS
420 "DETERMINED BE ITERATIVELY FINDING THE TIME NECESSARY TO BE
430 "ABLE TO PRODUCE ADJACENCY IN THE ALONG TRACK DIRECTION AT
440 "SWATH CENTER FOR SOME NOMINAL LATITUDE.  THIS TIME WAS
450 "FOUND TO BE .040105 SEC, AND COUPLED WITH A DUTY CYCLE OF
460 "80%, THE SWATH SCAN TIME WAS .016042 SEC.  THE SAMPLE PER-
470 "IOD WAS THUS 3.7 MICROSEC AT EQUAL INCREMENTS OF 1.923E-04
480 "RAD POLAR ANGLE WHICH YIELDED 4357 SAMPLES PER SWATH BEFORE
490 "MULTIPLYING BY THE 6 RESOLUTION ELEMENTS.
500 "      THE PROGRAM IS ORGANIZED SO THAT VARIOUS S/C OR SENSOR
510 "CONFIGURATIONS MAY BE SIMULATED, E.G. CIRCULAR SCAN, PITCH
520 "DOWN, OR PITCH UP.  THE LATER TWO ARE COMMONLY REFERRED TO
530 "AS NADIR SCANNING SINCE THE S/C NADIR POINT IS ALSO A DATA
540 "POINT.  IN ADDITION, ROLL OFFSET MANEUVERS MAY BE PERFORMED
550 "WHEREBY REGIONS TO THE LEFT OR RIGHT OF THE NORMAL SENSING
```

```
560 "AREA MAY BE INTERROGATED, HOWEVER, CARE SHOULD BE TAKEN TO
570 "ENSURE THAT IF A PITCH DOWN OR PITCH UP CONFIGURATION IS
580 "IN USE, THE PITCH VALUE IS MODIFIED TO FORCE THE SWATH
590 "CENTER TO LIE ON AN AXIS TRANSVERSE TO SENSOR LOCATION
600 "SINCE THE TRANSFORMATION MATRIX WITHIN THE PROGRAM USES
610 "TRUE EULER ROLL, PITCH, AND YAW ANGLES.
620 "      AS PRESENTLY ARRANGED, INPUT TO THE PROGRAM IS DONE
630 "THROUGH A DATA FILE LABELED 'FILL'.  FIVE PARAMETERS ARE
640 "PRESENTLY TRANSFERRED, SWATH NUMBER (1 OR 2), RESOLUTION
650 "ELEMENT NUMBER (+2178 TO -2178), CORNER NUMBER OF THE IFOV
660 "OF INTEREST (1 TO 4), PITCH ANGLE FOR NADIR OR CIRCULAR
670 "SCANNING, AND ROLL OFFSET.
680 "      ATTITUDES, ATTITUDE RATES, AND ATTITUDE ACCELERATIONS
690 "ARE NOT INPUTTED ALTHOUGH BY MODIFYING THE 'READ' STATE-
700 "MENT, THEY CAN BE.  ON THE EARTH, FACING IN THE DIRECTION
710 "OF INSTANTANEOUS S/C HEADING, THE CORNERS OF THE IFOV ARE
720 "LABELLED AS 1 FOR THE LEFT-BACK, 2 FOR THE RIGHT BACK,
730 "3 FOR THE LEFT FRONT, AND 4 FOR THE RIGHT FRONT. AS PRE-
740 "SENTLY ARRANGED ONLY TWO ADJACENT SWATHS MAY BE EXAMINED,
750 "ALTHOUGH WITH SOME MODIFICATIONS MANY SWATHS MAY BE
760 "TREATED
770 "      THE OUTPUT FROM THE PROGRAM CONSISTS OF 3 CATEGORIES,
780 "1) S/C DATA AT THE CENTER OF SWATH 1, 2) S/C DATA WHEN THE
790 "POINT IN QUESTION WAS SENSED, AND 3) LOCATION OF THE POINT
800 "ON THE EARTH IN TWO COORDINATE SYSTEMS.  OUTPUT 1 OF THE
810 "PROGRAM CONSISTS OF S/C LATITUDE, UNCERTAINTY IN THE ALT-
820 "ITUDE, ALTITUDE, LONGITUDE, LONGITUDE OF THE ORBITAL PLANE
830 "TERMINATOR, AND THE HEADING OF THE S/C.  OUTPUT 2 CONSISTS
840 "OF S/C LATITUDE, ALTITUDE, ORBITAL PLANE ANGLE MEASURED
850 "FROM THE TERMINATOR, AND ALTITUDE UNCERTAINTY.  OUTPUT 3
860 "CONSISTS OF LATITUDE AND LONGITUDE OF THE EARTH BASED POINT,
870 "(XEE,YEE,ZEE) COORDINATES IN A CARTESIAN SYSTEM TANGENT TO
880 "THE EARTH'S ELLIPSOID AT THE CENTER OF SWATH 1.  ALL CAL-
890 "CULATIONS ARE DONE IN DOUBLE PRECISION MODE AND ALL DIS-
900 "TANCES ARE MEASURED IN METERS, ALL TIMES IN SECONDS, AND
910 "ANGLES IN RADIANS (EXCEPT FOR IO WHEN DEGREES ARE USED).
920 "
930 "
940 "                    DEFINITION OF MAIN VARIABLES
950 "
960 "
970 "A=SEMI-MAJOR AXIS OF THE EARTH
980 "DGR=CONVERTS DEGREES TO RADIANS
990 "BETA=PITCH VARIABLE USED TO PRODUCE NADIR SCANNING
1000 "THETA=ROLL VARIABLE USED TO PRODUCE ROLL OFFSET
1010 "ECCN=ECCENTRICITY OF THE EARTH
1020 "GAMMA=HALF-CONE ANGLE OF THE SCANNER
1030 "ALP=COMPLEMENT OF ORBITAL INCLINATION
```

```
1040 "VO=TANGENTIAL VELOCITY OF S/C
1050 "RO=RADIUS OF ORBIT FROM CENTER OF EARTH
1060 "C1=ROTATION RATE OF THE EARTH
1070 "C3=CONSTANT USED TO DETERMINE RATE OF CHANGE OF ORBITAL ANGLE
1080 "      (MEASURED FROM THE CENTER OF THE EARTH)
1090 "TO=TIME TO SCAN ONE-HALF SWATH
1100 "CO=ANGULAR SCAN RATE OF SENSOR
1110 "B=SEMI-MINOR AXIS OF THE EARTH
1120 "THO=ORBITAL ANGLE DEFINED AS THE ANGLE SUBTENDED BY TWO
1130 "      LINES, ONE DRAWN FROM THE CENTER OF THE EARTH TO THE
1140 "      TERMINATOR AND ONE DRAWN FROM THE CENTER OF THE EARTH
1150 "      TO THE INSTANTANEOUS LOCATION OF THE S/C
1160 "XLSEO=LONGITUDE OF S/C AT SWATH 1 CENTER
1170 "PHISO=LATITUDE OF S/C AT SWATH 1 CENTER
1180 "HSEO=ALTITUDE OF S/C AT SWATH 1 CENTER
1190 "DELT=UNCERTAINTY IN S/C ALTITUDE AT SWATH 1 CENTER
1200 "XLPK=LONGITUDE OF TERMINATOR AT SWATH 1 CENTER
1210 "XKAPPO=YAW AT SWATH 1 CENTER
1220 "PHID=PITCH RATE AT SWATH 1 CENTER
1230 "PHIDD=PITCH ACCELERATION AT SWATH 1 CENTER
1240 "XKAPD=YAW RATE AT SWATH 1 CENTER
1250 "XKAPDD=YAW ACCELERATION AT SWATH 1 CENTER
1260 "TOO=ONE-HALF SWATH SCAN TIME OR TIME BETWEEN SWATHS DEPENDING
1270 "      IF SWATH 1 OR 2 IS BEING EXPLORED
1280 "WO=ROLL AT SWATH 1 CENTER
1290 "WD=ROLL RATE AT SWATH 1 CENTER
1300 "ETA=POLAR ANGLE OF SCANNER
1310 "ELL=RESOLUTION ELEMENT NUMBER (-2178 TO +2178)
1320 "WDD=ROLL ACCELERATION AT SWATH 1 CENTER
1330 "T=TIME MEASURED FROM THE START OF SWATH 1
1340 "PHIT=TIME VARYING CONTRIBUTION OF PITCH
1350 "XKAPT=TIME VARYING CONTRIBUTION OF YAW
1360 "WT=TIME VARYING CONTRIBUTION OF ROLL
1370 "PHI=NET INSTANTANEOUS PITCH
1380 "W=NET INSTANTANEOUS ROLL
1390 "XKAPPA=NET INSTANTANEOUS YAW
1400 "A(I,J)=TRANSFORMATION COEFFICIENTS FROM S/C ORIENTATION TO
1410 "      COORDINATE SYSTEM TANGENT TO THE ELIIPSOID
1420 "THT=INSTANTANEOUS ORBITAL ANGLE
1430 "XLSE=S/C LONGITUDE AT T
1440 "PHISE=S/C LATITUDE AT T
1450 "HSE=S/C ALTITUDE AT T
1460 "B(I,J)=TRANSFORMATION COEFFICIENTS FROM LOCAL COORDINATES TO
1470 "      GEOCENTRIC
1480 "XEE=X-COORDINATE OF POINT IN TANGENT PLANE SYSTEM
1490 "YEE=Y-COORDINATE OF POINT IN TANGENT PLANE SYSTEM
1500 "ZEE=Z-COORDINATE OF POINT IN TANGENT PLANE SYSTEM
1510 "XLAT=LATITUDE OF POINT BEING SENSED
```

```
1520 "XLNG=LØNGITUDE ØF PØINT BEING SENSED
1530 "ALPHA=HEADING ØF S/C AT T
1540 "AZØ=HEADING ØF S/C AT SWATH 1 CENTER
1550 "
1560 "
1570 "      THE TWØ SUBRØUTINES ARE LATLNG AND ASE WITH LATLNG
1580 "DETERMINING THE LATITUDE AND ALTITUDE ØF THE S/C FRØM
1590 "SØME GIVEN ØRBITAL ANGLE AND ASE DETERMINING THE HEADING ØF
1600 "THE S/C GIVEN SØME LATITUDE, ALTITUDE, AND ØRBITAL ANGLE
1610 REAL*8 GAMMA1,ETA1,BARG,ELL
1620 REAL*8 XLAT(18),XLNG(18),XEE(18),YEE(18),ZEE(18)
1630 REAL*8 A,DGR,ECCN,GAMMA,%
1640 BETA,THETA,ALP,V0,R0,C1,C3,T0,C0,B,TH0,XLSE0,PHIS0,HSE0,%
1641 "
1642 "
1643 "
1650 DELT,PHISD,XLPR,AZ0,XLPK,XLPKD,XX,XKAPP0,PHID,PHIDD,%
1660 XKAPD, XKAPDD,W0,WD,WDD,T,ETA,T00,CTX,CTY,CTZ,PHIT,XKAPT,%
1670 WT,PHI,W,XKAPPA,PHIE,C0N1,C0N2,C0N3,C0N4,C0N5,C0N6,A11,%
1680 A12,A13,A21,A22,A23,A31,A32,A33,CCX,CCY,CCZ,THT,THID,%
1690 XLSEP,XLSE,PHISE,HSE,B11,B12,B13,B21,B22,B23,B31,%
1700 B32,B33,E,UX,WX,R1,R2,R3,R4,R5,R6,BIGA,BIGB,BIGC,W1,U1,%
1710 V1,XLT,DIFF,AMT,P,EC0N2,EC0N,UP,VP,WP,UXX,WXX,ALPHA,HSEN
1720 A=6378388.
1730 CALL ØPEN(1,'FILL','INPUT')
1740 READ(1,*) NC0DE,ELL,NPT,BETA,THETA
1750 DGR=57.2957795131
1760 BETA=BETA/DGR
1770 THETA=THETA/DGR
1780 ECCN=0.082
1790 GAMMA=13.23/DGR
1800 ALP=9./DGR
1810 V0=7400.
1820 R0=7358288.
1830 C1=360./(86164.*DGR)
1840 C3=V0/R0
1850 T0=0.016042
1860 C0=48./(DGR*0.032084)
1870 B=A*DSQRT(1.-ECCN**2)
1880 TH0=60./DGR
1890 XLSE0=90./DGR
1900 CALL LATLNG(TH0,ALP,A,B,R0,ECCN,PHIS0,HSE0,DELT)
1910 PHISD=PHIS0*DGR
1920 30 XLPR=DATAN(DSIN(TH0)/(DC0S(TH0)*DSIN(ALP)))
1930 CALL ASE(A,ECCN,ALP,C3,C1,B,TH0,R0,PHIS0,HSE0,AZ0)
1940 XLPK=XLSE0-XLPR
1950 XLPKD=XLPK*DGR
1960 XX=XLSE0*DGR
```

```
1970 WRITE(6,*)PHISD,DELT,HSEO,XX,XLPKD,AZO
1980 XKAPPO=0.0612893939115
1990 PHID=0.0
2000 PHIDD=0.0
2010 XKAPD=0.0
2020 XKAPDD=0.0
2030 TOO=TO
2040 IF(NCODE.EQ.2) TOO=0.056147
2050 WO=0.0
2060 WD=0.0
2070 ETA=ELL*1.923E-04+9.615E-05
2080 WDD=0.0
2090 T=ETA/CO+TOO
2100 ETA1=ETA
2110 GAMMA1=GAMMA
2120 IF(NPT.EQ.4) GO TO 51
2130 IF(NPT-2) 50,51,53
2140 51 BARG=DCOS(GAMMA1)*(DCOS(4.4D-05)+DSIN(GAMMA1)*DSIN(ETA1)*%
2150 DSIN(4.4D-05)/DSQRT(1.-DSIN(ETA1)**2*DSIN(GAMMA1)**2))
2160 GAMMA=DATAN(DSQRT(1.-BARG**2)/BARG)
2170 BARG=DTAN(GAMMA1)*DCOS(ETA1)/DTAN(GAMMA)
2180 ETA=DATAN(DSQRT(1.-BARG**2)/BARG)
2190 IF(NPT.EQ.4) GO TO 53
2200 GO TO 50
2210 53 BARG=DCOS(GAMMA)*(DCOS(2.64D-04)+DSIN(GAMMA)*DCOS(ETA)*%
2220 DSIN(2.64D-04)/DSQRT(1.-DCOS(ETA)**2*DSIN(GAMMA)**2))
2230 GAMMA1=DATAN(DSQRT(1.-BARG**2)/BARG)
2240 BARG=DTAN(GAMMA)*DSIN(ETA)/DTAN(GAMMA1)
2250 ETA=DATAN(BARG/DSQRT(1.-BARG**2))
2260 GAMMA=GAMMA1
2270 50 IF((ETA1*ETA).LE.0.0) ETA=-ETA
2280 NSWAT=1
2290 NAB=1
2300 NSMAX=1
2310 NLOOP=1
2320 46 IF(NLOOP-1) 39,39,45
2330 39 CONTINUE
2340 48 ARG=DSQRT(1.0+(DCOS(GAMMA)/DSIN(GAMMA))**2)
2350 CTX=DCOS(ETA)/ARG
2360 CTY=-1.0*DSIN(ETA)/ARG
2370 CTZ=(DCOS(GAMMA)/DSIN(GAMMA))/ARG
2380 PHIT=PHISEO+PHID*(T-TO)+SIGN*PHIDD*(T-TO)**2/2.
2390 XKAPT=XKAPPO+XKAPD*(T-TO)+XKAPDD*(T-TO)**2/2.
2400 WT=WO+WD*(T-TO)+WDD*(T-TO)**2/2.
2410 PHI=PHIT+BETA
2420 W=WT+THETA
2430 XKAPPA=XKAPT
2440 PHIE=PHI
```

```
2450 CON1=DCOS(PHIE)
2460 CON2=DSIN(PHIE)
2470 CON3=DCOS(XKAPPA)
2480 CON4=DSIN(XKAPPA)
2490 CON5=DCOS(W)
2500 CON6=DSIN(W)
2510 A11=CON1*CON3-CON2*CON6*CON4
2520 A12=-CON5*CON4
2530 A13=CON2*CON3+CON1*CON6*CON4
2540 A21=CON1*CON4+CON2*CON6*CON3
2550 A22=CON5*CON3
2560 A23=CON2*CON4-CON1*CON6*CON3
2570 A31=-CON2*CON5
2580 A32=CON6
2590 A33=CON1*CON5
2600 CCX=(A11/CTX-A21/CTY)/(A23/CTY-A13/CTX)-(A11/CTX-A31/%
2610  CTZ)/(A33/CTZ-A13/CTX)
2620 CCY=(A22/CTY-A12/CTX)/(A23/CTY-A13/CTX)-(A32/CTZ-A12/%
2630  CTX)/(A33/CTZ-A13/CTX)
2640 CCZ=CCX*((A33/CTZ-A23/CTY)/(A32/CTZ-A22/CTY)-(A23/CTY%
2650  -A13/CTX)/(A22/CTY-A12/CTX))/((A21/CTY-A31/CTZ)/(A32/%
2660  CTZ-A22/CTY)-(A11/CTX-A21/CTY)/(A22/CTY-A12/CTX))
2670 THT=TH0+(V0/R0)*(T-T0)
2680 THID=THT*DGR
2690 XLSEP=DATAN(DSIN(THT)/(DCOS(THT)*DSIN(ALP)))
2700 XLSE=XLPK+XLSEP+C1*(T-T0)
2710 IF(XLSE-3.14159) 10,10,11
2720 11 XLSE=XLSE-6.2832
2730 10 CALL LATLNG(THT,ALP,A,B,R0,ECCN,PHISE,HSE,DELT)
2740 PHISD=PHISE*DGR
2750 2 WRITE(6,*)PHISD,HSE,THID,DELT
2760 CALL ASE(A,ECCN,ALP,C3,C1,B,THT,R0,PHISE,HSE,ALPHA)
2770 B11=DCOS(ALPHA)*DSIN(PHISE)
2780 B12=-DSIN(ALPHA)
2790 B13=-DCOS(ALPHA)*DCOS(PHISE)
2800 B21=DSIN(ALPHA)*DSIN(PHISE)
2810 B22=DCOS(ALPHA)
2820 B23=-DSIN(ALPHA)*DCOS(PHISE)
2830 B31=DCOS(PHISE)
2840 B32=0.0
2850 B33=DSIN(PHISE)
2860 E=A/DSQRT(1.0-ECCN**2*DSIN(PHISE)**2)
2870 UX=E*DCOS(PHISE)
2880 WX=E*(1.0-ECCN**2)*DSIN(PHISE)
2890 R1=(CCX*B11-CCY*B21)/(CCY*B23-CCX*B13)-(CCX*B11-CCZ*B31)%
2900  /(CCZ*B33-CCX*B13)
2910 R2=-CCX*(B11*UX+B13*WX)/(CCY*B23-CCX*B13)+CCX*(%
2920  B11*UX+B13*WX)/(CCZ*B33-CCX*B13)
```

```
2930 R3=(CCY*B22-CCX*B12)/(CCY*B23-CCX*B13)-(CCZ*B32-CCX*B12)%
2940  /(CCZ*B33-CCX*B13)
2950 R4=-CCY*(B21*UX+B23*WX)/(CCY*B23-CCX*B13)+CCZ*%
2960  (B31*UX+B33*WX+HSE)/(CCZ*B33-CCX*B13)
2970 R5=R1*((CCY*B23-CCX*B13)/(CCY*B22-CCX*B12)-(CCZ*B33-CCX*%
2980  B13)/(CCZ*B32-CCX*B12))/((CCX*B11-CCY*B21)/(CCY*B22-%
2990  CCX*B12)-(CCX*B11-CCZ*B31)/(CCZ*B32-CCX*B12))
3000 R6=R1*((-CCY*(B21*UX+B23*WX)+CCX*(B11*UX+B13*WX)%
3010  )/(CCY*B22-CCX*B12)-(-CCZ*(B31*UX+B33*WX+HSE)+CCX*%
3020  (B11*UX+B13*WX))/(CCZ*B32-CCX*B12))/((CCX*B11-CCY*%
3030  B21)/(CCY*B22-CCX*B12)-(CCX*B11-CCZ*B31)/(CCZ*B32-CCX*%
3040  B12))+R2
3050 BIGA=1.Ø/B**2+(R5**2/A**2)*(1./R1**2+1./R3**2)
3060 BIGB=(2.*R5/A**2)*((R6-R2)/R1**2+(R6-R4)/R3**2)
3070 BIGC=(R6-R2)**2/(A**2*R1**2)+(R6-R4)**2/(A**2*R3**2)-1.Ø
3080 W1=(-BIGB+DSQRT(BIGB**2-4.*BIGA*BIGC))/(2.*BIGA)
3090 U1=(1./R1)*(R5*W1+R6-R2)
3100 V1=(1./R3)*(R5*W1+R6-R4)
3110 3 DIFF=DATAN(V1/U1)
3120 XLT=XLSE-DIFF
3130 DIFF=DIFF*DGR
3140 NSUB=(NSWAT-1)*16+NLOOP+(NAB-1)*8
3150 XLNG(NSUB)=XLT*DGR
3160 AMT=W1/DSQRT(A**2*(1.-ECCN**2)**2+ECCN**2*W1**2)
3170 P=DATAN(AMT/DSQRT(1.-AMT**2))
3180 XLAT(NSUB)=P*DGR
3190 ECON2=A/DSQRT(1.-ECCN**2*DSIN(P)**2)
3200 ECON=A/DSQRT(1.-ECCN**2*DSIN(PHISO)**2)
3210 UP=ECON2*DCOS(P)*DCOS(XLSE0-XLT)
3220 VP=ECON2*DCOS(P)*DSIN(XLSE0-XLT)
3230 WP=ECON2*(1.-ECCN**2)*DSIN(P)
3240 UXX=ECON*DCOS(PHISO)
3250 WXX=ECON*(1.-ECCN**2)*DSIN(PHISO)
3260 B11=DCOS(AZO)*DSIN(PHISO)
3270 B12=-DSIN(AZO)
3280 B13=-DCOS(AZO)*DCOS(PHISO)
3290 B21=DSIN(AZO)*DSIN(PHISO)
3300 B22=DCOS(AZO)
3310 B23=-DSIN(AZO)*DCOS(PHISO)
3320 B31=DCOS(PHISO)
3330 B33=DSIN(PHISO)
3340 XEE(NSUB)=B11*(UP-UXX)+B12*VP+B13*(WP-WXX)
3350 YEE(NSUB)=B21*(UP-UXX)+B22*VP+B23*(WP-WXX)
3360 ZEE(NSUB)=B31*(UP-UXX)+B32*VP+B33*(WP-WXX)
3370 T=T+Ø.Ø22222222
3380 NLOOP=NLOOP+1
3390 GO TO 46
3400 45 WRITE(6,*)XLAT(1),XLNG(1),XEE(1),YEE(1),ZEE(1)
```

```
3410 STOP
3420 END
3430 SUBROUTINE LATLNG(THT,ALP,A,B,RO,ECCN,PHISE,HSE,DELT)
3440 REAL*8 THT,ALP,A,B,RO,ECCN,PHISE,HSE,DELT,HSEN
3450 HSEN=979000.
3460 NCT=1
3470 1 PHISE=DATAN(((A**2+A*HSEN)/(B**2+A*HSEN))*(DCOS(THT)*DCOS%
3480  (ALP)/DSQRT(DSIN(THT)**2+DCOS(THT)**2*DSIN(ALP)**2)))
3490 HSE=RO*DCOS(THT)*DCOS(ALP)/DSIN(PHISE)-A*(1.-ECCN**2)/DSQRT%
3500  (1.-ECCN**2*DSIN(PHISE)**2)
3510 DELT=DABS(HSEN-HSE)
3520 IF(DELT-1.0) 2,2,13
3530 13 IF(NCT-20) 14,2,2
3540 14 HSEN=HSE
3550 NCT=NCT+1
3560 GO TO 1
3570 2 RETURN
3580 END
3590 SUBROUTINE ASE(A,ECCN,ALP,C1,C2,B,THT,RO,PHISE,HSE,AZ)
3600 REAL*8 XO,YO,ZO,A,ECCN,ALP,C1,C2,B,THT,RO,PHISE,HSE,AZ,%
3610 EPP,PHO,X,Y,Z,UARG,C11,C22,C12,C21,C13,C23,PHISET,PHOT,%
3620 EPPT,XT,YT,ZT,CCC1,CCC2,ZETA,XETA,YETA,P1,P2,P3,DOT
3630 XO=RO*DSIN(THT)
3640 YO=RO*DCOS(THT)*DSIN(ALP)
3650 ZO=RO*DCOS(THT)*DCOS(ALP)
3660 EPP=A/DSQRT(1.-ECCN**2*DSIN(PHISE)**2)
3670 PHO=DATAN(DSIN(THT)/(DCOS(THT)*DSIN(ALP)))
3680 X=EPP*DCOS(PHISE)*DSIN(PHO)
3690 Y=EPP*DCOS(PHISE)*DCOS(PHO)
3700 Z=EPP*(1.-ECCN**2)*DSIN(PHISE)
3710 UARG=((A**2+A*HSE)/(B**2+A*HSE))*(DCOS(THT)*DCOS(ALP)/DSQRT%
3720  (DSIN(THT)**2+DCOS(THT)**2*DSIN(ALP)**2))
3730 C11=1.0
3740 C22=1.0
3750 C12=RO*DCOS(THT)*DCOS(ALP)*DCOS(PHISE)/DSIN(PHISE)**2+A*(%
3760  1.-ECCN**2)*ECCN*ECCN**2*DSIN(PHISE)*DCOS(PHISE)/(DSQRT(1.-%
3770  ECCN**2*DSIN(PHISE)**2))**3
3780 C21=(1./(1.+UARG**2))*(A*(A**2-B**2)/(B**2+HSE*A)**2)
3790 C13=-RO*DSIN(THT)*DCOS(ALP)/DSIN(PHISE)
3800 C23=((A**2+A*HSE)/(B**2+A*HSE))*(1./(1.+UARG**2))*(-DCOS%
3810 (ALP)*DSIN(THT)/(DSQRT(DSIN(THT)**2+DCOS(THT)**2*DSIN(ALP)%
3820 **2))**3)
3830 PHISET=((C13-C23*C11/C21)/(C12-C22*C11/C21))*C1
3840 PHOT=C1*DSIN(ALP)/(DCOS(THT)**2*DSIN(ALP)**2+DSIN(THT)%
3850 **2)
3860 EPPT=A*ECCN**2*DSIN(PHISE)*DCOS(PHISE)*PHISET/DSQRT%
3870  ((1.-ECCN**2*DSIN(PHISE)**2)**3)
3880 XT=DCOS(PHISE)*DSIN(PHO)*EPPT+EPP*DCOS(PHISE)*DCOS(PHO)*PHOT%
```

```
3890  -EPP*DSIN(PHO)*DSIN(PHISE)*PHISET
3900 YT=DCOS(PHISE)*DCOS(PHO)*EPPT-EPP*DCOS(PHISE)*DSIN(PHO)*PHOT%
3910  -EPP*DCOS(PHO)*DSIN(PHISE)*PHISET
3920 ZT=(1.-ECCN**2)*(DSIN(PHISE)*EPPT+EPP*DCOS(PHISE)*PHISET)
3930 CCC1=-(A**2/B**2)*Z/(X*DSIN(PHO)+Y*DCOS(PHO))
3940 CCC2=DSQRT(1./(1.+CCC1**2))
3950 ZETA=-CCC2
3960 XETA=-CCC1*DSIN(PHO)*CCC2
3970 YETA=-CCC1*DCOS(PHO)*CCC2
3980 P1=XETA*XT
3990 P2=YETA*YT
4000 P3=ZETA*ZT
4010 DOT=(P1+P2+P3)/DSQRT((XT**2+YT**2+ZT**2)*(XETA**2+YETA**2+%
4020  ZETA**2))
4030 AZ=DATAN(DSQRT(1.-DOT**2)/DOT)
4040 RETURN
4050 END
```

```
100 "     THIS PROGRAM CALCULATES THE VARIOUS CONICAL SCANNER IMAGE
110 "PARAMETERS NECESSARY TO PROJECT POINTS ON THE EARTH TO
120 "POSITIONS IN THE SEQUENTIALLY PREPARED DIGITAL TAPE.
130 "TO INITIALIZE THE PROGRAM, THE LOCATION OF THE S/C MUST
140 "BE KNOWN AT SOME TIME '0' ALONG WITH ITS ORIENTATION ELE-
150 "MENTS (ATTITUDES, ATTITUDE RATES, AND ATTITUDE ACCELERA-
160 "TIONS).  IN ADDITION, THE LATITUDE AND LONGITUDE OF THE
170 "POINT TO BE PROJECTED MUST BE GIVEN.  THE OUTPUT OF THE
180 "PROGRAM IS THE TIME FROM '0' WHEN THE POINT WAS SENSED,
190 "THE NUMBER OF SWATH INCREMENTS BEFORE THE POINT WAS SENSED,
200 "THE LATERAL RESOLUTION ELEMENT NUMBER, AND THE DETECTOR
210 "NUMBER WITHIN THE STACK OF SIX.
220 "     INITIALLY, THE LOCATION OF THE POINT IS FOUND IN
230 "SENSOR COORDINATES FOR THE GIVEN S/C LOCATION.  BASED ON
240 "REQUIRED ESTIMATES, SUCCESSIVE ITERATIONS ADVANCE OR RETREAT
250 "THE S/C TO THE POINT OF SENSING.  THE SWATH INCREMENTS ASSUME
260 "A LINEAR VELOCITY IN SENSOR COORDINATES CONSEQUENTLY CARE
270 "MUST BE TAKEN TO INSURE THAT EXCESSIVE SWATH INCREMENTATION
280 "DOES NOT OCCUR SINCE IN THAT CASE THE POINT WOULD BE
290 "SKIPPED IN THE FIRST PASS.  IF THE APPROACH IS MADE
300 "GRADUAL, THE POINT WILL NOT BE SKIPPED AND THE ACCESS
310 "TIME MAY BE FOUND IN ONE PASS, HOWEVER, SEVERAL PHASES OF
320 "SWATH INCREMENTATION MUST BE USED.
```

```
330 "      THE X-Y PLANE OF THE SENSOR COORDINATE SYSTEM WAS
340 "DIVIDED INTO FIVE ZONES.  IT SHOULD BE NOTED THAT THIS
350 "PROGRAM ASSUMES EITHER FORWARD SCANNING OR CIRCULAR
360 "SCANNING AND CANNOT HANDLE AFT SCANNING.  THE REGION WHERE
370 "X>0 IS LABELED AS 1, THE REGION WHERE X<0 AND X>XMAX
380 "WHERE XMAX IS THE X-COORDINATE OF THE FOREMOST (SMALLEST
390 "NEGATIVE) PORTION OF THE ACTIVE REGION OF THE SWATH IS
400 "LABELLED 2, THE REGION WHERE X<XMAX AND WHERE X IS NOT CON-
410 "TAINED WITHIN THE ACTIVE SWATH AREA IS LABELLED REGION 3,
420 "THE SWATH AREA IS LABELLED  AS REGION 4, AND ALL AREA
430 "BEHIND THE SWATH IS LABELLED REGION 5.
440 "      AT FIRST THE S/C POSTTION IS KNOWN AT SOME SWATH
450 "CENTER.  THE LOCATION OF THE GROUND POINT IN SENSOR
460 "COORDINATES IS COMPUTED FOR THE BEGINNING AND ENDING
470 "OF THAT SWATH.  SINCE THE SWATH SCAN TIME IS KNOWN,
480 "A LINEAR VELOCITY IN SENSOR COORDINATES MAY BE FOUND.
490 "IF THE POINT FALLS IN REGION 1, THE NUMBER OF SWATH
500 "INCREMENTS NECESSARY TO PLACE THE POINT JUST INSIDE REGION
510 "2 IS ESTIMATED USING A LINEAR VELOCITY APPROACH.
520 "THE PROGRAM RETURNS AND RECALCULATES THE TWO POINTS AGAIN
530 "FOR THE NEW TIME AND S/C LOCATION.  IF IT FALLS IN REGION
540 "2, THE NECESSARY SWATH INCREMENT TO BRING IT INTO REGION
550 "3 IS COMPUTED AS IN ABOVE.  HOWEVER, BECAUSE THE SWATH
560 "INCREMENTS ARE OVER ESTIMATED (TANGENTIAL RELATIONSHIP
570 " DUE TO INCREASED SLANT RANGE), A SCALE FACTOR OF 0.95
580 "IS USED. THE PROGRAM RETURNS AND LOCATES THE TWO POINTS FOR
590 "THE NEW TIME AND S/C LOCATION.  THE ABOVE PROCEDURE IS
600 "FOLLOWED UNTIL THE POINTS FALL INTO REGION 3. AGAIN
610 "REQUIRED SWATH INCREMENTS ARE CALCULATED, THIS TIME TO
620 "FORCE THE POINTS TO FALL INTO THE ACTIVE AREA OF THE
630 "SCANNER.  AS A PRECAUTION AGAINST OVER INCREMENTING, THE
640 "ESTIMATES ARE REDUCED BY 4 SWATHS AND THE PROGRAM RETURNS.
650 "IF THE POINT IS INITIALLY IN REGION 5, THE S/C IS MOVED
660 "BACK UNTIL IT FALLS IN REGION 3 AT WHICH TIME THE
670 "NORMAL PROCEDURE IS FOLLOWED FROM THAT POINT.
680 "ITERATION CONTINUES UNTIL THE POINT ASSOCIATED WITH THE
690 "END OF ONE SWATH FALLS WITHIN THE ACTIVE AREA.
700 "      AT THIS POINT INTERSWATH MODE IS BEGUN, THAT IS TO
710 "SAY, THE POINT WILL BE SENSED IN THAT SWATH OR THE ONE
720 "FOLLOWING IT.  BASED ON ITS LOCATION IN SENSOR COORDINATES,
730 "THE LATERAL RELOLUTION ELEMENT NUMBER IS ESTIMATED.  AT
740 "THIS POINT, THE GROUND POINT IS PROJECTED FOR ONLY ONE
750 "TIME, THAT TIME BEING ESTIMATED IN THE SAME MANNER AS THE
760 "LATERAL RESOLUTION ELEMENT.  BY PROJECTING THE POINT FOR
770 "VARIOUS ELEMENTS ABOUT THIS TIME, THE DETECTOR STACK MAY
780 "BE LOCATED.  IF AFTER SEVERAL ATTEMPTS (6) , THE STACK
790 "HAS NOT BEEN LOCATED, THE SWATH NUMBER IS INCREMENTED BY
800 "1 AND THE ABOVE PRODEDURE IS REPEATED.  ONCE THE STACK
```

```
810 "IS LOCATED, THE DETECTOR NUMBER (1 THROUGH 6) IS FOUND
820 "BY A MINIMUM DISTANCE TO CENTER CRITERION.  IF THE POINT IS
830 "NEVER SENSED DUE TO EARTH ROTATION GAPS, A STATEMENT IS
840 "PRINTED TO THE EFFECT THAT SWATH INCREMENTATION WAS TOO
850 "LARGE.
860 "     THE INPUT TO THE PROGRAM FROM A DATA FILE IS THE
870 "LATITUDE AND LONGITUDE OF THE POINT WHILE THE OUTPUT IS
880 "THE TIME FROM THE INITIAL S/C LOCATION, THE LATERAL REL-
890 "SOLUTION ELEMENT NUMBER, THE DETECTOR NUMBER, AND THE
900 "SWATH INCREMENT NUMBER.
910 "
920 "
930 "                  DEFINITION OF VARIABLES
940 "
950 "
960 "DGR=CONVERTS DEGREES TO RADIANS
970 "PLAT=LATITUDE OF GROUND POINT
980 "PLNG=LONGITUDE OF GROUND POINT
990 "A=SEMI-MAJOR AXIS OF THE EARTH
1000 "ECCN=ECCENTRICITY OF THE EARTH
1010 "GAMMA=CONE ANGLE OF THE SENSOR
1020 "BETA=PITCH USED TO PRODUCE FORWARD SCANNING
1030 "THETA=ROLL OFFSET
1040 "ALP=COMPLEMENT OF ORBITAL INCLINATION
1050 "VO=TANGENTIAL S/C VELOCITY
1060 "RO=RADIUS OF CIRCULAR ORBIT
1070 "C1=EARTH ROTATION RATE
1080 "C3=CONSTANT USED IN CONJUNCTION WITH ORBITAL ANGLE
1090 "TO=1/2 SWATH SCAN TIME
1100 "CO=SCANNER POLAR ANGLE SPEED
1110 "B=SEMI-MINOR AXIS OF THE EARTH
1120 "THT=ORBITAL ANGLE MEASURED BETWEEN THE TERMINATOR AND THE
1130 "     INSTANTANEOUS LOCATION OF THE S/C
1140 "PHISEO=PITCH AT TIME ZERO
1150 "PHID=PITCH RATE AT TIME ZERO
1160 "PHIDD=PITCH ACCELERATION AT TIME ZERO
1170 "XKAPPO=YAW AT TIME ZERO
1180 "XKAPD=YAW RATE AT TIME ZERO
1190 "XKAPDD=YAW ACCELERATION AT TIME ZERO
1200 "WO=ROLL AT TIME ZERO
1210 "WD=ROLL RATE AT TIME ZERO
1220 "WDD=ROLL ACCELERATION AT TIME ZERO
1230 "TOO=TIME BETWEEN SWATHS
1240 "XLSE=LONGITUDE OF S/C AT TIME T
1250 "TP=SWATH CENTER TIME INITIALLY 0
1260 "XLPK=LONGITUDE OF ORBITAL TERMINATOR
1270 "RAD=RADIUS OF SCAN AREA IN SENSOR COORDINATES USING A
1280 "     Z-DIMENSION OF 1.0
```

```
1290 "DEL=DISPLACEMENT OF SCAN AREA IN WHICH TWO CORCLES OF
1300 "      RADAII RAD OFFSET BY DEL WITH RESPECT TO ONE ANOTHER
1310 "      FORM THE ACTIVE SCAN AREA
1320 "T=THE INSTANTANEOUS TIME AT WHICH THE GROUND POINT IS TO
1330 "      BE PROJECTED
1340 "PHISE=LATITUDE OF S/C AT T
1350 "HSE=ALTITUDE OF S/C AT T
1360 "ALPHA=HEADING OF S/C AT T
1370 "PHIT=TIME VARYING CONTRIBUTION OF PITCH
1380 "XKAPT=TIME VARYING CONTRIBUTION OF YAW
1390 "WT=TIME VARYING CONTRIBUTION OF ROLL
1400 "PHI=PITCH AT TIME T
1410 "W=ROLL AT TIME T
1420 "XKAPPA=YAW AT TIME T
1430 "NCOUNT=THE LATERAL RELOLUTION ELEMENT NUMBER
1440 "NTST=THE TOTAL NO. OF SWATH INCREMENTS
1450 "ITEM=THE DETECTOR NO.
1460 "XT=TOP OF RESOLUTION ELEMENT STACK IN X
1470 "XB=BOTTOM OF RESOLUTION ELEMENT STACK IN X
1480 "YL=LEFT BOUND OF RES. ELE. STACK IN Y
1490 "YR=RIGHT BOUND OF RES. ELE. STACK IN Y
1500 "ETA0,ETA1,ETA2=POLAR ANGLES ASSOCIATED WITH THE SCANNER
1510 REAL*8 D(6)
1520 REAL*8  DELETA,PLAT,PLNG,A,DGR,ECCN,GAMMA,BETA, THETA,%
1530 ALP,V0,R0,C1,C3,T0,C0,D,THT,XKAPPO,PHISEO,PHID,PHIDD,XKAPD,%
1540 XKAPDD,W0,WD,WDD,T00,XLSE,TP,XLPR,XLPK,XLPKD,XX,RAD,DEL,XMAX,%
1550 XMIN,PHISE,HSE,DELT,PHISD,ALPHA,PHIT,TH0,XKAPT,WT,PHI,W,XKAPPA,%
1560 E1,E2,UP,VP,WP,UX,WX,B11,B21,B31,B12,B22,B32,B13,B23,B33,UR,%
1570 VR,WR,XE,YE,ZE,A11,A21,A31,A12,A22,A32,A13,A23,A33,XP,YP,ZP,%
1580 XP2,YP2,ZP2,XP1,YP1,ZP1,ETA1,XCAL,ETA2,VMX,XM,BB,XA,YA,EAT,%
1590 T,ETA0,XT,XB,ARG,GAM1,ARG2,YL,YR,PX1,PX2,PX3,PX4,PX5,PX6,CON,DUM,%
1600 PLATD,PLNGD
1610 INTEGER*4 ISW,NTEST,NT,IT,KMX,LOOP,NCOUNT,ITEM,NTST
1620 ISW=0
1630 DELETA=1.923E-04
1640 NTEST=0
1650 NTRY=0
1660 NT=0
1670 NPT=0
1680 DGR=57.2957795131
1690 CALL OPEN(1,'FOLL','INPUT')
1700 READ(1,*) PLAT,PLNG
1710 PLAT=PLAT/DGR
1720 PLNG=PLNG/DGR
1730 A=6378388.
1740 ECCN=.082
1750 NTST=0
1760 GAMMA=13.23/DGR
```

```
1770 PLATD=PLAT*DGR
1780 PLNGD=PLNG*DGR
1790 WRITE(6,500) PLATD,PLNGD -
1800 500 FORMAT(' THE LAT. OF THE POINT IS',F9.5//' THE LONG.%
1810  OF THE POINT IS',F9.5/)
1820 BETA=13.23/DGR
1830 THETA=0.0
1840 ALP=9./DGR
1850 V0=7400.
1860 R0=7358288.
1870 C1=360./(86164.*DGR)
1880 C3=V0/R0
1890 T0=0.016042
1900 C0=48./(DGR*0.032084)
1910 B=A*DSQRT(1.-ECCN**2)
1920 THT=60./DGR
1930 TH0=THT
1940 XKAPP0=0.0
1950 PHISE0=0.0
1960 PHID=0.0
1970 PHIDD=0.0
1980 XKAPD=0.0
1990 XKAPDD=0.0
2000 W0=0.0
2010 WD=0.0
2020 WDD=0.0
2030 T00=0.040105
2040 XLSE=90./DGR
2050 TP=0.0
2060 XLPR=DATAN(DSIN(THT)/(DCOS(THT)*DSIN(ALP)))
2070 XLPK=XLSE-XLPR
2080 XLPKD=XLPK*DGR
2090 XX=XLSE*DGR
2100 IT=0
2110 RAD=DSIN(GAMMA)
2120 DEL=RAD-DSIN(GAMMA-2.64E-04)
2130 XMAX=-RAD*DCOS(24./DGR)+DEL
2140 XMIN=-RAD
2150 1 CONTINUE
2160 IF(IT.EQ.0) T=TP-T0
2170 IF(IT.EQ.1) T=TP+T0
2180 2 THT=TH0+(V0/R0)*T
2190 XLSE=XLPK+C1*T+DATAN(DSIN(THT)/(DCOS(THT)*DSIN(ALP)))
2200 CALL LATLNG(THT,ALP,A,B,R0,ECCN,PHISE,HSE,DELT)
2210 PHISD=PHISE*DGR
2220 CALL ASE(A,ECCN,ALP,C3,C1,B,THT,R0,PHISE,HSE,ALPHA)
2230 PHIT=PHISE0+PHID*T+PHIDD*T**2/2
2240 XKAPT=XKAPP0+XKAPD*T+XKAPDD*T**2/2
```

```
2250 WT=W0+WD*T+WDD*T**2/2
2260 PHI=-(PHIT+BETA)
2270 W=-(WT+ THETA)
2280 XKAPPA=-XKAPT
2290 E1=A/DSQRT(1.-ECCN**2*DSIN(PLAT)**2)
2300 E2=A/DSQRT(1.-ECCN**2*DSIN(PHISE)**2)
2310 UP=E1*DCOS(PLAT)*DCOS(XLSE-PLNG)
2320 VP=E1*DCOS(PLAT)*DSIN(XLSE-PLNG)
2330 WP=E1*(1.-ECCN**2)*DSIN(PLAT)
2340 UX=E2*DCOS(PHISE)
2350 WX=E2*(1.-ECCN**2)*DSIN(PHISE)
2360 B11=DCOS(ALPHA)*DSIN(PHISE)
2370 B21=DSIN(ALPHA)*DSIN(PHISE)
2380 B31=DCOS(PHISE)
2390 B12=-DSIN(ALPHA)
2400 B22=DCOS(ALPHA)
2410 B32=0.0
2420 B13=-DCOS(ALPHA)*DCOS(PHISE)
2430 B23=-DSIN(ALPHA)*DCOS(PHISE)
2440 B33=DSIN(PHISE)
2450 UR=UP-UX
2460 VR=VP
2470 WR=WP-WX
2480 XE=B11*UR+B12*VR+B13*WR
2490 YE=B21*UR+B22*VR+B23*WR
2500 ZE=B31*UR+B32*VR+B33*WR
2510 A11=DCOS(PHI)*DCOS(XKAPPA)-DSIN(PHI)*DSIN(W)*DSIN(XKAPPA)
2520 A21=-DCOS(W)*DSIN(XKAPPA)
2530 A31=DSIN(PHI)*DCOS(XKAPPA)+DCOS(PHI)*DSIN(W)*DSIN(XKAPPA)
2540 A12=DCOS(PHI)*DSIN(XKAPPA)+DSIN(PHI)*DSIN(W)*DCOS(XKAPPA)
2550 A22=DCOS(W)*DCOS(XKAPPA)
2560 A32=DSIN(PHI)*DSIN(XKAPPA)-DCOS(PHI)*DSIN(W)*DCOS(XKAPPA)
2570 A13=-DSIN(PHI)*DCOS(W)
2580 A23=DSIN(W)
2590 A33=DCOS(PHI)*DCOS(W)
2600 XP=A11*XE+A12*YE+A13*(ZE-HSE)
2610 YP=A21*XE+A22*YE+A23*(ZE-HSE)
2620 ZP=A31*XE+A32*YE+A33*(ZE-HSE)
2630 IF(IT.EQ.0) GO TO 3
2640 XP2=XP
2650 YP2=YP
2660 ZP2=ZP
2670 IT=0
2680 GO TO 4
2690 3 XP1=XP
2700 YP1=YP
2710 ZP1=ZP
2720 IT=1
```

```
2730 IF(ISW.EQ.1) GO TO 18
2740 IF(ISW.GE.2) GO TO 25
2750 GO TO 1
2760 4 XP1=-XP1/ZP1
2770 YP1=-YP1/ZP1
2780 ZP1=1.0
2790 XP2=-XP2/ZP2
2800 YP2=-YP2/ZP2
2810 ZP2=1.0
2820 IF(XP2.GT.0.0) GO TO 10
2830 IF(XP2.GT.XMAX) GO TO 11
2840 ETA1=DATAN(YP2/(DEL-XP2))
2850 XCAL=-DSIN(GAMMA)*DCOS(ETA1)+DEL
2860 IF(XP2.GT.XCAL) GO TO 12
2870 ETA2=DATAN(YP1/(-XP1))
2880 XCAL=-DSIN(GAMMA)*DCOS(ETA2)
2890 IF(XP1.LT.XCAL) GO TO 14
2900 GO TO 17
2910 10 VMX=(XP2-XP1)/(2.*T0)
2920 KMX=-XP2/(VMX*T00)
2930 KMX=KMX+5
2940 TP=TP+DFLOAT(KMX)*T00
2950 NTEST=1
2960 NTST=NTST+KMX
2970 GO TO 1
2980 11 XM=(YP2-YP1)/(XP2-XP1)
2990 BB=YP2-XM*XP2
3000 XINT=(DEL-XM*BB-DSQRT(DSIN(GAMMA)**2*(1.+XM**2)-(XM*DEL+BB)%
3010 **2))/(1.+XM**2)
3020 VMX=(XP2-XP1)/(2.*T0)
3030 KMX=0.9*(XMAX-XP2)/(VMX*T00)
3040 KMX=KMX+1
3050 IF(NT.EQ.1) KMX=KMX+110*KMX/(100*KMX)
3060 TP=TP+DFLOAT(KMX)*T00
3070 NT=NT+1
3080 NTST=NTST+KMX
3090 NTEST=1
3100 GO TO 1
3110 12 VMX=(XP2-XP1)/(2.*T0)
3120 KMX=(XCAL-XP2)/(VMX*T00)
3130 KMX=KMX-2
3140 IF(NPT.GE.1) KMX=1
3150 NPT=NPT+1
3160 TP=TP+DFLOAT(KMX)*T00
3170 NTST=NTST+KMX
3180 NTEST=1
3190 GO TO 1
3200 14 IF(NTEST.EQ.0) GO TO 15
```

```
3210 WRITE(6,104)
3220 104 FORMAT(' THE POINT HAS BEEN SKIPPED SOMEHOW,  TOO MANY %
3230 SWATH INCREMENTS AT SOME POINT')
3240 STOP
3250 15 VMX=(XP2-XP1)/(2.*T0)
3260 KMX=(XMIN-XP1)/(VMX*T00)
3270 KMX=KMX-50
3280 TP=TP+DFLOAT(KMX)*T00
3290 NTST=NTST+KMX
3300 GO TO 1
3310 17 WRITE(6,107)
3320 107 FORMAT(' INTERSWATH MODE HAS BEGUN')
3330 LOOP=0
3340 XA=(XP1+XP2)/2.
3350 YA=(YP1+YP2)/2.
3360 EAT=DATAN(-YA/XA)
3370 NCOUNT=EAT/DELETA
3380 NCOUNT=NCOUNT-5
3390 T=TP+ T0*1.923E-04*DFLOAT(NCOUNT)*DGR/24.
3400 ISW=1
3410 GO TO 2
3420 18 EAT=DATAN(-YP1/XP1)
3430 ISW=ISW+1
3440 NCOUNT=EAT/DELETA
3450 NCOUNT=NCOUNT-2
3460 25 XP1=-XP1/ZP1
3470 YP1=-YP1/ZP1
3480 LOOP=LOOP+1
3490 IT=0
3500 ETA0=DFLOAT(NCOUNT)*DELETA
3510 XT=-DSIN(GAMMA)*DCOS(ETA0)
3520 XB=XT+DEL
3530 ARG=DCOS(GAMMA)*(DCOS(2.2D-05)-DSIN(GAMMA)*DSIN(ETA0)*%
3540 DSIN(2.2D-05)/DSQRT(1.-DSIN(ETA0)**2*DSIN(GAMMA)**2))
3550 GAM1=DATAN(DSQRT(1.-ARG**2)/ARG)
3560 ARG2=DSIN(GAMMA)*DCOS(GAM1)*DCOS(ETA0)/(DCOS(GAMMA)*DSIN%
3570 (GAM1))
3580 ETA1=DATAN(DSQRT(1.-ARG2**2)/ARG2)
3590 YL=DSIN(GAM1)*DSIN(ETA1)
3600 IF(NCOUNT.LT.0) YL=-YL
3610 ARG=DCOS(GAMMA)*(DCOS(2.2D-05)+DSIN(GAMMA)*DSIN(ETA0)*%
3620 DSIN(2.2D-05)/DSQRT(1.-DSIN(ETA0)**2*DSIN(GAMMA)**2))
3630 GAM1=DATAN(DSQRT(1.-ARG**2)/ARG)
3640 ARG2=DSIN(GAMMA)*DCOS(GAM1)*DCOS(ETA0)/(DCOS(GAMMA)*DSIN(%
3650 GAM1))
3660 ETA1=DATAN(DSQRT(1.-ARG2**2)/ARG2)
3670 YR=DSIN(GAM1)*DSIN(ETA1)
3680 IF(NCOUNT.LT.0) YR=-YR
```

```
3690 IF(NCOUNT.GE.0) GO TO 42
3700 40 DUM=YL
3710 YL=YR
3720 YR=DUM
3730 42 CONTINUE
3740 IF(XP1.LT.XB) GO TO 19
3750 T=T+TO*1.923D-04*DGR/24.
3760 NCOUNT=NCOUNT+1
3770 GO TO 24
3780 19 IF(XP1.GT.XT) GO TO 20
3790 WRITE(6,111)
3800 111 FORMAT(' THE POINT IS HIGH, IT WILL NOT BE SENSED  ')
3810 STOP
3820 20 IF(YP1.LT.YR) GO TO 22
3830 T=T+TO*1.923D-04*DGR/24.
3840 NCOUNT=NCOUNT+1
3850 GO TO 24
3860 22 IF(YP1.GT.YL) GO TO 23
3870 WRITE(6,113)
3880 113 FORMAT(' THE POINT IS TO  THE LEFT')
3890 STOP
3900 23 CONTINUE
3910 PX1=-(XT-XB)/12.+XT
3920 PX2=-(XT-XB)/4.+XT
3930 PX3=-(XT-XB)*5./12.+XT
3940 PX4=-(XT-XB)*7./12.+XT
3950 PX5=-(XT-XB)*3./4.+XT
3960 PX6=-(XT-XB)*11./12.+XT
3970 D(1)=DABS(XP1-PX1)
3980 D(2)=DABS(XP1-PX2)
3990 D(3)=DABS(XP1-PX3)
4000 D(4)=DABS(XP1-PX4)
4010 D(5)=DABS(XP1-PX5)
4020 D(6)=DABS(XP1-PX6)
4030 CON=D(1)
4040 ITEM=1
4050 DO 31 I=2,6
4060 IF(CON.LT.D(I)) GO TO 31
4070 CON=D(I)
4080 ITEM=I
4090 31 CONTINUE
4100 WRITE(6,115) TP,NCOUNT,ITEM
4110 115 FORMAT(' THE FINAL TIME IS',F9.5,' THE ELEMENT NO. IS',%
4120 I5/' THE ELEMENT WITHIN  THE STACK IS',I5)
4130 WRITE(6,403) NTST
4140 403 FORMAT('  THE TOTAL NO. OF SWATH INCRE. IS ',I6/)
4150 STOP
4160 24 CONTINUE
```

```
4170 IF(LOOP.GE.6) GO TO 26
4180 GO TO 2
4190 26 CONTINUE
4200 ISW=0
4210 TP=TP+TOO
4220 IF(NTRY.EQ.2) STOP
4230 NTRY=NTRY+1
4240 GO TO 1
4250 END
4260 SUBROUTINE LATLNG(THT,ALP,A,B,RO,ECCN,PHISE,HSE,DELT)
4270 REAL*8 THT,ALP,A,B,RO,ECCN,PHISE,HSE,DELT,HSEN
4280 HSEN=979000.
4290 NCT=1
4300 1 PHISE=DATAN(((A**2+A*HSEN)/(B**2+A*HSEN))*(DCOS(THT)*DCOS%
4310  (ALP)/DSQRT(DSIN(THT)**2+DCOS(THT)**2*DSIN(ALP)**2)))
4320 HSE=RO*DCOS(THT)*DCOS(ALP)/DSIN(PHISE)-A*(1.-ECCN**2)/DSQRT%
4330  (1.-ECCN**2*DSIN(PHISE)**2)
4340 DELT=DABS(HSEN-HSE)
4350 IF(DELT-1.0) 2,2,13
4360 13 IF(NCT-20) 14,2,2
4370 14 HSEN=HSE
4380 NCT=NCT+1
4390 GO TO 1
4400 2 RETURN
4410 END
4420 SUBROUTINE ASE(A,ECCN,ALP,C1,C2,B,THT,RO,PHISE,HSE,AZ)
4430 REAL*8 XO,YO,ZO,A,ECCN,ALP,C1,C2,B,THT,RO,PHISE,HSE,AZ,%
4440 EPP,PHO,X,Y,Z,UARG,C11,C22,C12,C21,C13,C23,PHISET,PHOT,%
4450 EPPT,XT,YT,ZT,CCC1,CCC2,ZETA,XETA,YETA,P1,P2,P3,DOT
4460 XO=RO*DSIN(THT)
4470 YO=RO*DCOS(THT)*DSIN(ALP)
4480 ZO=RO*DCOS(THT)*DCOS(ALP)
4490 EPP=A/DSQRT(1.-ECCN**2*DSIN(PHISE)**2)
4500 PHO=DATAN(DSIN(THT)/(DCOS(THT)*DSIN(ALP)))
4510 X=EPP*DCOS(PHISE)*DSIN(PHO)
4520 Y=EPP*DCOS(PHISE)*DCOS(PHO)
4530 Z=EPP*(1.-ECCN**2)*DSIN(PHISE)
4540 UARG=((A**2+A*HSE)/(B**2+A*HSE))*(DCOS(THT)*DCOS(ALP)/DSQRT%
4550  (DSIN(THT)**2+DCOS(THT)**2*DSIN(ALP)**2))
4560 C11=1.0
4570 C22=1.0
4580 C12=RO*DCOS(THT)*DCOS(ALP)*DCOS(PHISE)/DSIN(PHISE)**2+A*(%
4590  1.-ECCN**2)*ECCN*ECCN**2*DSIN(PHISE)*DCOS(PHISE)/(DSQRT(1.-%
4600  ECCN**2*DSIN(PHISE)**2))**3
4610 C21=(1./(1.+UARG**2))*(A*(A**2-B**2)/(B**2+HSE*A)**2)
4620 C13=-RO*DSIN(THT)*DCOS(ALP)/DSIN(PHISE)
4630 C23=((A**2+A*HSE)/(B**2+A*HSE))*(1./(1.+UARG**2))*(-DCOS%
4640 (ALP)*DSIN(THT)/(DSQRT(DSIN(THT)**2+DCOS(THT)**2*DSIN(ALP)%
```

```
4650 **2))**3)
4660 PHISET=((C13-C23*C11/C21)/(C12-C22*C11/C21))*C1
4670 PHOT=C1*DSIN(ALP)/(DCOS(THT)**2*DSIN(ALP)**2+DSIN(THT)%
4680 **2)
4690 EPPT=A*ECCN**2*DSIN(PHISE)*DCOS(PHISE)*PHISET/DSQRT%
4700  ((1.-ECCN**2*DSIN(PHISE)**2)**3)
4710 YT=DCOS(PHISE)*DSIN(PHO)*EPPT+EPP*DCOS(PHISE)*DCOS(PHO)*PHOT%
4720  -EPP*DSIN(PHO)*DSIN(PHISE)*PHISET
4730 YT=DCOS(PHISE)*DCOS(PHO)*EPPT-EPP*DCOS(PHISE)*DSIN(PHO)*PHOT%
4740  -EPP*DCOS(PHO)*DSIN(PHISE)*PHISET
4750 ZT=(1.-ECCN**2)*(DSIN(PHISE)*EPPT+EPP*DCOS(PHISE)*PHISET)
4760 CCC1=-(A**2/B**2)*Z/(X*DSIN(PHO)+Y*DCOS(PHO))
4770 CCC2=DSQRT(1./(1.+CCC1**2))
4780 ZETA=-CCC2
4790 XETA=-CCC1*DSIN(PHO)*CCC2
4800 YETA=-CCC1*DCOS(PHO)*CCC2
4810 P1=XETA*XT
4820 P2=YETA*YT
4830 P3=ZETA*ZT
4840 DOT=(P1+P2+P3)/DSQRT((XT**2+YT**2+ZT**2)*(XETA**2+YETA**2+%
4850  ZETA**2))
4860 AZ=DATAN(DSQRT(1.-DOT**2)/DOT)
4870 RETURN
4880 END
```

APPENDIX B

USER REQUIREMENT SURVEY

R. J. Ouellette

B.1 INTRODUCTION

The purpose of the user requirement survey was to determine the ground resolution-cell sizes required for the different anticipated observation needs of major users. A second purpose was to provide a unified base of data from which sensor resolution, registration, and positioning requirements can be determined in the future.

The survey first determined what observations are of interest to users. The user group consisted of ten agencies in four government departments and represented the majority of government users. The survey consisted of telephone interviews with fourteen technical personnel within these four departments. These interviews are listed as entries in the list of sources at the end of this section. The observations given by this user group were classified by basic shape and size. From this shape and size information an estimate of the required ground resolution cell size was derived. The views expressed in this section summarize the information received from the telephone conversations. In the summarization some amount of subjectivity has inevitably been introduced. It is hoped that as little misinterpretation as possible has occurred.

In Section B.2 user observations are grouped into three major categories: land use, hydrology/geology, and cartography. Each of these categories is discussed in detail in terms of specific observations and their respective ground sizes and shapes.

In Section B.3 ground observations are categorized by shape and dimension, and a summary table is given with estimates of the percentage of the total observations each categorized group represents. Also the size and shape groups are related to required ground resolution cell sizes for these observations.

As a preface to the rest of this study two preliminary considerations merit discussion here. The first is related to the fact that there has been a basic lack of satellite imagery available to users to evaluate. This lack of experience with the raw data sometimes results in the users not knowing what is required of satellite imagery for a desired observation. This lack of experience is also the main reason for this study considering observations in terms of ground size and shape since these are values readily known by the user.

The second consideration relates to the types of users of satellite images. One type of user is interested in high resolution imagery over a large area but does not need multiple coverage. Another user is interested in repetitive coverage over large areas but does not need high resolution. Still a third type of user needs high resolution and repetitive coverage but only over small areas. The second group is the major user group.

The second type of user generally represents the largest portion of the user group and is best suited to having his observation needs met by satellite imagery. The two other types of users can have some of their observations needs met by satellite imagery, and thus can profitably participate in the satellite program by sharing image data with the second group.

The most significant outcome of the survey is that the great majority of the user observational needs would be met with a 30-to-70 meter ground resolution cell size. To have a significant further impact on the user observation needs, a ground resolution cell size less than 10 meters would be required. (Ground resolution cell size as used here refers to the linear dimension on the ground defined, in a pure geometric sense, by the resolution element of the sensor.)

B.2 USER OBSERVATION NEEDS

B.2.1 Background

United States Government agencies interested in aerial image data were contacted to evaluate their observation needs for possible satellite image data. These government agencies include the Department of Interior, Department of Agriculture, Department of Commerce, and Army Corps of Engineers.

The Departments of Agriculture and Interior will probably be the largest users within this group. Of these two, The Department of Interior has the largest amount of equipment with which to analyze raw satellite data. The Department of Agriculture is working with the NASA/MSC Science and Applications Directorate, Houston, Texas, to develop the data analysis techniques for the observations that the Department is interested in.

Major government users regard satellite image data as part of a multi-layered data acquisition system. Satellite data represents the coarsest upper layer of data while aircraft imagery and ground data acquisition represent the medium and fine resolution layers of the system.

Three qualifying statements should be made before presenting the data of this section. The first is that this survey restricts itself to land-based as opposed to ocean-based, observational

needs, because land-based observations have the most stringent resolution registration and positioning requirements.

The second is that for this study observations that require size, shape, texture, and shadow analyses of objects 10 meters or less in diameter have not been considered. Satellite imagery of higher resolution (10 meters diameter or less) is impractical for large-area coverage because of the high data volume. If high resolution image data were acquired over the whole earth surface, image data volumes would be extremely high. For example, the continental United States, mapped at 10 meter square ground areas, would yield 6.6×10^{11} bits of image data (6 bit digitization). At anticipated satellite mapping rates this surface would be remapped every 18 days. There is an increased computer cost with an increase in image volume. Data rates increase as the inverse square of the decrease in resolution element size. Very high resolution pointable sensors would solve some of the problems of large amounts of image data but would make it more difficult to cover small specific areas of interest situated throughout a large ground surface area.

The third qualifying statement is that only the geometric measurements involved in spectral signature analysis were considered for this survey. Spectral signature analysis is the use of radiometric signals from a surface separated into several spectral regions to define surface characteristics, such as crop species identification. The radiometric aspects of signature analysis were not considered a part of this task. Geometric aspects were used to the extent they were needed for the detection of spot, linear and area features by temporal and spatial signature differences. By temporal signature difference is meant change detection of the radiometric surface signal from one satellite pass to another, over the same area. Spatial signature difference refers to difference between a particular area and the surrounding area.

Observational needs are considered in three basic areas: land use, hydrology/geology, and cartography. These basic areas and their sub-groups are given in Table B-1. Within each area the observations of interest are discussed below, and size and shape information are presented. Observations will be categorized into one or more of the three basic ground shapes of spot, linear, and area features.

B.2.2 Land Use

General

Land use involves the specific areas of agriculture, forestry, and private/public/commercial land development. A general observational need common to each of these specific areas is boundary delineation.

Table B-1 - Observational Need Categories

1. Land Use
   - A. Agriculture
   - B. Forestry
   - C. Private/Public/Commercial
2. Hydrology/Geology
   - A. Control
   - B. Survey
3. Cartography

Boundary delineation of the following interfaces are of interest: grass/brush/timberland/desert/water/crop/bare soil/culturally developed. Some interface boundaries are sharp, due to inherent differences between the areas (e.g., water/grass interface) or the presence of linear objects at the boundaries (e.g., rivers, roads, or tree rows). Other interface boundaries are less well defined because of smaller inherent differences between the areas (e.g., boundaries between different crop types).

Boundary delineation involves linear and area features. For these observations linear features have ground dimensions from ten meters (tree rows, small rivers) to fifty meters (large rivers, major highways). In cases where surface differences (spatial and spectral) define the boundaries the boundary width will appear to be at least several meters wide in the image data.

Agriculture

Observational needs in the area of Agriculture include: inventory, crop species identification, stress analysis, and soil survey (both type and moisture content). The Department of Agriculture is heavily involved in crop inventory and species identification through the Agricultural Stabilization and Conservation Service. Species identification measurements include surface crop identification, surface area measurement, and crop species identification.

Crop fields range in size from four tenths of a hectare (one acre) while ownership plots range from four hectares to hundreds or even thousands of hectares. Average field size varies from area to area within the country and is dependent upon the type of crops planted. High-value crops such as fruits and vegetables tend to be planted in smaller fields, while grain crops are planted in larger fields. Fields

in coastal and heavily populated regions tend to be smaller and discontinuous, while fields in the Midwest tend to be larger and more grouped together.

Stress analysis detects infestation in plant life. Spectral signature changes are the basic data measurements. Surface areas of interest vary from single plant areas to entire crop fields. This corresponds to spot features of a fraction of a meter in diameter to area features as large as few tens of hectares. Larger area features represent the major portion of stress analysis observations.

Soil surveys are carried out in large part by the Soil Conservation Service of the Department of Agriculture. Soil survey measurements (for the type of analysis that can be provided by remote imagery) involve identification of soils in terms of surface area, location, type, and moisture content. Presently, black and white aerial photos are used as base maps and for delineation of different soil surface areas. Direct ground samples are the basic sources for present soil classification. Area features for soil survey observations have sizes that range from a fraction of a hectare to tens of hectares. The distribution of observations through this range is fairly balanced.

Forestry

Observational needs for forestry include tree inventory, species identification, and stress analysis. Forest inventory and species identification are done within the Department of Agriculture. The Forest Service is involved with Federal forest lands whereas the Soil Conservation Service is involved with farmland forest management.

Measurement for forest inventory and species identification include surface area delineation and area measurement. Species identification from space imagery can be done by signature analysis. Sizes of the areas of interest for tree inventories will range from four tenths of a hectare (one acre) to hundreds of hectares. Observations involving Federal forest lands have area sizes generally larger than observations involving farmland forest management. Also Federal forest land observations represent the majority of the total observations.

Stress analysis will require smaller analysis areas than species identification. One of the specific questions to be answered by the first satellite imagery will be: How small an infestation area can be detected from space? When the infestation areas are small, low-contrast spot detection from space will be required. Infestation areas range from three meters to three hundred meters in diameter. The majority of the observations occur in the middle of this size range.

Private/Public/Commercial

A third land area concerns private/public/commercial development. All of the government agencies contacted have some interest in this area. Observational needs are transportation and communication route studies which require inventory and development information. Other needs include private and commercial land use and development studies which require change detection analysis in large part. Data measurements here include spot and linear feature detection and surface area measurement.

Spot features range in size from twenty to a few hundred meters in diameter with the major number of observations occurring in the lower part of the range. Linear features for transportation and communication route studies range in width from five to seventy meters with the majority of the observations falling in the mid to upper part of this range. Area sizes of interest from four tenths of a hectare (one acre) to a few tens of hectares with the majority of the observations grouped in the lower half of this size range.

B.2.3 Hydrology/Geology

Flood Control

Government agencies interested in flood control include the Army Corp of Engineers and the Department of Agriculture. Flood control involves dam construction, snow studies, flood plain delineation, and ice jam detection. Observation needs in this area are water basin information for dam construction, snow cover change detection to predict water run off, and ice jam detection for flood control.

Spot, linear, and area feature measurements are needed for general control studies in the areas of hydrology/geology. Spot features range from three to a few hundred meters in diameter. Linear features range from five to a few hundred meters in width. The lower end of these size ranges is related to small water basin and small dam construction on farmland while the upper end of the size range relates to large water basins and country and state dam construction. Area features range in size from a tenth of a hectare (one quarter acre), for example, for small water basins, to a few hundred hectares for snow cover studies. Spot and linear feature observations are dispersed uniformly throughout respective ranges. The majority of the area feature observations occur in the lower part of the size range.

Inventory Survey

Land surface survey consists of inventory and thematic mapping. Inventory survey is directed at answering questions such as follows. How much of a particular measured quantity is present (e.g., water surface survey)? What is the observed change in a measured

quantity (e.g., soil erosion survey)? Thematic mapping is more involved with the surface location of some measured quantity (e.g., geological feature mapping).

Inventory surveys measure ground water, erosion, sedimentary patterns, water pollution, mineral/petroleum, heavy metal, construction material, and natural disaster phenomena. Thematic mapping includes geological features, river basins, water-sheds, and coastal areas.

Data needs for hydrology/geology surveys include spot, linear, and area features. Spot feature sizes range from about ten meters to one hundred meters. The great majority of measurements fall in the upper part of this size range. Geologic features represent the major observations. Linear feature widths range from five to one hundred meters. The majority of the measurements fall in the upper part of this size range. Geologic features and linear boundaries comprise the major observations. Area features, including spectral signature ground surface areas, fall in the size range from four tenths of a hectare (one acre) to over one hundred hectares. The largest number of measurements occur in the upper half of this range. The majority of the observations involve ground water, medium to broad geological structures, and material location.

B.2.4 Cartography

The Department of Interior is the government agency most interested in the use of earth resources satellite imagery to make or revise standard topographic maps. These maps will be used as data bases for most large-area remote sensing observations.

At the present the United States is completely mapped at 1/250,000 scale. There is considerable interest among the different users for satellite imagery at 1/250,000 scale. This is interesting, in light of some of the high resolutions and small dimensions stated to be of interest. Ideally, the satellite imagery should be made available at the largest scale consistent with resolution and the scales of data base materials to be used for comparison. Information available from well-detailed imagery at 1/1,000,000 scale is believed to be appropriate for the 1/250,000 scale maps in areas that are poorly mapped.

Table B-2 lists the ground surface widths of a thin line (0.1 mm) drawn on maps of different map scales. These ground dimensions are not necessarily the minimum feature widths to be shown on the maps, as can be seen from the table. Some care is needed in attempting to relate image resolution, map symbol size, and importance of the feature for a particular map. If the image is substituted for a line map, the higher information content of the image must be made available to the map user. Linear features of smaller widths can be seen in the image because of the eye's inherent ability to pick out line features.

Table B-2 - Map Scale Versus Projected Ground Size
For A 0.1-MM Line Drawn On A Map of That Scale

Map Scale	Ground Size (m)
1/1,000,000	100
1/250,000	25
1/100,000	10
1/62,500	6
1/50,000	5
1/24,000	2.4

Area measurements can be made where minimum breadth is only a few times the minimum spot resolution.

B.3 SUMMARY

Measurement Needs of Users

Satellite imagery for land surface measurements will be used for the specific measurement categories of spot, linear, and area features.

Table B-3 lists the three classes of features and the ground dimension ranges associated with fine, medium, and coarse observations of these features. For a particular feature type an estimate is given of the percentage of total observation each of the groups represents. An estimate is given of the required ground resolution element cell size range for each group. The numbers in this table are not absolute values, but trends indicated by the stated observational needs. Now consider the size class groupings in Table B-3 in terms of the major observations that make up each size group. For spot features the major fine size observation is agricultural stress measurement. Medium size spot features are made up of a broad set of observations covering each of the basic observational need areas covered in Section B.2. The same is true of the observational make-up of coarse size spot features. The two sub-groups within the medium size group represent agricultural stress analysis, private/commercial land use, and hydrology/geology control observations for the smaller sub-group and forest stress analysis and hydrology/geology survey observations for the larger size sub-group. The great majority of spot feature measurements are represented by the medium and coarse size classes.

Fine size linear features are made up of observations from public and commercial land use and the hydrology/geology flood control

Table B-3 - Ground Surface Dimensions, Percentage of Total Number of Observations, and Required Ground Resolution Element Range for Spot, Linear, and Area Features

Feature Type		Size Classes			
		Fine	Medium		Coarse
Spot	Dimension (m)	< 3	3 - 10	10 - 30	> 30
	GRE Range*	A	A - B	A - B - C	B - C
	Percent of Total	5	15	30	50
Linear	Width	< 10	10 - 30		> 30
	GRE Range	A	B - C		> C
	Percent of Total	10	70		20
Area	Dimension on a Side (m)	< 65	65 - 200	200 - 400	> 400
	GRE Range	A	B - C	C	> C
	Percent of Total	5	25	35	35

*Ground Resolution Element Range
(dimensions given are for one side of a square ground cell)

A	B	C
< 20 m	20 m to 40 m	40 m to 70 m

and inventory survey measurements. The great majority of linear feature measurements are represented by the medium size class. Boundary delineation and communication and transportation route studies represent the major observations. The majority of the observations for coarse size linear features are hydrology/geology flood control and inventory survey measurements.

Observations of fine-size area features include hydrology/geology flood control measurements, and agriculture and forestry stress analysis. The great majority of area feature measurements are represented by the medium size class. Observations in this size class are a broad representation of each basic observation area. The breakdown of the medium size group into two sub-groups represents the separation between small crop fields, farmland forest management, and public/commercial observations for the smaller size sub-group, and large crop field, Federal

forest management, and hydrology/geology flood control observations for the larger size sub-group. Coarse size area feature observations cover the entire set of basic observation areas but represent a smaller part of the total number of area feature measurements than the medium size class.

The final discussion in this subsection will concern itself with the relationship between the three types of data measurement features (spot, linear, and area) and ground resolution cell sizes.

Spot feature measurements made on satellite imagery can include spot features whose surface dimensions are smaller than a ground-resolution-element cell size (e.g., ice jam detection in inland waterways for flood control). Since the spot feature is smaller in dimension than the ground resolution cell size, the inherent ground contrast of the spot feature is degraded by the fact that the spot energy is averaged over the ground area of the resolution cell. Spot features which are several times smaller than the ground resolution cell will be detectable only when the spot feature has a very high ground contrast.

Linear feature detection involves location of features whose short dimensions can be several times smaller than a ground resolution element. The width of the linear feature can be measured when its dimension is equal to or greater than a ground resolution element. Detectability of a linear feature whose short dimension is smaller than a ground resolution element will be determined by its resultant image plane contrast ratio.

For linear boundaries between well defined areas the boundary location will be no worse than one ground resolution cell size. Linear boundaries between areas with little surface or area signal differences, can have an error in locating the linear boundary, of several ground cell sizes.

Recent studies indicate that linear feature detection for roadway analysis is completely reliably only when the width of the roadway is at least 1/3 of the ground resolution cell (Source 17, p. 855). However, Apollo space photography has detected roadways that were 1/10 ground resolution cell size (Source 6, p. 33). Thus very high contrast linear features whose widths are as much as one tenth the ground resolution cell size are detectable from satellite imagery.

Measurement of ground surface areas requires that the area be resolved by the sensor. Areas are delineated by linear boundary detection and ground surface differences such as surface structure and spectral signature. Signature analysis of large ground surface areas is relatively independent of the ground resolution cell size. Spectral signature identification of large area agricultural crops is the same for 66 to 100 meter ground resolution images as it is for 3 to 6 meter ultra-high resolution images. Spectral signatures of large area crop are distinct from one another and therefore lend themselves readily to multi-spectral signature analysis. (Source 11, p. 1193).

In general for spot, linear, and area features, if the surface area of a feature is not resolved, dimensional measurement cannot be made. It is still possible to detect the presence of the feature if the resultant image contrast is enough to make the feature discernible from the background. It should be noted that area measurements near the resolution limits are prone to a larger percentage of error since they require near-perfect transmitting and collection media. Also a general comment to spot, linear, and area features: recent studies indicate that gross geological area features, fine linear features, and high contrast spot features can be identified from satellite imagery which has a ground resolution size from 50 to 100 meters (Source 2, p. 499).

B.4 LIST OF SOURCES CONSULTED FOR USER REQUIREMENT SURVEY

1. Addess, S., Topographic Division, U. S. Geological Survey, U. S. Department of Interior, Goddard Space Flight Center, Greenbelt, Maryland, (Telephone conversation 5/15/72).
2. Amsbury, D. L., "Geological Comparison of Spacecraft and Aircraft Photographs of the Potrillo Mountains, New Mexico, and Franklin Mountains, Texas," Proceedings of the Sixth International Symposium on Remote Sensing of Environment, Volume 1, pp. 493-501, (October 13-16, 1969).
3. Borgason, W., Topographic Division U. S. Geological Survey, U. S. Department of Interior, McLean, Virginia, (Telephone conversation 5/15/72).
4. Clifton, J. W., Agricultural Stabilization and Conservation Service, U. S. Department of Agriculture, Washington, D. C., (Telephone conversation 5/17/72).
5. Colvocoresses, A. P., "Image Resolutions for ERTS, SKYLAB and GEMINI/APOLLO," Photogrammetric Engineering, pp. 33-35, (January, 1972).
6. Fischetti, T. L. and Bondeen, W. R., "Earth Observatory Satellite Mission Review Group (EOSMRG)," NASA Washington, D. C., Final Report (1971).
7. Fisher, W. A., "Projected Uses of Observations of the Earth from Space---The EROS Program of the Department of the Interior," Proceedings of AIAA Earth Resources Observation and Information Systems Meeting, (March 2-4, 1970).
8. Heller, R. C., Forest Service, U. S. Department of Agriculture, Berkely, California, (Telephone conversation 5/18/72).
9. Goddard Space Flight Center, "Earth Observatory Satellite (EOS) Definition Phase Report," Greenbelt, Maryland, (August, 1971).

10. Jarmon, J., Civil Works Directorate, U. S. Army Corp of Engineers, Washington, D. C. (Telephone conversation 5/19/72).

11. Lauer, D. T. and Thamon, R. R., "Information Content of Simulated Space Photographs as a Function of Various Levels of Image Resolution," Proceedings of the 7th International Symposium on Remote Sensing of Environment, Volume II, pp. 1191-1204, (May 17-21, 1971).

12. McLaurin, J., Topographic Division, U. S. Geological Survey, U. S. Department of Interior, McLean, Virginia, (Telephone conversation 5/11/72).

13. Miller, R. H., Research Department, U. S. Department of Agriculture, Washington, D. C., (Telephone conversation 5/9/72).

14. Mohr, J. E., Van der Meer, C., and Krishnaununni, K., "Evaluation of Hyperaltitude Photography for Geological Mapping," Proceedings of the 7th International Symposium on Remote Sensing of Environment, Volume III, pp. 2307-18, (May 17-21, 1971).

15. Orvedal, A., Soil Conversation Service, U. S. Department of Agriculture, Washington, D. C., (Telephone conversation 5/19/72).

16. Scheps, B. B., Engineer Topographic Laboratory, U. S. Army Corp of Engineers, Fort Belvair, Virginia, (Telephone conservation 5/18/72).

17. Simonett, D. S., Henderson, F. M., and Egbert, D. D., "On the Use of Space Photography for Identifying Transportation Routes: A Summary of Problems," Proceedings of Sixth International Symposium on Remote Sensing of Environment, Volume II, pp. 855-877, (October 13-16, 1969).

18. Smith, C. R. and Wood, P., "Multi-Discipline Applications for Earth Resources Satellite Data," Presented at AIAA Earth Resources Observations and Information Systems Meeting, Annapolis, Maryland, (March 2-4, 1970).

19. Tueller, P. T. and Garwin, L., "Environmental Analysis of the Lake Tahoe Basin from Small Scale Multispectral Imagery," Proceedings of the 7th International Symposium on Remote Sensing of the Environment, Volume I, pp. 453-63, (May 17-21, 1971).

20. Von Steen, D. H., Statistical Reporting Service, U. S. Department of Agriculture, Washington, D. C., (Telephone conversation 5/16/72).

21. Weinstein, O., Miller, B. P., and Barletta, J., "Simulation of ERTS RBV Imagery," Proceedings of 7th International Symposium on Remote Sensing of the Environment, Volume II, pp. 1177-89, (May 17-21, 1971).

22. Wiegand, C., Agricultural Research Service, U. S. Department of Agricultural, Wesaco, Texas, (Telephone conversation 5/10/72).

23. Wiesnet, C., National Environment Satellite Service, U. S. Department of Commerce, Suitland, Maryland, (Telephone conversation 5/11/72).

24. Wood, P., "User Requirements for Earth Resources Satellite Data," Proceedings of Electronic and Aerospace Systems Convention (EASCON), Washington, D. C., pp. 14-20, (October 26-28, 1970).

REFERENCES

1. NASA/GSFC. Earth Observatory Satellite (EOS) Definition Phase Report. Greenbelt, Maryland. August 1971.

2. NASA. Earth Observatory Satellite Mission Review Group (EOSMRG) Final Report. Washington, D. C. November 1971.

3. Conversations with R. Predmore, NASA/GSFC. April - August 1972.

4. K. W. Wong. Geometric Analysis of RBV Television System. 38th Annual Meeting, American Society of Photogrammetry. Washington, D. C. March 1972.

5. T. J. Stansell, Jr. Transit, the Navy Satellite Navigation System. Navigation, Vol. 18 (1). Spring 1971.

6. E. M. Gaposchkin and K. Lambeck. Earth's Gravity Field to Sixteenth Degree and Station Coordinates from Satellite and Terrestrial Data. Journal of Geophysical Research, Vol. 76 (20). July 1971.

7. Conversations with J. L. Cooley, NASA/GSFC. April - August 1972.

8. J. L. Cooley. Orbital and Earth Modeling for EOS Mapping Accuracy Study, memorandum to W. L. Alford, NASA/GSFC. April 1972.

9. J. L. Cooley. Orbital Selection Considerations for Earth Observatory Satellites. NASA/GSFC preprint X-551-72-145. Greenbelt, Maryland. April 1972.

10. H. H. Schmid. Remarks at 12th International Congress of Photogrammetry, Ottawa, Canada. August 1972.

11. H. H. Schmid. Applications of Photogrammetry to Three-Dimensional Geodesy (Photogrammetric Satellite Triangulation). Invited paper, 11th International Congress of Photogrammetry, Lausanne, Switzerland. July 1968.

12. H. H. Schmid. Accuracy Aspects of A Worldwide Passive Satellite Triangulation System. Photogrammetric Engineering, Vol. 21 (1). January 1965. Pages 104-117.

13. B. K. Meade. High-Precision Transcontinental ESSA/USC&GS Traverse Survey. Annual Convention, American Society of Photogrammetry. Washington, D. C. March 1966.

14. J. C. Trinder. Relationship Between Pointing Precision, Spread Function, and Modulation Transfer Function. Presented paper, 12th International Congress of Photogrammetry. Ottawa, Canada. August 1972.

15. S. A. Hempenius. The Role of Image Quality in Photogrammetric Pointing Accuracy. Final Report, Contract DA-91-591-EUC-3721, U.S. Army. 1969.

16. C. E. K. Mees and T. H. James. Theory of the Photographic Process. Third Edition. New York. 1966.

17. R. B. Forrest. RBV Image Geometry. ERTS Technical Memorandum ERTM-H-184. Undated.

18. R. B. Forrest. MSS Image Geometry. ERTS Technical Memorandum ERTM-H-185. Undated.

19. General Electric Co. ERTS OCC and DPF Final Report. Systems Studies. Book 2, NASA/GSFC Contract No. NAS5-11529. Philadelphia, Pennsylvania. April 1970.

20. Conversations with Dr. Arun K. Guha, NASA/GSFC. April - August 1972.

21. B. Hallert. Photogrammetry. New York. 1960.

22. American Society of Photogrammetry. Manual of Photogrammetry. Third Edition. Falls Church, Virginia. 1966.

23. G. Ogletree, J. Coccoli, R. McKern, M. Smith, and R. White. Candidate Configuration Trade Study, Stellar-Inertial Measurement System, (SIMS) for an Earth Observation Satellite (EOS). NASA Contract NAS9-4065, MIT Charles Stark Draper Laboratory. Cambridge Massachusetts. Interim Technical Report No. 1. November 1971.

24. Ibid. Interim Technical Report No. 2. January 1972.

25. Ibid. Interim Technical Report No. 3. June 1972.

26. Bendix Aerospace Systems Division. Multispectral Picture Registration Study. Final Technical Report. NASA Contract NAS5-11699. Ann Arbor, Michigan. November 1969.

27. G. L. Hobrough and T. B. Hobrough. Image Correlator Speed Limits. Photogrammetric Engineering, Vol. 37(10). October 1971. Pages 1045-1053.

28. W. E. Chapelle, A. E. Whiteside, and J. E. Bybee. Automation in Photogrammetric Compilation. Presented paper, 11th International Congress of Photogrammetry, Lausanne, Switzerland. July 1968.

29. D. I. Barnea and H. F. Silverman. A Class of Algorithms for Fast Digital Image Registration. IEEE Transactions on Computers, Vol. C-21(2). February 1972. Pages 179-187.

30. H. F. Silverman. On the Uses of Transforms for Satellite Image Processing. Proceedings of the Seventh International Symposium on Remote Sensing of Environment. University of Michigan, Institute of Science and Technology. Ann Arbor, Michigan. May 1971.

31. H. H. Schmid. Some Problems Connected with the Execution of Photogrammetric Multi-Station Triangulations. Proceedings of the Symposium on Geodesy in the Space Age. The Ohio State University. Columbus. 1961. Page 59.